UNIVERSITY OF SOUTHAMPTON

FACULTY OF ENGINEERING, SCIENCE & MATHEMATICS

School of Chemistry

High-Throughput Studies of Polymer Electrolytes for Battery and Fuel Cell Applications

by

Hannah Jane Alcock BSc (Hons)

Thesis for the degree of Doctor of Philosophy

DATE 03/04/2009

ABSTRACT

New methods for the high-throughput characterisation of polymer electrolytes have been developed. Polymer electrolytes for use in lithium ion batteries have been prepared in a novel systematic manner that involves parallel preparation and subsequent high-throughput conductivity measurements of up to 64 individual compositions in a multi-electrode cell. The method of casting the polymer electrolytes directly onto the substrate also allows high-throughput characterisation by x-ray diffraction. The technique was applied specifically to a ternary system of PVdF-HFP, LiTFSI and PC. By preparing a vast array of samples across the composition range, it was found that the conductivity reached a maximum value when the weight fraction composition was 0.45/0.45/0.1 of PVdF-HFP/LiTFSI/PC with completely free standing samples. The trend of increasing conductivity tended towards the maximum liquid conductivity of LiTFSI/PC.

Due to limitations of this method with highly conductive polymer electrolytes, a second novel alternative polymer synthesis, preparation and measurement technique was developed for proton conducting polymers for fuel cell applications. In addition a second multi-electrode cell was designed and constructed specifically allowing AC Impedance measurements to be taken whilst allowing the polymer electrolytes to be subjected to temperature and relative humidity effects. The multi-electrode cell was calibrated using commercially available Nafion samples before being used with synthesised samples. PEEK was sulfonated to SPEEK using varying temperatures and reaction times to obtain many samples with differing DS values. The conductivity of the samples was measured *in situ* using an in-plane 4 electrode impedance measurement, over a range of environmental conditions. It was found that water loss caused significant conductivity decay under PEMFC conditions for Nafion but not for SPEEK samples. SPEEK with a DS of 75 % was found to have the maximum SPEEK equilibration conductivity of 0.177 S cm^{-1}, a value comparable to that of commercial membranes. By blending this sample with a lower DS SPEEK, high conductivity values could be maintained at temperatures of 105 °C and 75 % relative humidity with maintained mechanical integrity. When an inorganic additive ($Zr(HPO_4)_2$) was introduced into the blended samples, the conductivity was enhanced further due to increased water retention within the phosphate structure.

Table of Contents

Chapter 1 Introduction

Chapter 2 AC Impedance as a Method for Studying Polymer Electrolytes

Chapter 3 Lithium Ion Gel Polymer Electrolytes

Chapter 4 Experimental – H^+ Conducting PEM's

Chapter 5 Multi-electrode Cell Design and Method Validation

Chapter 6 Temperature and Relative Humidity Effects on H^+ Membranes

DECLARATION OF AUTHORSHIP

I, Hannah Jane Alcock, declare that the thesis entitled

"High-Throughput Studies of Polymer Electrolytes for Battery and Fuel Cell Applications"

and the work presented in the thesis are both my own, and have been generated by me as the result of my own original research.

- this work was done wholly or mainly while in candidature for a research degree at this University;

- where any part of this thesis has previously been submitted for a degree or any other qualification at this University or any other institution, this is always clearly attributed;

- where I have quoted from the work of others, the source is always given. With the exception of such quotations, this thesis is entirely my own work;

- I have acknowledged all main sources of help;

- where the thesis is based on work done by myself jointly with others, I have made clear exactly what was done by others and what I have contributed myself;

- none of this work has been published before submission.

Signed:

Date:

Acknowledgements

I would like to thank Professor John Owen who has provided invaluable discussions and personal insights throughout my studies. I am particularly grateful for the opportunities he gave me through my international conference participation that was encouraged (even though I had to go on my own!). Secondly, Dr Matthew Roberts, Dr Girts Vitins were key in assisting with the initial education of combinatorial and high-throughput chemistry, while Dr Thierry Le Gall and Ilika Technologies provided an industrial view on the work along with sponsorship. Professor Derek Pletcher, my advisor, remained a source of knowledge and sensibility over the 3 years and also had unlimited supplies of membranes for me. Cheers!

All the members of the Owen Group during my studies in Southampton have been key in providing help at some stage, but more importantly provided good healthy banter! Those who have not already been mentioned, Yasu (The Wakster), Phil (green cake) Johns, Ken, James Mason and Paaaaan I thank you, Pan especially, as you replaced me as the tiniest person in the Owen Group and upped the female contingent from one to two for a while! From the neighbouring groups, Maria, Chris, Katie and Maciej, Staff Club and coffee times would have been dull without you!

Lastly for Southampton, I should not forget the technical staff, namely Alistair and the workshop guys, who have been involved with endless HT cell designs over my time here.

More personally, I would like to thank Neal for starting me off on a path of dealing with all the data I produced with the VBA coding. You also put up with my whinging on a daily basis, took me touring round Europe and to grand prixs for a bit of light relief!

Finally, and most importantly, I would like to thank my parents and brother, Peter, who have supported and inspired me while I have been studying at Southampton and previously. To my Mum and Dad, thank you for buying my new laptop to write this thesis on. It would have been an impossibly slow process otherwise with all this (high-throughput) data!

List of Symbols

ΔG	Gibbs energy	
ΔG_f	Gibbs energy of formation	
ΔH	Enthalpy	J
ΔS	Entropy	$J\ K^{-1}$
A	Area	cm^2
a	Activity	
B	Pseudo-activation energy	
C	Capacitance	F
c	Concentration	mol
C_b	Bulk capacitance	F
C_{dl}	Double layer capacitance	$F\ cm^{-2}$
CPE	Constant phase element	
e	Electron	
E	Voltage	V
E_a	Activation energy	$J\ mol^{-1}$
E_f	Electric field	
F	Faraday constant (98645)	$C\ mol^{-1}$
f	Frequency	Hz
f_f	final frequency	Hz
f_i	Initial frequency	Hz
G	Conductance	S
h	Sample thickness	cm
I	Current	A
j	Complex number operator ($\sqrt{-1}$)	
$\hat{J}$	Current density vector	
k	Width of electrode	cm
l	Distance between electrodes	cm
L	Inductance	H
Ł	Average film thickness	cm
M_{dry}	Dry weight	g
M_{wet}	Wet weight	g
N	Avogadros Constant ($6.023x10^{23}$)	mol^{-1}
N’	Amount of material	mol
N_d	Point per decade	
N_f	Number of frequencies	
P	Pressure	Pa
p_W	Partial pressure of water	Pa
p_{WS}	Saturation vapour pressure of water	Pa
R	Resistance	Ω
Ř	Average resistance	Ω
Ŗ	Gas constant (8.314)	$J\ K^{-1}\ mol^{-1}$
R_b	Bulk resistance	Ω
r_p	Pore radius	
s_σ	Standard deviation of conductivity	
T	Temperature	°C

t	Time	s
T_{exp}	Experiment time	h
T_{wait}	Wait period	
$\tilde{V}$	Partial molar volume	
V’	Volume	cm^3
V_{pp}	Peak to peak amplitude	mV
W	Sample width	cm
W’	Sample weight	g
X	Reactance	Ω
Y	Admittance	S
Z	Impedance	Ω
Z'	Real impedance	Ω
-Z"	Imaginary Impedance	Ω
Z*	Complex Impedance	Ω
α	Any phase	
ε	Dielectric constant	
ε_0	Vacuum permitivity ($8.85x10^{-14}$)	F cm^{-1}
λ	Water content	mol/mol
μ	Chemical potential	J mol^{-1}
ξ	Surface tension	N m^{-1}
Π	Pressure	Pa
ρ	Electrical resistivity	Ω m
σ	Conductivity	S cm^{-1}
σ_{MAX}	Conductivity maximum	S cm^{-1}
σ_P	Conductivity plateau	S cm^{-1}
τ	Time constant	s
ψ	Other potentials	
ω	Angular frequency	r s^{-1}
Ä	Pre exponential factor	

List of Abbreviations

AC	Alternating Current
ACN	Acetonitrile
ALD	Aldrich
BAM	Ballard Advanced Materials
B_{pt}	Boiling Point
CP	Cyclopentanone
CPE	Constant Phase Element
CPE-P	Constant Phase Element Phase Angle
DBP	Dibutyl Phthalate
DC	Direct Current
DI	De-ionised
DMAc	Dimethyl acetamide
DMC	Dimethyl Carbonate
DMF	Dimethyl formamide
DMSO	Dimethyl sulfoxide
DMSO-d_6	Dimethyl sulfoxide-deuterated
DS	Degree of Sulfonation
DSC	Differential Scanning Calorimetry
EC	Ethylene Carbonate
EDX	Energy Dispersive X-ray Spectroscopy
EW	Equivalent Weight
HT	High-throughput
ICE	Internal Combustion Engine
IDE	Integrated Drive Electronics
IEC	Ion-Exchange Capacity
JM	Johnson Matthey
L	Inductor
LiTFSI	Lithium bis(trifluoromethane) sulfonimide salt
MACOR	Machinable Glass Ceramic
M_n	Molecular Number
M_W	Molecular Weight
NMP	N-methyl-2-pyrrolidinone
NMR	Nuclear Magnetic Resonance
PAN	Poly(acrylonitrile)
PBI	Poly(benzimidazole)
PC	Propylene Carbonate
PCB	Printed Circuit Board
PE	Poly(ethylene)
PEEK	Poly(ether ether ketone)
PEG	Poly(ethylene glycol)
PEI	Poly(ethylene imide)
PEM	Proton Exchange Membrane
PEMFC	Proton Exchange Membrane Fuel Cell
PEO	Poly(ethylene oxide)
PFS	Perfluorosulfonate
PFSI	Perfluorosulfonated Ionomer

PP	Poly(propylene)
PPO	Poly(propylene oxide)
PPSU	Poly(phenyl sulfone)
PSU	Poly(sulfone)
PTFE	Poly(tetrafluoro ethylene)
PVdF	Poly(vinylidene fluoride)
PVdF-HFP	Poly(vinylidene fluoride-co-hexafluoropropylene)
PVP	Poly(vinyl pyrrolidone)
RH	Relative Humidity
SANS	Small Angle Neutron Scattering
SAXS	Small Angle X-ray Scattering
SN	Succinonitrile
SPEEK	Sulfonated poly(ether ether ketone)
T_c	Crystallisation Temperature
T_g	Glass Transition Temperature
T_m	Melting Temperature
T_{max}	Maximum Temperature
TMS	Tetramethyl siloxane
VB	Visual Basic
VMP	Variable Multi-Channel Potentiostat
VTF	Vogel-Tamman-Fulcher
wt.	Weight
WU	Water Uptake
XRD	X-ray Diffraction
ZrP	Zirconium Phosphate

Chapter 1

Introduction

Chapter 1 Introduction

Energy conversion devices play a fundamental role in everyday society and electrical power demand is increasing at a rate that is not sustainable using fossil fuels. In addition to this is the growing concern from a political stance over "global warming". Wind farms and solar panels are becoming commonplace in the UK and most of the developed world, and are able to meet demands for domestic power in most cases.

Producing electrical power for other devices has in the past few decades seen rapid technological advancements allowing smaller and more powerful electronics to be developed in such portable devices as laptops and mobile phones. However, motor vehicles powered by internal combustion engines (ICE's) are thought to be a major contributing factor to current and future environmental problems. Therefore other renewable and green energy sources have attracted more attention such that the global automotive market has re-evaluated automotive power with the majority of manufacturers having hybrid or fuel cell cars in the market today.

Batteries and fuel cells are being seen as the near future replacements for the ICE, with a key component of both these power sources being a polymer electrolyte. Polymer electrolytes are solid membranes that have comparable properties to that of liquid electrolytes. They have attracted increasing interest due to the variety of possible applications. Initially they showed promising use in rechargeable lithium ion batteries, and have since been utilised in such solid state electrochemical devices as electrochromic windows, supercapacitors and proton exchange membrane fuel cells (PEMFC) for example. The polymer electrolytes effectively act as the separators between the two electrodes in an electrochemical cell, preventing electrical short circuits whilst still allowing ionic current to flow through it. The drive to make these devices has never been greater, and although the technology is available for use now, improvements can still be made.

1.1 Polymer Electrolytes in Battery Applications

Typical commercial lithium ion batteries contain polymers which are used as separators between the anode and cathode of the cell as seen in Figure 1.1.1. The batteries also contain a lithium salt dissolved in an organic solvent which is used as the electrolyte.

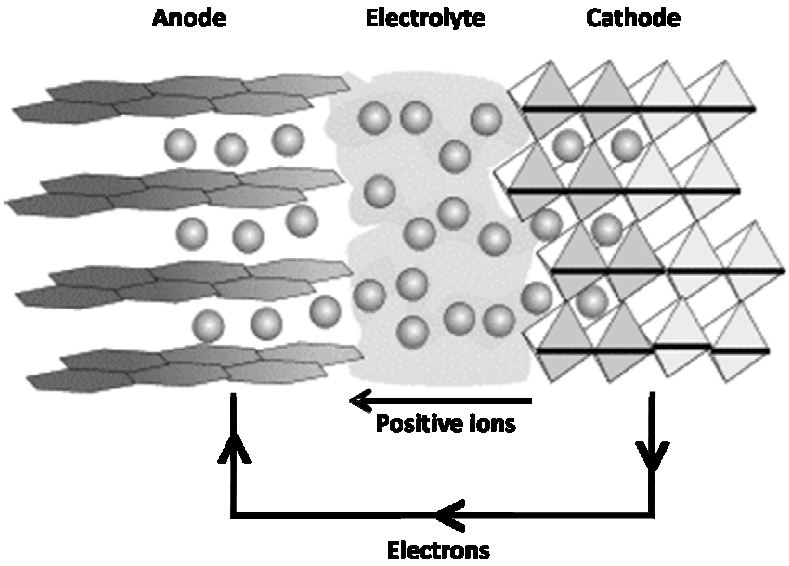

Figure 1.1.1 Schematic diagram of a lithium ion cell. The balls represent lithium ions that move through the electrolyte to compensate for electrons passing in and out of the electrodes while current passes in the external circuit.

Polymers such as poly(propylene) (PP) and poly(ethylene) (PE) are the most frequently used polymers for these separators. They provide an insulating barrier whilst still allowing flow of the liquid battery electrolyte between the two electrodes. The liquid electrolyte contains a lithium salt and provides the path from a lithium cathode compound to the anode where lithium is inserted. Such a reaction can be seen in Equation 1.1.1 for a lithium cobalt oxide cathode and a carbon anode.

$$LiC_6 + CoO_2 \leftrightarrow C_6 + LiCoO_2$$

Equation 1.1.1

However, there are safety issues with using volatile liquid electrolytes. One such instance is the spate of exploding batteries in small devices thought to be caused by the organic solvents present within the cell. Any accidental exposure to abnormal temperatures, can affect the system by decreasing the electrolyte resistance and causing self perpetuating reactions with detrimental effects. With the type of solvents used in battery electrolytes, the risk of an event occurring are higher than would be preferred by manufacturers. By removing this and using alternative materials, it is hoped that the safety issues can be addressed, whilst retaining the desirable qualities such as high storage capacity. Currently commercialised technologies are using polymers such as poly(vinylidene fluoride) (PVdF) gelled with conventional battery salts and a reduced quantity of battery solvent to address some the safety issue. However, more recently, manufacturers have been concentrating on lithium ion polymer batteries, whereby the electrolyte is a solid polymer such as poly(ethylene oxide) (PEO) or poly(acrylonitrile) (PAN) that contains the conducting salt and other additives. In these cases, volatile organic solvents are completely removed and the cell is thought to be more robust. The specific design of the cell is often governed by the purpose which it is to be used. Therefore, many different polymer electrolytes are still being investigated as a matter of course.

1.2 Polymer Electrolytes in Fuel Cells

With regards to automotive applications, the efficiency of hydrogen fuel cells is between 30 and 50 %. This is though, an improvement on the 20 % efficiency of the ICE. However, the initial offset costs of components and fuel production remains large leaving opportunities for improvement using new materials and may ultimately lead to an improved system on current setup methods.

A schematic of a typical PEM fuel cell can be seen in Figure 1.2.1.

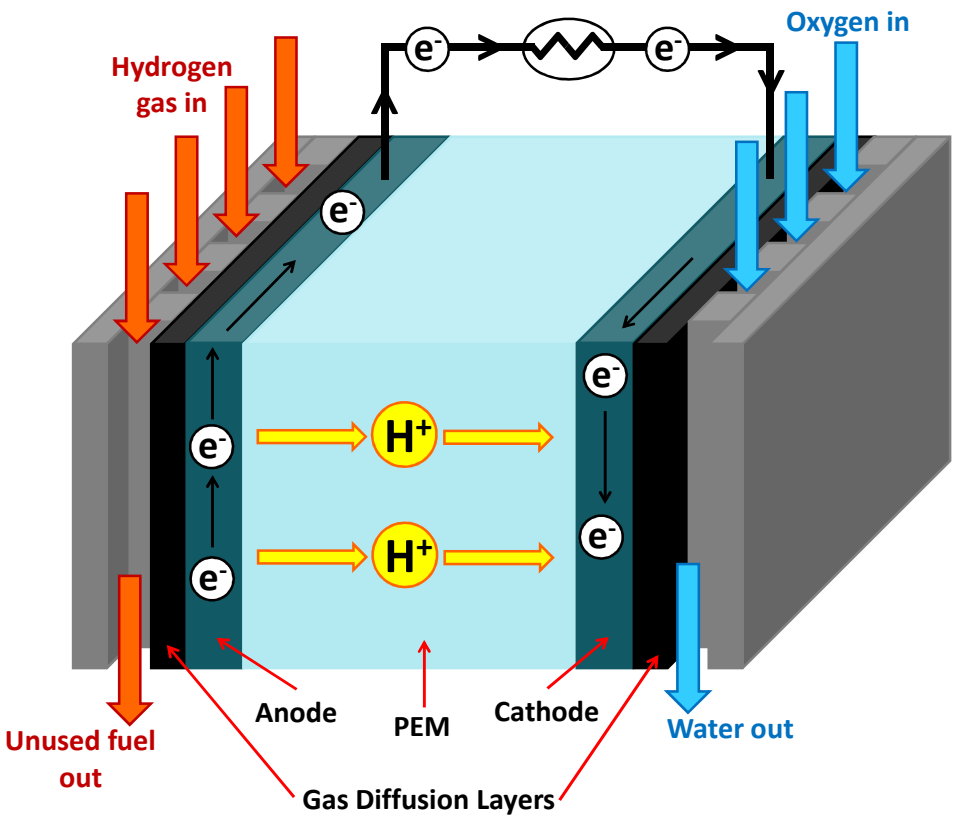

Figure 1.2.1 Schematic of fuel cell.

The diagram in Figure 1.2.1 illustrates how the different components of a fuel cell are setup. The PEM is sandwiched between the anode and the cathode which are normally constructed by using the ionomer as a binder. This also provides ionic conduction making a more favourable interface between the PEM and the electrodes. By constructing the electrode and membrane in this manner, a low resistance ionic contact that is stable with time is achieved [1]. The fuel cell converts chemical energy from the

hydrogen fuel into electrical energy. The oxidation and reduction half cell reactions can be seen respectively in Equation 1.2.1 and Equation 1.2.2, with the membrane allowing transport of protons required for the reaction to be completed.

$$\textbf{\textit{Anode}} \qquad H_2 \rightarrow 2H^+ + 2e^-$$

Equation 1.2.1

$$\textbf{\textit{Cathode}} \qquad \tfrac{1}{2}O_2 + 2H^+ + 2e^- \rightarrow H_2O$$

Equation 1.2.2

This gives the overall reaction shown in Equation 1.2.3.

$$\textbf{\textit{Overall}} \qquad H_2 + \tfrac{1}{2}O_2 \rightarrow H_2O$$

Equation 1.2.3

For each molecule of hydrogen used and each water molecule to be produced, two electrons pass around the external circuit. Therefore when one mole of hydrogen is consumed, 2*N* electrons pass around the external circuit. When –e is the charge on one electron, the charge that flows is defined by Equation 1.2.4,

$$-2Ne = -2F$$

Equation 1.2.4

where *N* is Avogadro's number and *F* is the Faraday constant or the charge on one mole of electrons.

The electrical work done to move this charge around the circuit can be defined by, Equation 1.2.5, where *E* is the voltage of the fuel cell.

$$Electrical\ work\ done = charge\ x\ voltage = -2FE$$

Equation 1.2.5

For reversible systems, or those which have no losses, the electrical work done is equal to the Gibbs free energy released, ΔG as seen in Equation 1.2.6 and rearranged to give Equation 1.2.7.

$$\Delta G = -2FE$$

Equation 1.2.6

$$E = \frac{\Delta G}{2F}$$

Equation 1.2.7

For the reaction shown in Equation 1.2.3, the Gibbs free energy is defined by Equation 1.2.8.

$$\Delta G = \sum \Delta G_{f_{products}} - \sum \Delta G_{f_{reactants}} = \Delta G_{(H_2O)} - \Delta G_{(H_2)} - \frac{1}{2}\Delta G_{(O_2)}$$

Equation 1.2.8

Each individual ΔG value can be calculated using the changes in enthalpy, ΔH, and entropy, ΔS, (Equation 1.2.9) using values which are readily available (Table 1.2.1).

$$\Delta G = \Delta H - T\Delta S$$

Equation 1.2.9

However, the Gibbs free energy of formation is not constant, changing with temperature and depending on whether the product, water, is formed in the liquid or gaseous state. Some ΔG values for the reaction in Equation 1.2.3 can be seen in Table 1.2.1

Table 1.2.1 ΔG_f values for the reaction $H_2 + {}^1/_2 O_2 \rightarrow H_2O$ at different temperatures.

Temperature / °C	ΔG_f / kJ mol^{-1}	Product state
25	-237.2	Liquid
80	-228.2	Liquid
80	-226.1	Gas
100	-225.2	Gas
200	-220.4	Gas
400	-210.3	Gas
1000	-177.4	Gas

The theoretical potential of a hydrogen/air fuel cell operating at 25 °C is calculated using Equation 1.2.7 to yield 1.229 V as shown in Equation 1.2.10.

$$E = \frac{237200}{2\,x\,96485} = 1.229\,V$$

Equation 1.2.10

While an increase in the temperature to 80 °C yields a theoretical potential of 1.185 V for liquid state product. At 80 °C with a gaseous state product, the theoretical potential is lowered to 1.171 V.

These three values are based upon true reversibility. However practically, the voltage obtained is a lot lower, usually around 0.7 V due to voltage drops caused by four main factors –

- Mass transport losses due to concentration changes in the reactants at the surface of the electrodes.
- Activation losses due to the speed of the reactions taking place on the surface of the electrodes.
- Fuel crossover through the membrane, which is normally minimal.
- Ohmic losses due to the resistance to the flow of ions in the electrolyte membrane.

The PEM directly affects two of these factors. It is assumed that there will always be a minimal amount of fuel crossover, and this only causes a significant effect at low temperatures. The key parameter is the ohmic loss due to the membrane resistance. Both the ionomer within the electrodes and the membrane itself require high water contents to achieve their optimum conductivities. This limits the operating conditions of the fuel cell to less than 100 °C so that highly humidified gases can be used. However, operating the fuel cell at temperatures around 120 °C, lowers CO poisoning of the membrane and increases the kinetics of the system, mainly at the electrodes.

The membrane must therefore be kept as thin as possible to minimise resistive losses until new membranes are found which possess a lower dependence on water content.

Research is therefore continued due to the polymers currently used having some form of flaw in either its physical, chemical or electrochemical properties. Any newly developed "*ideal membranes*" for use in a fuel cells are required to provide at least the following properties [2] -:

- High proton conductivity with zero electronic conductivity to prevent shorting.
- Low water drag.
- Chemical and physical strength.
- Tough mechanical properties.
- Low gas permeability for reduced crossover.
- Moisture control in cell stack.
- Low cost.

Any other properties will then be of additional benefit and specific for the type of fuel cell it will be used in.

1.3 Review on Polymer Electrolytes

There are a number of different categories of polymer electrolyte which are used in batteries and fuel cells that can be categorised depending on such properties as composition, additives, and ionically conducting species as described below.

1.3.1 Solvent Free Polymer Electrolytes

Solvent free polymer electrolytes have been around for many years when in the 1970's studies were first done on PEO, the structure of which is seen in Figure 1.3.1 is a typical crystalline polymer.

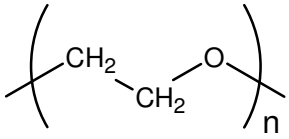

Figure 1.3.1 Structural formula of PEO.

It has a high solvating power along with high chemical and thermal stability. Due to the flexibility of PEO from the lack of double bonds, it is possible to coordinate with a number of different metal ions at the electron lone pair of the ether oxygen. It has been found that PEO was able to form coordinates with alkali metal ions and attain conductivities in the region of 1x 10^{-8} S cm^{-1} [3]. This was also reported on several years later [4] where it was found that the complexing power of PEO showed some dependency on the size of the anion. The polymers such as PEO, poly(propylene oxide) (PPO) and poly(ethylene imine) (PEI), that fall into this category are effectively high molecular weight (M_w) solvents in which the salt is dissolved into a polar polymer matrix. These solid polymer electrolytes are typically used in lithium ion batteries [5, 6] due to their conductive properties. The structure of the crystalline complexes that form between PEO and lithium salts is relatively unknown. Powder x-ray diffraction studies on PEO/LiTFSI complexes found that the PEO chains adopted a helical conformation with no interchain links [7]. There has also been interest is designing lithium salts that will be more suited for battery application. Ionic conductivity can be

enhanced by using anions that do not easily form ion-pairs. Studies have focused on non-coordinating anions that are relatively large and have significantly delocalised negative charges as they require little solvation. The electrolyte formation is expected to follow the order of soft to hard bases from left to right as shown in Scheme 1.3.1 [8].

$$F^- \ll Cl^- < I^- \sim SCN^- < ClO_4^- \sim CF_3SO_3^- < BF_4^- \sim AsF_6^-$$

Scheme 1.3.1

Synthesis of large anion lithium salts has been documented [9] and applied to PEO systems [10]. These new salts such as bis(trifluoromethane) sulfonimide lithium salt (LiTFSI) seen in Figure 1.3.2, had been found by DSC experiments to have reduced the crystalline melting point leading to a subsequent increase in conductivity due to spreading of the polymer chains within the matrix.

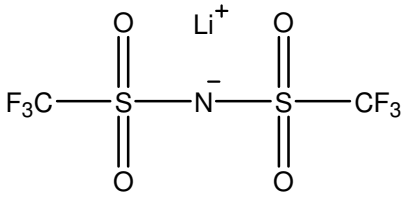

Figure 1.3.2 Structural formula of LiTFSI.

These salts possess the ability to plasticise certain crystalline polymers without the presence of a solvent. In a bid to improve the room temperature ionic conductivity of PEO with lithium salts, the use of additives in the system has been explored [11]. By partial substitution of the high M_w PEO by a lower M_w PEO, the solubility of the crystalline polymer-salt complex had been increased along with increases in the conductivity at 40 ° C to 1 x 10^{-4} S cm^{-1}. Other low M_w polymers have been added to PEO such as poly(ethylene glycol) (PEG) [12]. Whilst PEO and PEG possess the same repeat unit, PEO is synthesised from the monomer ethylene oxide *via* ring-opening polymerisation to form high M_w polymers. By contrast, PEG is synthesised from ethane-1,2-diol and polymerises *via* a condensation reaction to form polymers with generally low M_w (M_w < 20,000). Although the conductivity achievable is adequate for

battery use these low molecular weight polymer systems should realistically be grouped as gel polymer electrolytes.

1.3.2 Gel Polymer Electrolytes

This kind of polymer electrolyte may be defined as those containing a conductive additive such as a salt which is dissolved into the matrix of the polymer with the aid of a liquid solvent or plasticiser. Poly(vinylidene fluoride) (PVdF) has been used as a gel polymer electrolyte in when it was incorporated with ethylene carbonate (EC) or propylene carbonate (PC) and lithium trifluoromethanesulfonate ($LiCF_3SO_3$) [13]. The electrochemical properties were studied by impedance spectroscopy after the polymer electrolyte film had been cast and used as the separator in an electrochemical cell. Varying amounts of plasticiser and lithium salt were tested without the presence of the polymer, and the results showed that the maximum room temperature conductivity appeared at 25 % weight lithium salt. An interesting observation was in that by addition of a small amount of salt, the conductivity increased by two orders of magnitude. This was also observed by [14] who performed a more thorough investigation into the physical and mechanical properties of the polymer films with respect to their conductivity. The PVdF gels were found to favour one phase in their pure form but change to a secondary phase in the presence of the salt. Differential scanning calorimetry (DSC) experiments showed that the polymer crystallinity was only slightly reduced by the presence of salt and that conductivity values upon heating and cooling showed no hysteresis. This led to the conclusion that ionic conductivity was independent of the mechanical state of the gel. This polymer however is fully crystalline and it is assumed that no complexes are formed with lithium salts. The solvent free polymer electrolytes mentioned in the previous section such as PEO are also crystalline but are capable of forming complexes that are ionically conducting. Since ionic mobility in a non-complexing crystalline polymer requires plasticisation, a semi-crystalline or amorphous polymer should have enhanced levels of conductivity, due to the ions with their coordinated solvent having greater mobility. This has been addressed by using a copolymer of PVdF namely poly(vinylidene fluoride-co-hexafluoro propylene) (PVdF-HFP) shown in Figure 1.3.3. The hexafluoro propylene group provides an amorphous domain while the PVdF region still remains crystalline.

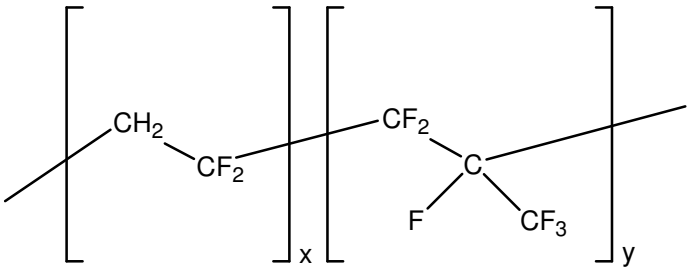

Figure 1.3.3 Structural formula of PVdF-HFP.

Alterations to the structure of PVdF-HFP have been performed using phase inversion techniques [15]. The nanoporous films that were prepared were used as a separator in a lithium ion battery that had been fabricated using a nanostructured lithium chromium manganese oxide ($LiCrMnO_4$) cathode material. The polymer was combined with a battery electrolyte, namely lithium hexafluorophosphate ($LiPF_6$) in ethylene carbonate/dimethyl carbonate (EC/DMC). It was found that the nanostructured cathode required this specific nanostructured PVdF-HFP film to enable a high retention of the specific capacity over a number of cycles.

Studies on the effects of additives on the ionic conductivity of porous PVdF-HFP membranes have also been performed [16]. A linear increase in the conductivity with increasing porosity was found, mainly due to the ability of the membrane to trap more battery electrolyte in the pores. However, the conductivity of the membrane was also affected by the additives that were used. Dibutyl phthalate (DBP), PEG, and poly(vinyl pyrrolidone) (PVP). PVP decreased the overall crystallinity of the system and provided samples with the highest ionic conductivity at 0.49 mS cm^{-1}. This shows how much of an effect structure has on the ionic conductivity. When comparing this value to samples that were prepared using conventional solution casting techniques, the porous sample has a much lower value. A number of different compositions of PVdF-HFP with lithium tetrafluoroborate ($LiBF_4$) in EC/PC were prepared [17]. The most conductive sample was found to be that with a composition of 15 wt % PVdF-HFP and 80 wt % EC/PC and 5 wt % $LiBF_4$ with a conductivity value of 6.4 mS cm^{-1}. Although the conductivity was high, other properties such as the mechanical stability of the sample suffered the low wt % of polymer.

PVdF and its co-polymers are not the only gel polymer electrolytes studied in the literature. Spectroscopic studies have been undertaken on PAN and LiTFSI complexes using PC as the plasticiser. It was revealed that a phase transition occurred in the complexes. The salt initially dissolved into the polymer with the number of acrylonitrile repeat units being 6. It was suggested however, that the polymer would then dissolve in the salt when the number of acrylonitrile units was lower at two, eliminating the majority of the crystalline domains [18, 19].

The majority of research in the area of the gel polymer electrolytes found that the higher conductivity values are only obtained when samples contain high levels of plasticiser. This means that the membranes have very poor mechanical properties and often behave more as gels than as solids. To provide additional mechanical strength to the samples, it was found that by adding succinonitrile (SN) to PAN and using a co-salt system of lithium perchlorate ($LiClO_4$) and LiTFSI, a semi-solid organic plastic electrolyte was formed [20]. In this case, even lower wt % of PAN could be used (*c.a.* 7.5 wt %), with a 92.5 wt % of LiTFSI/$LiClO_4$ in SN. When the mechanical properties were investigated, the electrolyte, LiTFSI/$LiClO_4$ in SN was said to have infinite strain with a negligibly small applied stress as Young's Modulus tended to zero. This meant that the electrolyte on its own, behaved as a liquid under applied stress. With the addition of the PAN, a dramatic change occurred in the elastic properties. The Young's Modulus was increased from approximately 0.01 to 0.4 MPa as the amount of PAN was increased. It was suggested that the inclusion of PAN had resulted in converting a semi-solid $LiClO_4$-SN to a solid system with a certain degree of elasticity.

1.3.3 Proton Conducting Polymer Electrolytes

Proton conducting polymers generally consist of an inert main chain with a functionalised pendant chain or group. It is this functionalised group that facilitates the ionic transport within the polymer matrix. When referring to proton conducting polymer electrolytes it would be normal to associate this term with such membranes as Nafion, as this was one of the first membranes to be commercialised when it was used in the Chlor-Alkali cell [21] to produce chlorine gas from the electrolysis of brine. However since this time a number of alternative polymer membranes have been and

continue to be developed. The different types of polymer used can be defined by some general categories as follows.

1.3.3.1 *Perfluorinated Proton Conducting Polymer Electrolytes*

Nafion is the most commonly known PEM in this category. The molecular structure is shown in Figure 1.3.4.

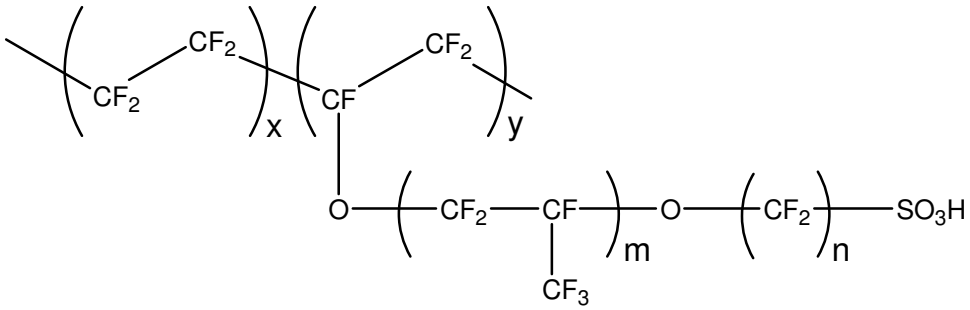

Figure 1.3.4 Structural formula of Nafion.

The structure consists of a poly(tetrafluoro ethylene) (PTFE) backbone with a pendant sidechain that is also fluorinated and terminated by a sulfonic acid group. It is precisely because the polymer is so highly fluorinated that it possesses such superior physical resistance to both oxidative and reducing environments. However the downfall of such a structure is that the degree of fluorination means the matrix is highly hydrophobic. It is only the sulfonic acid groups at the end of the chains that are hydrophilic in nature, a property which is needed for proton transport in H_2 / air fuel cells.

The earlier research into Nafion was more focused on modelling its morphology. Evidence of the behaviour of clustering was first presented in a model by Yeager [22]. This model shown in Figure 1.3.5 was also derived by considering findings of [23] who described three phases within the polymer structure that were attributed to fluorocarbon microcrystallites, ionic water clusters and a second ionic region of lower ion content.

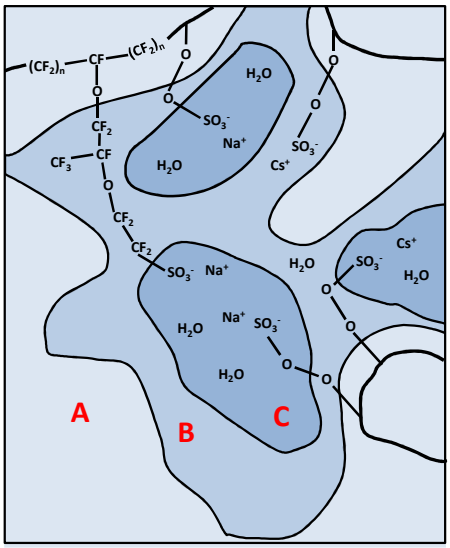

Figure 1.3.5 Three region structural model for Nafion, (A - fluorocarbon region, B - interfacial zone, C - ionic clusters) [22].

The work by [22] had concentrated on the self-diffusion coefficients for Nafion that had been ion exchanged with sodium and caesium ions. The results indicated that the cations may exist in two distinct regions, with the proportion of cations in each being dependent on ion size and charge density. The model was proposed whereby the fluorocarbon main chain would remain separate, while an interfacial region containing some pendant side chains, sulfonic acid sites and a small quantity of counter-ions and sorbed water was between that and the majority of sulfonic acid sites, sorbed water and counter-ions in the third region. This three phase Nafion system was also reported after small angle x-ray scattering (SAXS) and small angle neutron scattering (SANS) experiments with Nafion in acid and neutralised forms with varying water contents [24, 25]. Other experimental and simulation studies [26, 27] using SAXS concluded in agreement with [28] that the three phase system could be more likely described by a core of ionic clusters surrounded by a shell of fluorocarbon chains which would then be encapsulated by the intermediate ionic phase.

A few years later another model was presented for the cluster network behaviour of Nafion [29]. The Gierke Model shown in Figure 1.3.6 was an idealised model which was used as a basis for calculations and comparisons with experimental data [30].

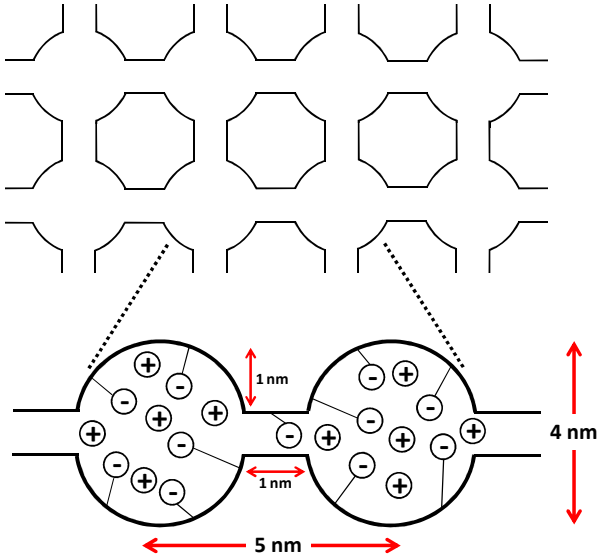

Figure 1.3.6 Schematic based on the Gierke cluster model of Nafion.

The model similarly depicts the swollen state of Nafion as an inverted micellar structure. This appears as spherical clusters of fixed sulfonic acid groups with counter-ions, in a uniform repeating manner, connected by narrow channels. The dimensional variations in cluster size were proposed to increase as the water content was increased by both expansion of cluster size and redistribution of sulfonic acid sites generating fewer clusters when the polymer was fully hydrated. The model did not include any indication of any secondary ionic phases.

Recently, the literature has seen adaptations of the aforementioned models to more fully describe the evolution of perfluorosulfonated ionomer (PFSI) membrane structure with increasing water content [31]. Using SANS and SAXS, data was obtained on the small-angle scattering maximum which was shown to shift towards a smaller angle as the water content increased. This was thought to be due to a size increase in the ionic aggregates. When the conductivity data was considered, some change was observed at water contents over 50 %. The conductivity began to decrease until the membrane was so highly swollen that it was considered to behave as a solution. At the point the conductivity had begun to decrease, the ionic clusters were deemed to have reached their maximum swelling point and a further structural change where the ionic groups were diluted had occurred. From this point the structure was defined as being in rod like structures as seen in Figure 1.3.7.

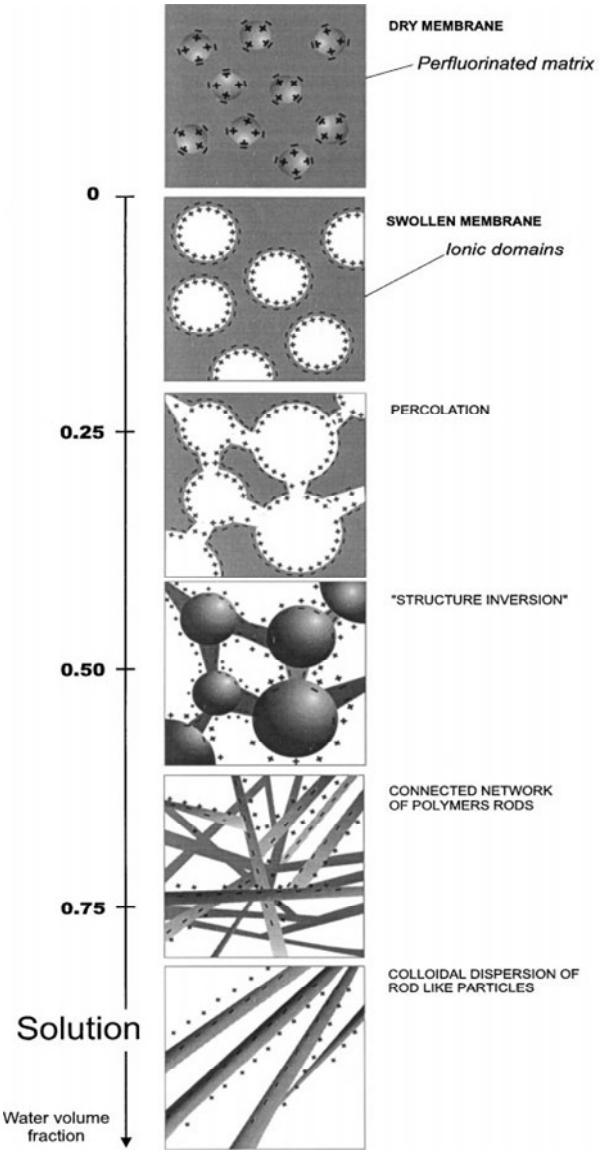

Figure 1.3.7 Gebel representation of PFSI structure with increasing water content [31].

Since Nafion has been considered to be the prototype material for use in PEM fuel cells there has been no shortage of research into not only structural properties but other physical, chemical and electrochemical behaviour. In particular, the conductivity is of great interest and has been well documented in the literature. There is however some ambiguity pertaining to the actual value due to various methods of measurement and experimental conditions. Due to this it is often difficult to make direct comparisons between literature values. Some of the results in the literature have been compiled and can be seen in Table 1.3.1.

Table 1.3.1 Comparison of conductivity measurements of Nafion membranes.

Nafion membrane	Electrolyte	Temperature (° C)	Electrode configuration	Conductivity direction	Conductivity (S cm^{-1})	Ref.
117	Water vapour (100 %)	30	2 x stainless steel	Through plane	0.0178	[32]
117	Water vapour (100 %)	90	2 x stainless steel	Through plane	0.0224	[32]
117	Water vapour (100 %)	100	2 x stainless steel	Through plane	0.0251	[32]
117	Immersed in H_2O	80	2 x stainless steel	Through plane	0.08	[33]
117	Water vapour (100 %)	25	2 x wire	In plane	0.09	[34]
117	Water vapour (100 %)	25	Co-axial probe	Through plane	0.024	[35]
117	Water vapour (100 %)	25	Co-axial probe	In plane	0.086	[35]
117	Water vapour (80 %)	25	Co-axial probe	In plane	0.00618	[36]
117	Water vapour (93 %)	25	Co-axial probe	In plane	0.0136	[36]
117	Water vapour (100 %)	25	Co-axial probe	In plane	0.0661	[36]
117	Water vapour (95 %)	80	2 x wire	In plane	0.021	[37]
115	Water vapour (95 %)	80	2 x wire	In plane	0.037	[37]
112	Water vapour (95 %)	80	2 x wire	In plane	0.055	[37]
117	Water vapour (95 %)	80	4 x wire	In plane	0.075	[37]
115	Water vapour (95 %)	80	4 x wire	In plane	0.094	[37]
112	Water vapour (95 %)	80	4 x wire	In plane	0.115	[37]
117	Immersed in H_2O	30	2 x electrode	Through plane	0.1	[38, 39]

In addition to the information in Table 1.3.1, there have been other reports of high conductivity values of Nafion 117. However the experiments utilised an acid electrolyte as opposed to water [40-43]. Since the conductivity of the acid itself is greater than the membrane could achieve, analysing the results as a comparison is of no true value.

A number of other companies have processed similar perfluorosulfonate (PFS) polymers based on Nafion with differing ratios of chain lengths [44]. Based generally on the structure seen in Figure 1.3.4 the variations can be seen in Table 1.3.2.

Table 1.3.2 Commercial perfluorosulfonate polymers with specific chain lengths.

	Chain length			
Commercial Polymers	**x**	**y**	**m**	**n**
Nafion® (DuPont)	5 – 13.5	1	1	2
Flemion® (Asahi Glass)	5 – 13.5	1	0.1	1 – 5
Aciplex® (Asahi Chemicals)	1.5 – 15	1	0	2 – 5
Dow® (Dow Chemicals)	3.6 – 10	1	0	2
Hyflon® (Solvay Solexis)	6.5	1	0	2
3M® Membrane	x	y	0	4

The exclusion of the CF_3 group in both Hyflon and 3M membranes has produced a polymer that has a much higher T_g than Nafion, enhanced oxidative stability, higher conductivity at lower equivalent weights and improved mechanical properties at hot and dry conditions [45]. The Dow membrane with a shortened side chain has been found to perform better in PEM fuel cells. The range of Dow membranes has been found to

possess lower solvent transport with regards to water and methanol in direct methanol fuel cells, as a result of reduced swelling properties [46]. It has been anticipated that by combining a high ion-exchange capacity (IEC) with increased crystallinity, an increase in proton conductivity and preservation of the morphology of the membrane occurs.

Included in this category of membranes, is a subset of partially fluorinated polymer membranes. Ballard Advanced Materials (BAM) has produced a PTFE styrene derivative membrane seen in Figure 1.3.8.

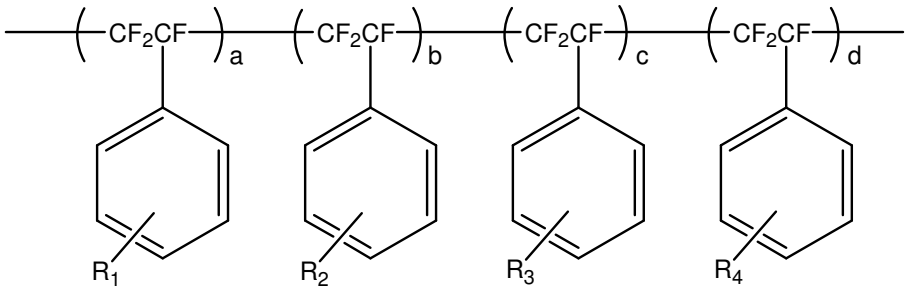

Figure 1.3.8 Structural formula of BAM membrane.

This membrane possesses good thermal, mechanical and chemical resistance properties as it retains the fluorinated backbone, and the pendent styrene groups can easy be functionalised by simple organic reactions. The process of adding a functional group is necessary in order to change the polymer from an insulator to an ionic conductor by the addition of a sulfonic acid group for example. A similar membrane has been synthesised by electron beam irradiation of PVdF polymer films followed by styrene graft polymerisation and sulfonation [47]. This also keeps the desirable properties associated with a fluorinated polymer backbone, but has a secondary layer that can easily be functionalised. In this case a much higher ion exchange capacity can be achieved due to the number of styrene groups present.

1.3.3.2 Non-fluorinated Proton Conducting Polymer Electrolytes

This category contains new membranes such as aromatic polymers namely poly(ether ether ketone) (PEEK), poly(sulfone) (PSU), along with some high performance polymers such as poly(benzimidazole) (PBI) seen in Figure 1.3.9.

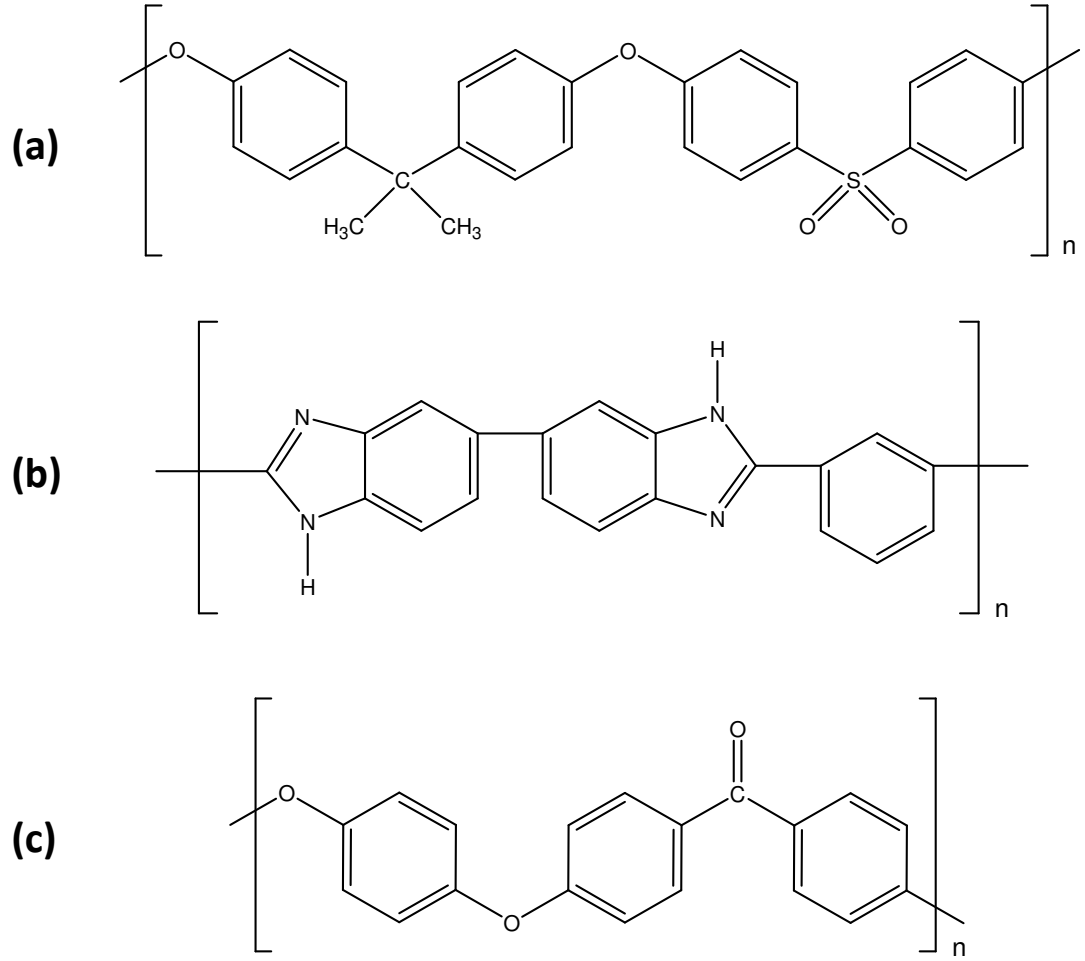

Figure 1.3.9 Structural formulae of some sulfonated proton conducting polymers, (a) PSU, (b) PBI, (c) PEEK.

These membranes are hoped to be used for higher temperature fuel cells, and similarly to the BAM membrane, these polymers need a functional group that will facilitate ionic conduction. The simplest method of doing this has been to sulfonate one of the benzene rings. In the case of PSU, the sulfone unit was added to the monomer unit before the polymerisation step [48] , and this has also been reported as a method for synthesising sulfonated-PEEK (SPEEK) [49, 50]. It was reported that this method of sulfonation is

suitable for all polymer which form soluble lithium salts and that the sulfonic acid group is introduced in the more hydrolysis stable part of the arylene polymer system [51]. By contrast the literature has many references to post sulfonation of a polymer unit. Similarly to the BAM membranes mentioned in the previous section, the sulfonic acid group is introduced to a benzene ring in the polymer chain as performed with PEEK [52-55]. The benefit of these aromatic membranes is the high compatibility they have when different polymers are combined within a system. SPEEK has been blended with poly(phenylsulfone) (PPSU) in order to control the physicochemical characteristics of SPEEK. The blends were found to have increased and stable conductivity up to temperatures of 120 °C [56]. Alternative work on SPEEK and PBI blends found that structures of composite membranes became more compact than that of SPEEK. This was documented to be due to the acid-base interaction between the sulfonic acid groups and amine groups, which could lead to the increase of mechanical properties and the reduction of excess swelling. The performances of the composite membranes were characterised and showed that the proton conductivity of the composite membranes was dependent on PBI content. The thermal stabilities, mechanical properties and swelling properties of the SPEEK membranes was improved greatly, with only moderate increases in the ion-exchange capacity [57]. Similar property changes have also been found for numerous other acid-base blended membranes [58].

1.3.3.3 Composite Membranes

The membranes aforementioned that have been synthesised and documented in literature, not excluding commercial membranes all possess some property detrimental to their performance. Similarly to $LiClO_4$/LiTFSI in SN samples mentioned previously, where PAN was added to provide additional mechanical integrity, proton conducting polymers have been modified to enhance different physical properties.

Experimental work has been performed in synthesising membranes containing silicates and layered metal phosphates in an attempt to reduce the water dependence of fluorinated membranes [59]. Later studies on composite membranes of zironcium phosphate and Nafion [60] found that samples with metal phosphates were able to

obtain the same conductivities as standard membranes but with a lower water activity. The addition of these inorganic additives often does provide a degree of mechanical stability to the membranes, but unless the additive facilitates proton conduction, the mass of active material for example the ion-exchange capacity. Titanates and silicates have been added to a number of membranes [61-63] with some beneficial effects, but higher conductivities and mechanical stability have been found with acid-base inorganic additives [64].

1.3.3.4 *Conduction Mechanisms*

Electrical conductivity occurs in polymer electrolytes due to the motion of ionic charge which is dependent on ionic mobility. In lithium batteries, the lithium ions move through the electrolyte as the ionic species. In fuel cells, specifically PEM, it is hydrogen ions that are the ionic species. Proton mobility in water is relatively high compared with other cations [65]. The explanation has been documented in terms of proton hopping between water molecules as defined by the *Grotthus* mechanism [66] and shown in Figure 1.3.10.

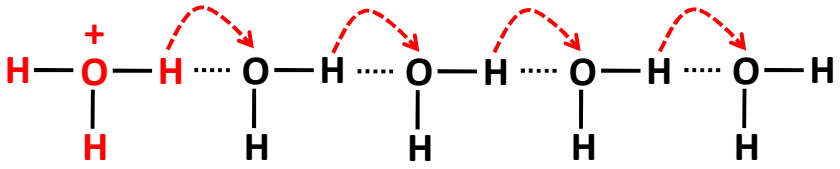

Figure 1.3.10 Schematic representation of the proton hopping process.

The exact details of the mechanism are still being debated but recently it has been proposed that two hydrated proton species namely the Zundel ($H_5O_2^+$) and Eigen cations ($H_9O_4^+$) seen in Figure 1.3.11 are favoured in aqueous solutions [67] and that in liquid solutions a continuous dynamical exchange exists between all configurations of ions [68-70].

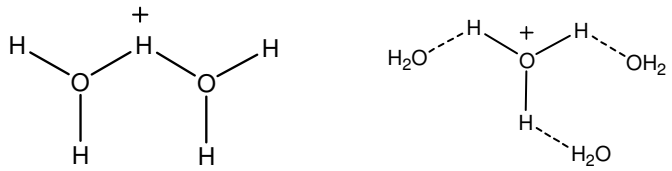

(a) (b)

Figure 1.3.11 Structure of (a) Zundel and (b) Eigen cations.

In polymer membranes that have pendent sulfonic acid groups (SO_3H), the proton has the ability to dissociate to leave an ionised sulfonate group (SO_3^-), and in the presence of water, these protons would be strongly associated with the water molecules. Polymer membranes with sulfonate groups can be considered to follow the aqueous conditions as the nature of the functional groups makes it highly acidic. Predominantly, the mechanism would occur via on of two further suggested mechanisms. Firstly, the Zundel and Eigen cations would act as the main transporters from one hydronium ion (H_3O^+) to the next. Secondly, using the time constants for proton hopping from experimental nuclear magnetic resonance (NMR) data, the hopping mechanism would proceed via an Eigen to Zundel to Eigen process [71]. This was determined after it was revealed through computational mechanics that the cation begins in the Eigen state and then transforms to the Zundel state as the transfer of the proton occurs.

1.4 Review on Combinatorial and High-throughput methods

Combinatorial methods have been used in the pharmaceutical industry over the past few decades. One of the first detailed methods was that of rapid concurrent synthesis of a large number of peptides on solid polymer supports which would hopefully be antibody specific [72]. The technique was then further developed a few years later [73] for similar compounds. This method enabled much larger numbers of products to be synthesised which in turn leads to a greater chance of finding desirable compounds. The specifics of the method are detailed in Figure 1.4.1 whereby a "split and pool" synthesis method is used. This involves simple division and recombination to generate the large numbers of unique compounds in a single reaction vessel. Organic chemistry has been up until recently the main branch of science that has utilised the methodology. However, the techniques are quickly being adapted to suit other material types and most materials sciences have adopted some form of combinatorial practices.

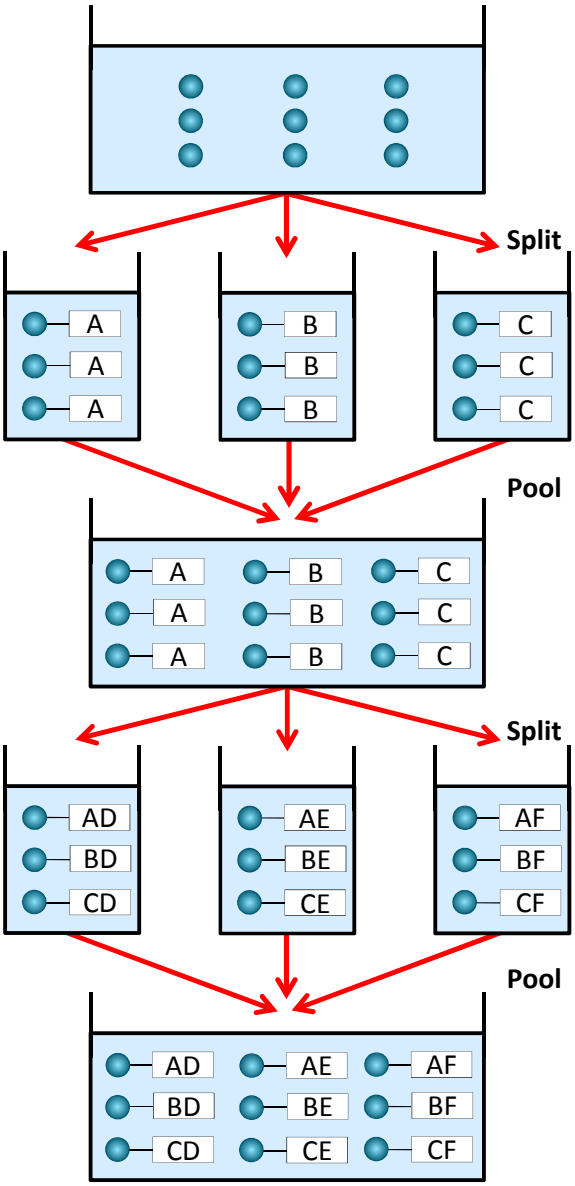

Figure 1.4.1 Flow chart depicting a combinatorial synthesis method.

The terms combinatorial and high-throughput are often used interchangeably, but for clarity, combinatorial should only describe the simultaneous preparation and analysis of samples within a single vessel as shown in Figure 1.4.1. The term high-throughput describes synthesis or characterisation that is performed in parallel or very quickly. Some of the more recent examples of combinatorial and high-throughput materials that have been explored can be seen in Table 1.4.1.

Table 1.4.1 A brief example of some materials that have been studied using combinatorial and high-throughput techniques.

Material Type	Reference
Complex fluids - rheology	[74]
Direct Methanol Fuel Cells	[75]
Electrocatalysts	[76]
Enantioselective catalysts	[77]
Electropolymerisation	[78]
Fuel cell anodes	[79]
Hydrogen storage	[80]
Gas sensors	[81]
Lithium batteries – negative electrodes	[82, 83]
Lithium batteries – positive electrodes	[84-86]
Luminescent inorganic oxides	[87, 88]
Magnetoresistive compounds	[89]
Organic – supported catalysts	[90]
Polymer biomaterials	[91]
Polymers– design	[92]
Polymers – solubility	[93]
Polymers - thickness	[94]
Reactive dyes – catalysts	[95]
Solar cells – thin film	[96]
Zeolite - films	[97]

Although it can be seen in Table 1.4.1 that there are numerous references to combinatorial and high-throughput methods being used in polymer synthesis, and also battery and fuel cell materials, the literature has yet to show any indications that a study on an amalgamation of the two has been done.

1.5 Aims of This Project

As mentioned in the previous section, literature studies when starting this project found that no data was held pertaining to high-throughput or combinatorial studies of polymer electrolytes for battery and fuel cell use. It can often be difficult to perform syntheses of polymer electrolytes and equally problematic performing accurate electrochemical measurements on them. Therefore, scaling to multiple samples may be a daunting prospect with no prior knowledge of combinatorial and high-throughput methods.

The work in this project aimed to use research methods in the literature for other materials to assist in the work, but also develop new ones which would be specific for the synthesis and characterisation of polymer electrolytes for battery and fuel cell applications.

The first part of the research was to investigate known lithium-ion polymer electrolytes, namely PVdF-HFP with a lithium salt and plasticiser. An established high-throughput technique would be adapted to this system with verification of the method.

The second aim was to study a proton conducting system, in which a parallel synthesis step would be introduced to allow compositional variations of the samples. A completely novel electrochemical cell and measurement method would also be designed in order that the conductivity of the samples could be measured while varying the temperature and relative humidity. It is anticipated that this will allow real time effects of environmental conditions on the polymer electrolytes to be investigated.

1.6 Chapter 1 References

1. T. Zawodzinski, *Electrolytes for Fuel Cells*, Fuel Cell Workshop Presentation, Los Alamos National Laboratory, 2001.

2. B. Smitha, S. Sridhar and A. A. Khan, *Journal of Membrane Science*, 2005, **259**, 10-26.

3. D. E. Fenton, J. M. Parker and P. V. Wright, *Polymer*, 1973, **14**, 589-589.

4. J. M. C. M.B. Armand, M. Duclot, , 2nd International Meeting on Solid Electrolytes, St. Andrews, Scotland, 1978.

5. F. Croce, L. Settimi, B. Scrosati and D. Zane, *Journal of New Materials for Electrochemical Systems*, 2006, **9**, 3-9.

6. S. Passerini, G. B. Appetecchi, P. Villano, M. Carewska and M. G. Puppo, *Batteries and Supercapacitors*, 2003, 529-534.

7. P. Lightfoot, M. A. Mehta and P. G. Bruce, *Science*, 1993, **262**, 883-885.

8. F. M. Gray, in *RSC Materials Monographs*, ed. J. A. Conner, The Royal Society of Chemistry, Cambridge, 1997, p. 12.

9. M. Armand, W. Gorecki and R. Andreani, in *Second International Symposium on Polymer Electrolytes*, ed. B. Scrosati, Elsevier, London, 1990, p. 91.

10. D. Benrabah, D. Baril, J. Y. Sanchez, M. Armand and G. G. Gard, *Journal of the Chemical Society-Faraday Transactions*, 1993, **89**, 355-359.

11. I. E. Kelly, J. R. Owen and B. C. H. Steele, *Journal of Power Sources*, 1985, **14**, 13-21.

12. Y. Ito, K. Kanehori, K. Miyauchi and T. Kudo, *Journal of Materials Science*, 1987, **22**, 1845-1849.

13. N. S. Mohamed and A. K. Arof, *Journal of Power Sources*, 2004, **132**, 229-234.

14. A. M. Voice, G. R. Davies and I. M. Ward, *Polymer Gels and Networks*, 1997, **5**, 123-144.

15. A. Manuel Stephan and D. Teeters, *Electrochimica Acta*, 2003, **48**, 2143-2148.

16. J.-H. Cao, B.-K. Zhu and Y.-Y. Xu, *Journal of Membrane Science*, 2006, **281**, 446-453.

17. P. Periasamy, K. Tatsumi, M. Shikano, T. Fujieda, Y. Saito, T. Sakai, M. Mizuhata, A. Kajinami and S. Deki, *Journal of Power Sources*, 2000, **88**, 269-273.

18. J. Z. Li, X. J. Huang and L. Q. Chen, *Journal of The Electrochemical Society*, 2000, **147**, 2653-2657.

19. Z. X. Wang, W. D. Gao, X. J. Huang, Y. J. Mo and L. Q. Chen, *Electrochemical and Solid State Letters*, 2001, **4**, A132-A135.

20. M. Patel, K. G. Chandrappa and A. J. Bhattacharyya, *Electrochimica Acta*, 2008, **54**, 209-215.

21. R. S. Yeo and J. McBreen, *Journal of The Electrochemical Society*, 1979, **126**, 1682-1687.

22. H. L. Yeager and A. Steck, *Journal of The Electrochemical Society*, 1981, **128**, 1880-1884.

23. R. Duplessix, M. Escoubez, B. Rodmacq, F. Volino, E. Roche, A. Eisenberg and M. Pineri, *Abstracts of Papers of the American Chemical Society*, 1979, 19-19.

24. E. J. Roche, M. Pineri, R. Duplessix and A. M. Levelut, *Journal of Polymer Science Part B-Polymer Physics*, 1981, **19**, 1-11.

25. E. J. Roche, M. Pineri and R. Duplessix, *Journal of Polymer Science Part B-Polymer Physics*, 1982, **20**, 107-116.

26. M. Fujimura, T. Hashimoto and H. Kawai, *Macromolecules*, 1981, **14**, 1309-1315.

27. M. Fujimura, T. Hashimoto and H. Kawai, *Macromolecules*, 1982, **15**, 136-144.

28. E. J. Roche, R. S. Stein, T. P. Russell and W. J. Macknight, *Journal of Polymer Science Part B-Polymer Physics*, 1980, **18**, 1497-1512.

29. W. Y. Hsu and T. D. Gierke, *Journal of Membrane Science*, 1983, **13**, 307-326.

30. T. A. Davies, J. D. Genders and D. Pletcher, The Electrochemical Consultancy, Romsey, UK, 1997, p. 69.

31. G. Gebel, *Polymer*, 2000, **41**, 5829-5838.

32. A. K. Sahu, G. Selvarani, S. Pitchumani, P. Sridhar, A. K. Shukla, N. Narayanan, A. Banerjee and N. Chandrakumar, *Journal of The Electrochemical Society*, 2008, **155**, B686-B695.

33. S. L. Zhong, X. J. Cui, T. Z. Fu and H. Na, *Journal of Power Sources*, 2008, **180**, 23-28.

34. A. Siu, J. Schmeisser and S. Holdcroft, *Journal of Physical Chemistry B*, 2006, **110**, 6072-6080.

35. C. L. Gardner and A. V. Anantaraman, *Journal of Electroanalytical Chemistry*, 1998, **449**, 209-214.

36. A. V. Anantaraman and C. L. Gardner, *Journal of Electroanalytical Chemistry*, 1996, **414**, 115-120.

37. C. H. Lee, H. B. Park, Y. M. Lee and R. D. Lee, *Industrial & Engineering Chemistry Research*, 2005, **44**, 7617-7626.

38. DuPont, *Nafion Membranes, Extrusion-Cast Technical Information*, http://www2.dupont.com/Fuel_Cells/en_US/assets/downloads/dfc101.pdf.

39. T. A. Zawodzinski, M. Neeman, L. O. Sillerud and S. Gottesfeld, *Journal of Physical Chemistry*, 1991, **95**, 6040-6044.

40. M. Yoshitake, M. Tamura, N. Yoshida and T. Ishisaki, *Denki Kagaku*, 1996, **64**, 727-736.

41. N. Yoshida, T. Ishisaki, A. Watakabe and M. Yoshitake, *Electrochimica Acta*, 1998, **43**, 3749-3754.

42. M. W. Verbrugge, E. W. Schneider, R. S. Conell and R. F. Hill, *Journal of The Electrochemical Society*, 1992, **139**, 3421-3428.

43. M. W. Verbrugge and R. F. Hill, *Journal of The Electrochemical Society*, 1990, **137**, 3770-3777.

44. M. Ulbricht, *Polymer*, 2006, **47**, 2217-2262.

45. A. Graichen, *3M Brennstoffzellen Technologie*, http://www.fuelcell-nrw.de/fileadmin/daten/jahrestreffen/Vortraege/15-Graichen-3M.pdf.

46. K. D. Kreuer, M. Schuster, B. Obliers, O. Diat, U. Traub, A. Fuchs, U. Klock, S. J. Paddison and J. Maier, *Journal of Power Sources*, 2008, **178**, 499-509.

47. S. D. Flint and R. C. T. Slade, *Solid State Ionics*, 1997, **97**, 299-307.

48. J. A. Kerres and A. J. Van Zyl, *Journal of Applied Polymer Science*, 1999, **74**, 428-438.

49. X. Li, Z. Wang, H. Lu, C. Zhao, H. Na and C. Zhao, *Journal of Membrane Science*, 2005, **254**, 147-155.

50. C. Zhao, X. Li, Z. Wang, Z. Dou, S. Zhong and H. Na, *Journal of Membrane Science*, 2006, **280**, 643-650.

51. J. Kerres, W. Cui and S. Reichle, *Journal of Polymer Science Part a-Polymer Chemistry*, 1996, **34**, 2421-2438.

52. S. Kaliaguine, S. D. Mikhailenko, K. P. Wang, P. Xing, G. Robertson and M. Guiver, *Catalysis Today*, 2003, **82**, 213-222.

53. X. F. Li, C. P. Liu, H. Lu, C. J. Zhao, Z. Wang, W. Xing and H. Na, *Journal of Membrane Science*, 2005, **255**, 149-155.

54. S. M. J. Zaidi, S. D. Mikhailenko and S. Kaliaguine, *New Materials for Electrochemical Systems IV. Extended Abstracts of the Fourth International Symposium on New Materials for Electrochemical Systems*, 2001, 315-316.

55. S. M. J. Zaidi, S. D. Mikhailenko, G. P. Robertson, M. D. Guiver and S. Kaliaguine, *Journal of Membrane Science*, 2000, **173**, 17-34.

56. M. L. Di Vona, A. D'Epifanio, D. Marani, M. Trombetta, E. Traversa and S. Licoccia, *Journal of Membrane Science*, 2006, **279**, 186-191.

57. H. Zhang, X. Li, C. Zhao, T. Fu, Y. Shi and H. Na, *Journal of Membrane Science*, 2008, **308**, 66-74.

58. A. U. J. Kerres, Th. Haring, M. Baldauf, U. Gebhardt, W. Preidel, *Journal of New Materials for Electrochemical Systems*, 2000, **3**, 129-239.

59. G. Alberti and M. Casciola, *Annual Review of Materials Research*, 2003, **33**, 129-154.

60. F. Bauer and M. Willert-Porada, *Solid State Ionics*, 2006, **177**, 2391-2396.

61. M. L. Di Vona, Z. Ahmed, S. Bellitto, A. Lenci, E. Traversa and S. Licoccia, *Journal of Membrane Science*, 2007, **296**, 156-161.

62. S. Licoccia, M. L. Di Vona, A. D'Epifanio, Z. Ahmed, S. Bellitto, D. Marani, B. Mecheri, C. de Bonis, M. Trombetta and E. Traversa, *Journal of Power Sources*, 2007, **167**, 79-83.

63. A. Sacca, A. Carbone, E. Passalacqua, A. D'Epifanio, S. Licoccia, E. Traversa, E. Sala, F. Traini and R. Ornelas, *Journal of Power Sources*, 2005, **152**, 16-21.

64. R. K. Nagarale, G. S. Gohil, V. K. Shahi and R. Rangarajan, *Macromolecules*, 2004, **37**, 10023-10030.

65. M. Kunst and J. M. Warman, *Nature*, 1980, **288**, 465-467.

66. C. J. D. Grotthuss, *Ann. Chim. LVIII*, 1806, 54-73.

67. O. F. Mohammed, D. Pines, J. Dreyer, E. Pines and E. T. J. Nibbering, *Science*, 2005, **310**, 83-86.

68. H. Lapid, N. Agmon, M. K. Petersen and G. A. Voth, *Journal of Chemical Physics*, 2005, **122**, -.

69. D. Marx, M. E. Tuckerman, J. Hutter and M. Parrinello, *Nature*, 1999, **397**, 601-604.

70. R. Vuilleumier and D. Borgis, *Journal of Chemical Physics*, 1999, **111**, 4251-4266.

71. N. Agmon, *Chemical Physics Letters*, 1995, **244**, 456-462.

72. H. M. Geysen, R. H. Meloen and S. J. Barteling, *Proceedings of the National Academy of Sciences of the United States of America-Biological Sciences*, 1984, **81**, 3998-4002.

73. H. M. Geysen, S. J. Rodda and T. J. Mason, *Molecular Immunology*, 1986, **23**, 709-715.

74. V. Breedveld and D. J. Pine, *Journal of Materials Science*, 2003, **38**, 4461-4470.

75. R. Z. Jiang, C. Rong and D. Chu, *Journal of Combinatorial Chemistry*, 2005, **7**, 272-278.

76. E. Reddington, A. Sapienza, B. Gurau, R. Viswanathan, S. Sarangapani, E. S. Smotkin and T. E. Mallouk, *Science*, 1998, **280**, 1735-1737.

77. M. T. Reetz, M. H. Becker, K. M. Kuhling and A. Holzwarth, *Angewandte Chemie-International Edition*, 1998, **37**, 2647-2650.

78. V. Kulikov and V. M. Mirsky, *Measurement Science & Technology*, 2004, **15**, 49-54.

79. P. Strasser, Q. Fan, M. Devenney, W. H. Weinberg, P. Liu and J. K. Norskov, *Journal of Physical Chemistry B*, 2003, **107**, 11013-11021.

80. C. H. Olk, *Measurement Science & Technology*, 2005, **16**, 14-20.

81. U. Simon, D. Sanders, J. Jockel and T. Brinz, *Journal of Combinatorial Chemistry*, 2005, **7**, 682-687.

82. J. R. Dahn, R. E. Mar and A. Abouzeid, *Journal of The Electrochemical Society*, 2006, **153**, A361-A365.

83. M. D. Fleischauer, T. D. Hatchard, A. Bonakdarpour and J. R. Dahn, *Measurement Science & Technology*, 2005, **16**, 212-220.

84. M. R. Roberts, A. D. Spong, G. Vitins and J. R. Owen, *Journal of The Electrochemical Society*, 2007, **154**, A921-A928.

85. M. R. Roberts, G. Vitins and J. R. Owen, *Journal of Power Sources*, 2008, **179**, 754-762.

86. A. D. Spong, G. Vitins, S. Guerin, B. E. Hayden, A. E. Russell and J. R. Owen, *Journal of Power Sources*, 2003, **119**, 778-783.

87. E. Danielson, M. Devenney, D. M. Giaquinta, J. H. Golden, R. C. Haushalter, E. W. McFarland, D. M. Poojary, C. M. Reaves, W. H. Weinberg and X. D. Wu, *Science*, 1998, **279**, 837-839.

88. E. Danielson, M. Devenney, D. M. Giaquinta, J. H. Golden, R. G. Haushalter, E. W. McFarland, D. M. Poojary, C. M. Reaves, W. H. Weinberg and X. Di Wu, *Journal of Molecular Structure*, 1998, **470**, 229-235.

89. G. Briceno, H. Y. Chang, X. D. Sun, P. G. Schultz and X. D. Xiang, *Science*, 1995, **270**, 273-275.

90. S. Kobayashi and R. Akiyama, *Pure and Applied Chemistry*, 2001, **73**, 1103-1111.

91. S. Brocchini, K. S. James, V. Tangpasuthadol and J. Kohn, *Abstracts of Papers of the American Chemical Society*, 1997, **213**, 257-BIOT.

92. S. Brocchini, K. James, V. Tangpasuthadol and J. Kohn, *Journal of the American Chemical Society*, 1997, **119**, 4553-4554.

93. C. L. Bray, B. Tan, C. D. Wood and A. I. Cooper, *Journal of Materials Chemistry*, 2005, **15**, 456-459.

94. J. C. Grunlan, A. R. Mehrabi and T. Ly, *Measurement Science & Technology*, 2005, **16**, 153-161.

95. A. C. Cooper, L. H. McAlexander, D. H. Lee, M. T. Torres and R. H. Crabtree, *Journal of the American Chemical Society*, 1998, **120**, 9971-9972.

96. H. Hansel, H. Zettl, G. Krausch, C. Schmitz, R. Kisselev, M. Thelakkat and H. W. Schmidt, *Applied Physics Letters*, 2002, **81**, 2106-2108.

97. R. Lai, B. S. Kang and G. R. Gavalas, *Angewandte Chemie-International Edition*, 2001, **40**, 408-411.

Chapter 2

AC Impedance as a Method for Studying Polymer Electrolytes

Chapter 2 AC Impedance as a Method for Studying Polymer Electrolytes

2.1 Introduction

In the late 18th and early 19th centuries, initial findings relating to the electrical properties of materials were released in the scientific world. It is over this timescale that impedance spectroscopy has developed to the methods that we now use today. Even since early studies on electrode interfaces and electrolyte resistances [1], there is still contributions to be made to advance the techniques further.

The electrical behaviour of all materials can be described by its conductance, *G*, which is the reciprocal of the resistance, *R* (Equation 2.1.1).

$$G = \frac{1}{R} = \frac{I}{V}$$

Equation 2.1.1

Conductance in metals provides charge movement due to electrons, while conductance in electrolytes is due to the motion of ionic charge which is dependent on ionic mobility. In a solid material such as a polymer electrolyte, the conductance reflects the ability of ions within the system to conduct electricity whilst behaving in a manner normally associated with liquid systems. The conductance follows that of *Ohm's Law* when the material is purely resistive and not a complex system. The conductance of a cross sectional object can be defined by Equation 2.1.2,

$$G = \frac{\sigma A}{l}$$

Equation 2.1.2

where *A* is the cross sectional area and *l* is the distance between the electrodes.

To find the resistance and conductivity of ionically conducting materials, alternating current (AC) methods such as AC Impedance may be used to overcome problems arising from the electrode-electrolyte interface.

2.2 AC Impedance Principles

AC Impedance is a method of characterising a number of different electrical properties of a material. Direct current (DC) measurements work well with ohmic systems such as purely electronic conductors, but offer limited detail about ionically conducting system. The AC method is required to avoid effects of polarisation at the electrode-electrolyte interface, provide data on the long-range migration of ions and also grain boundary effects. It has been well documented for the measurement of solid state materials [2, 3] and in particular with regards to polymer electrolytes [4, 5].

The principle of impedance is that a sinusoidal voltage is applied to a cell and the sinusoidal current passing through the cell as a result is measured. The sinusoidal voltage can be defined as by Equation 2.2.1,

$$E = \Delta E \sin \omega t$$

Equation 2.2.1

where *E* is the potential value, *ΔE* is the amplitude and *ω* is the angular frequency.

The angular frequency, ω, is equal to $2\pi f$ (where *f* is the sinusoidal frequency measured in Hz). The current that is measured, *I,* will be in phase with *E* in the case of ohmic systems, however it may out of phase with the potential by an angle θ as defined in Equation 2.2.2.

$$I = \Delta I \sin(\omega t + \theta)$$

Equation 2.2.2

This phase shift may be seen in Figure 2.2.1.

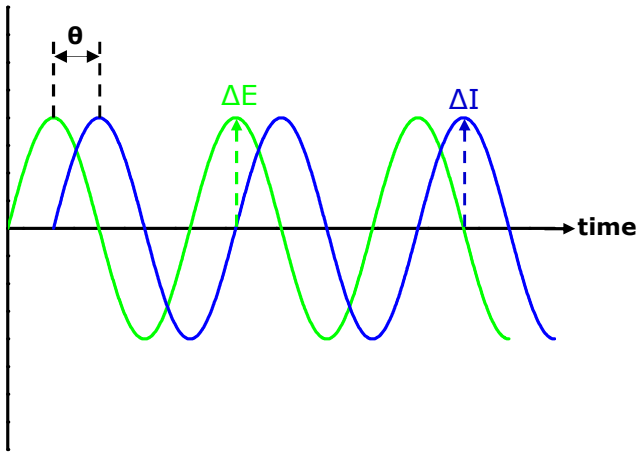

Figure 2.2.1 Sinusoidal voltage and phase-shifted current.

Using Equation 2.2.1 and Equation 2.2.2, an impedance, Z, can be defined analogously to the resistance of D.C. measurements. The magnitude of the impedance is defined by Equation 2.2.3, where both the phase angle and the magnitude of the impedance are both functions of the applied frequency.

$$|Z| = \frac{|\Delta E|}{|\Delta I|} = |Z(\omega)| = \frac{|\Delta E(\omega)|}{|\Delta I(\omega)|}$$

Equation 2.2.3

This frequency dependent behaviour of an impedance is the reason that further information may be obtained about different electrical properties of a sample or cell.

The impedance of a cell can be defined as a vector quantity, since it has both magnitude and phase. On a vector diagram, there is a separate point for each frequency that is

measured. The phase angle for each point is the angle of the vector from the origin to each point relative to the x-axis, which corresponds to the phase difference between E and *I*. The distance from each point to the origin relates to the magnitude of the impedance. A representation of such a vector diagram can be seen in Figure 2.2.2 which is commonly termed a complex plane or Nyquist plot as it is similar to the representation of a complex number.

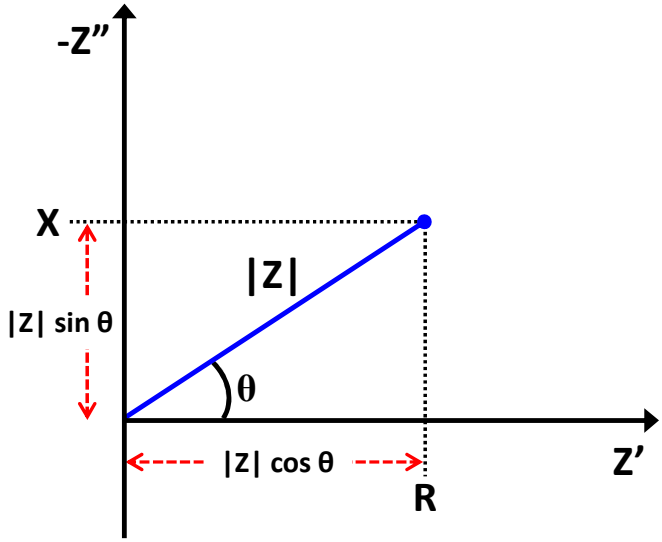

Figure 2.2.2 Representative Argand diagram showing the impedance of a sample.

Here, the real part of the impedance, *Z’*, may be defined purely as the resistance, *R*, where there is no phase shift between the current and the voltage. The imaginary part of the impedance can be defined as the reactance, *X*, which induces a phase shift of -90 ° between the voltage and current. The complex impedance of a sample, *Z**, is represented by the sum of both the real and imaginary parts (Equation 2.2.4) inclusive of the complex number operator, *j*, which has the value of √-1.

$$Z^* = Z' + jZ''$$

Equation 2.2.4

When determining the impedance of a sample, circuit models based on equivalent physical components are used. The most commonly used components are resistors (R), capacitors (C), constant phase elements (CPE) and inductors (L). The way in which some of these components appear in a Nyquist plot can be seen in Figure 2.2.3 and Figure 2.2.4.

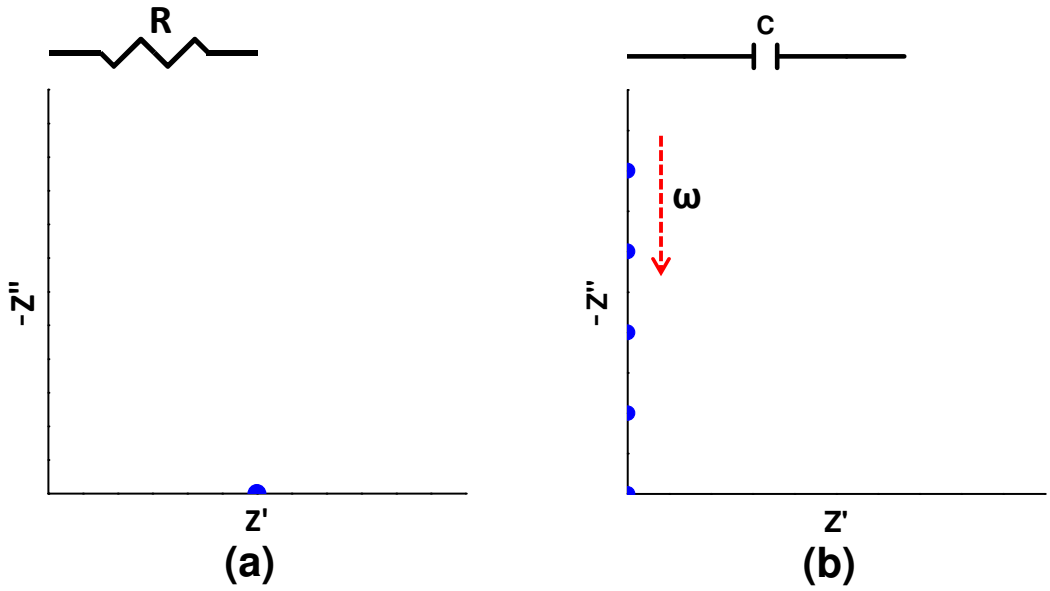

Figure 2.2.3 Representation of (a) a resistor, *R*, and (b) a capacitor, *C*, in a Nyquist plot.

When a sinusoidal voltage is applied across a resistor, it is always in phase with the current passing through it. The magnitude of the impedance is given by Equation 2.2.5.

$$Z_R^* = R$$

Equation 2.2.5

The impedance of a resistor is therefore independent of frequency and only a single value on the real axis at the resistance value is seen for all applied frequencies (Figure 2.2.3 (a)).

For a capacitor, *C*, the impedance is purely reactive. The voltage leads the current by 90 °, so that $\theta = -\pi / 2$. In this case a series of points appears on the imaginary axis

(Figure 2.2.3 (b)) with the high frequency points being nearest the origin. The magnitude of the impedance in this case is frequency dependent, and is defined by Equation 2.2.6.

$$Z_C^* = \frac{1}{j\omega C} = -\frac{j}{\omega C}$$

Equation 2.2.6

A capacitor can consist of two conductors separated by a dielectric. When an AC current is driven through it, it will accumulate an equal and opposite charge on each side until the current changes sign and the charge begins to dissipate. At high frequencies during a period of a wave, the voltage build up is less as the time is short. At low frequencies the voltage build up is greater as the period is much longer before its sign change, leading to a smaller opposition to the current.

Normally in real systems a combination of components are present in a more complicated manner. If a number of components are connected together in a series circuit, the impedances are simply summed as shown in Equation 2.2.7.

$$Z_{total} = Z_1 + Z_2 + \ldots + Z_n$$

Equation 2.2.7

However, if they are connected in parallel the impedances cannot be directly added. The admittances, where $Y = 1 / Z$, are additive (Equation 2.2.8).

$$Y_{total} = Y_1 + Y_2 + \ldots + Y_n$$

Equation 2.2.8

This leads to the complex impedance in a parallel system being defined as in Equation 2.2.9.

$$Z = \left[\frac{1}{Z_1} + \frac{1}{Z_2}\right]^{-1}$$

Equation 2.2.9

An example of a resistor and capacitor in series can be seen in Figure 2.2.4 (a). The vertical spur of the capacitive component is shifted away from the origin by the value of the resistance. At high frequencies only the capacitive part is visible due to less charge accumulation and so current flows only through the capacitor. At low frequencies the capacitor behaves as an open circuit as no current flows through the dielectric. The resistor then dominates and so as the frequency decreases, the points tend towards the real axis at the value of the resistor. The complex impedance of such a series combination is given by Equation 2.2.10.

$$Z^*_{total} = R - \frac{j}{\omega C}$$

Equation 2.2.10

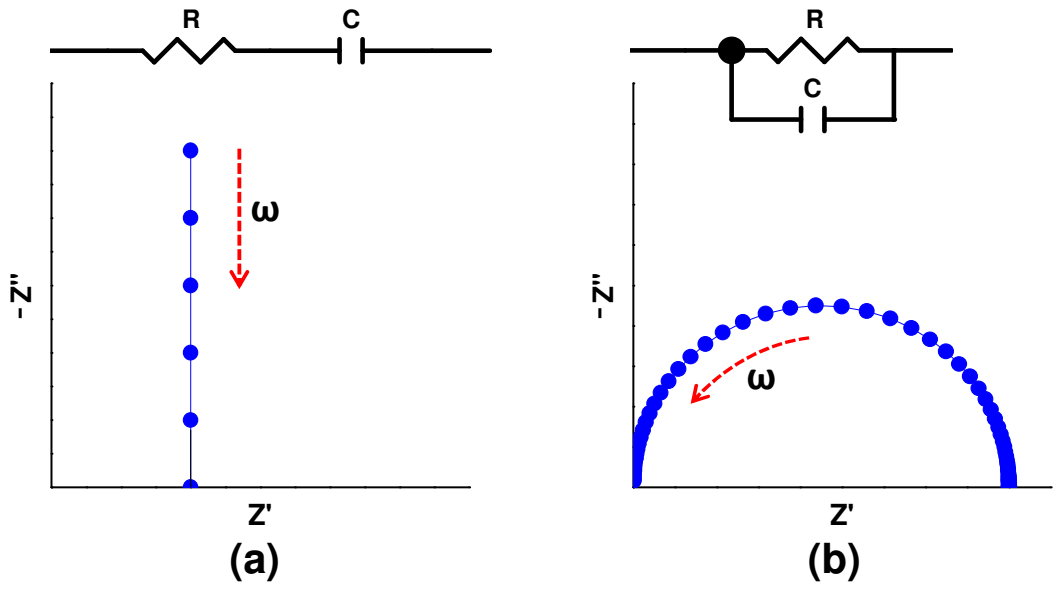

Figure 2.2.4 Representation of (a) a resistor capacitor in series and (b) a resistor and capacitor in parallel in a Nyquist plot.

If these components are then arranged in a parallel configuration as shown in Figure 2.2.4 (b), a semi-circle is visible, provided that the axes are arranged with equal spacing of units. The high frequency points are seen to intercept the real axis at the origin, while the low frequency points intercept the real axis at the value of the resistor. As with the series combination, the high frequencies favour the capacitive part of the circuit. As the frequency is decreased, the current flows through both elements producing the semi-circle, which then returns to the real axis at low frequency as the current flows only through the resistor. The complex impedance for a parallel combination of a resistor and capacitor can be defined by Equation 2.2.11.

$$Z^*_{total} = \frac{1}{\left(\frac{1}{R} + j\omega C\right)}$$

Equation 2.2.11

2.3 Impedance in Solid State Electrochemistry

A simple electrochemistry experiment can be performed by placing an ionically conducting sample between two blocking electrodes (Figure 2.3.1). With blocking electrodes the ionic species does not enter the electrode, but simply migrates between each electrode in phase with the voltage.

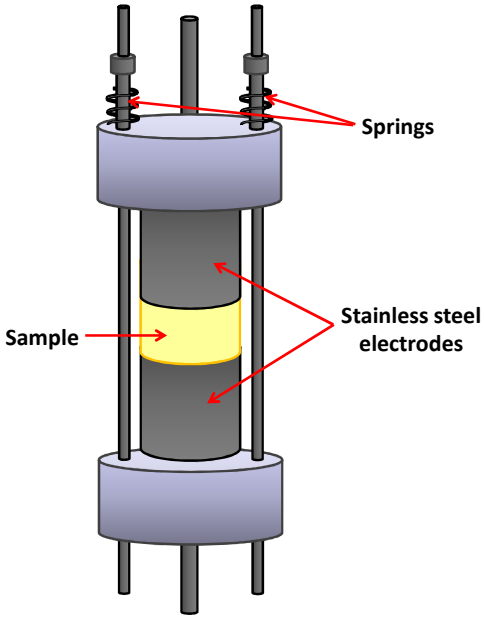

Figure 2.3.1 Schematic of a 2 electrode cell configuration.

The electrodes behave as capacitors whereby the ionic species will accumulate at the electrode – electrolyte interface represented by a double layer capacitance with a typical value of 10^{-6} F cm^{-2}.

There is also the capacitance associated with the polarisation of the material to the alternating field to be termed the dielectric or bulk capacitance. The polarisation of a solid electrolytes and the migration of ions under an alternating field occur simultaneously and are therefore said to be in parallel with each other. A simple equivalent circuit to represent the impedance of this type of two electrode cell is depicted in Figure 2.3.2, where C_{dl} is the electrode capacitance, R_b is the bulk electrolyte resistance and C_b is the bulk electrolyte capacitance.

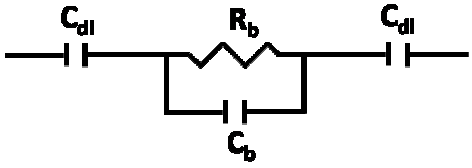

Figure 2.3.2 Equivalent circuit for an ideal blocking two electrode setup.

The bulk electrolyte capacitance, C_b, is related to the dielectric constant of the polymer as in Equation 2.3.1.

$$C_b = \frac{\varepsilon\, \varepsilon_o\, A}{l}$$

Equation 2.3.1

Where ε is the dielectric constant of the polymer sample, ε_o is the vacuum permittivity (8.85×10^{-14} F cm^{-1}), l is the electrode separation and A is the electrode surface area.

For the case of an equivalent circuit such as in Figure 2.3.2, the Nyquist plot will appear as in Figure 2.3.3 whereby the semi-circle appears at high frequency, the lower end of the semi-circle being the R_b component. The electrode capacitance appears at low frequency as the vertical spur in series with the electrolyte resistance.

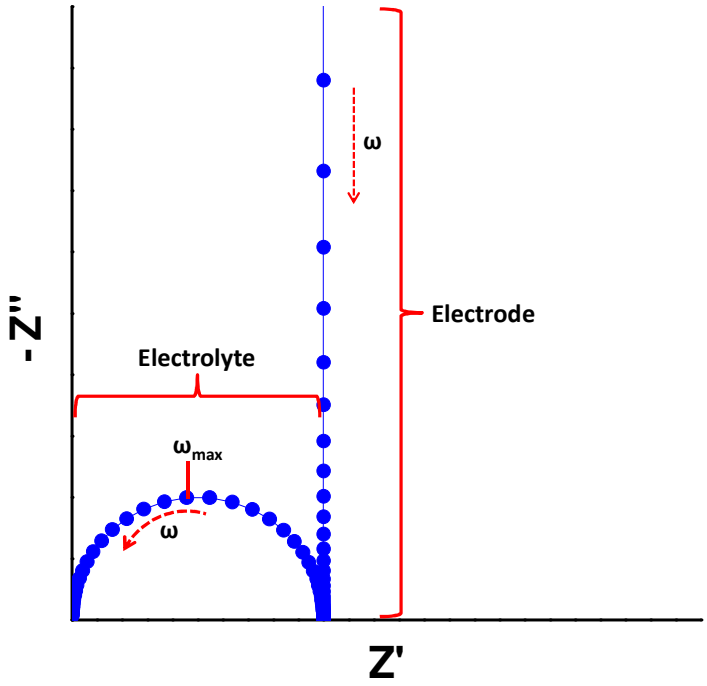

Figure 2.3.3 Nyquist plot representing an ideal two blocking electrode cell with ionically conducting species.

The relaxation time constant, which is the product of an RC component, is a useful concept in describing the response time of a sample to any applied signal.

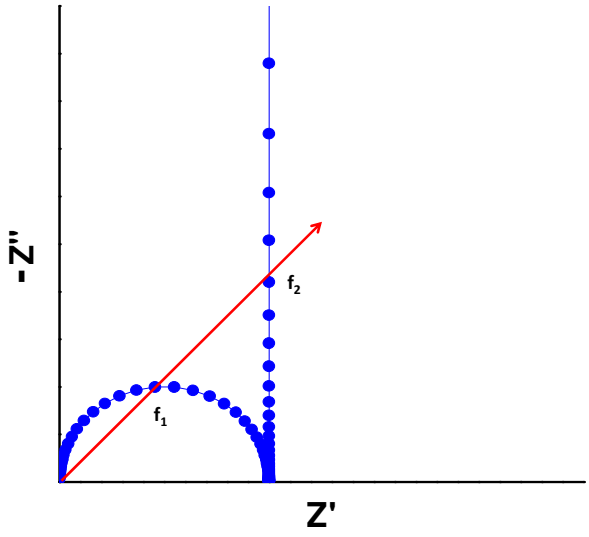

Figure 2.3.4 Nyquist plot of blocking electrode system. Red line indicates when Z' and Z'' are equal.

In Figure 2.3.4, a 45 ° line was drawn from the origin relative to the x-axis, where at any point on the line, both the real and imaginary parts of the impedance are equal. It can be seen that the line crosses both the semi-circle and the vertical spur. At these points, there is an associated frequency, f^*, with the RC product time constant. At the top of the semi-circle, f_1, the time constant is associated with the relaxation of the bulk material, while at the point on the vertical spur, f_2, it is the relaxation of the electrode capacitance through the resistance of the sample. When Z' is equal to Z" the time constant can be defined as in Equation 2.3.2.

$$\tau = RC = \frac{1}{2\pi f^*}$$

Equation 2.3.2

The time constant associated with this type of RC component needs a particular frequency to be visible. Figure 2.3.4 shows two frequencies, f_1 and f_2. For the specific shape, *i.e*; the semi-circle maximum, to be visible in the Nyquist plot, the f_1 frequency must be within the instrumental measured range. If it is not, then the characteristic shape will not be visible in the spectra.

An ideal system can be represented by model components. Real experimental systems do not behave in this manner. The capacitance of experimental electrodes is generally non ideal as the assumption of a uniformly active electrode is not valid [6]. Surface roughness, non-homogeneity of the electrode or a porous structure, are all thought to affect the capacitance by causing a time constant dispersion. In these cases, the capacitance part of the equivalent circuit is normally replaced by a constant phase element. The impedance of a CPE can be defined by Equation 2.3.3.

$$Z^*_{CPE} = \frac{1}{T_{CPE}(j\omega)^P}$$

Equation 2.3.3

In this equation T_{CPE}, is the magnitude of the CPE. The value of P is related to the phase angle of the impedance. In a capacitor the phase angle is at a constant 90 ° which leads to a CPE-P value of 1. If the CPE-P value is zero, the phase angle is also zero and the component can be deemed to be a resistor. If the phase angle is 45 ° then the CPE-P value is 0.5 and depicts a Warburg element. In the case of blocking electrodes, a CPE-P value between 0.5 and 1 can be seen. In the case of a polymer electrolyte-blocking electrode system, more commonly values of 0.75 to 0.9 are seen, which corresponds to a phase angles of approximately 67-88 °. This is attributed to the capacitive behaviour that is non ideal, and so the angle tends towards 90 ° rather than zero. When the equivalent circuit model seen in Figure 2.3.2 has the capacitors replaced by constant phase elements as in Figure 2.3.5, a Nyquist plot similar to that in Figure 2.3.6 is seen.

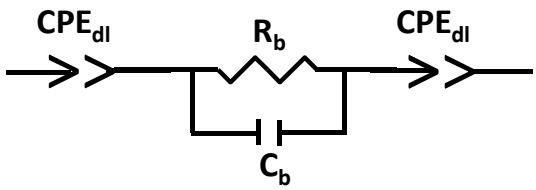

Figure 2.3.5 Equivalent circuit of 2 blocking electrodes in an experimental system.

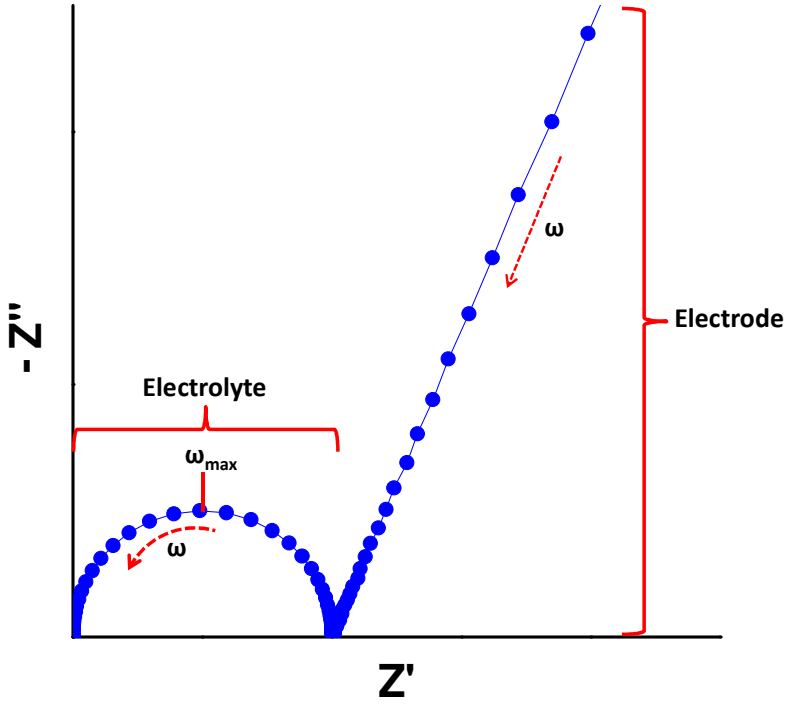

Figure 2.3.6 Nyquist plot of an experimental 2 blocking electrode system.

The electrode behaviour now exhibits a non vertical spur at low frequency corresponding to the value of P. When the Nyquist plot exhibits a parallel RC component, the bulk capacitance of an electrolyte can be calculated by using the frequency corresponding to the maximum point of the semicircle, ω_{max} [7]. At this point the magnitude of the resistor and capacitor are equal and the resistance at ω_{max} follows Equation 2.3.4.

$$C_b = \frac{1}{\omega_{max} R}$$

Equation 2.3.4

The bulk electrolyte resistance can be calculated from the extrapolation of the low frequency spur to the real axis or the low frequency part of the semi-circle and subsequently used to calculate the electrolyte conductivity.

2.4 Cell Geometry and Impedance

As seen in the previous section, the impedance of a solid electrolyte can be measured between two electrodes in order to obtain the electrolyte resistance. In this case the impedance is measured through the plane of the sample. The orientation of impedance measurements is not limited to one direction. The impedance may also be measured in the plane of the sample as depicted in Figure 2.4.1.

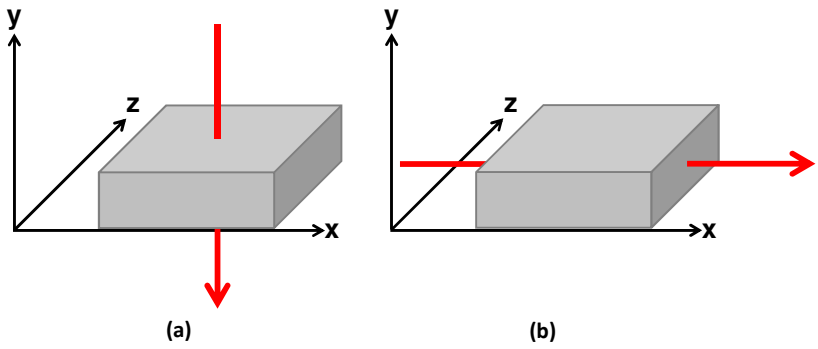

Figure 2.4.1 Schematic showing (a) through-plane and (b) in-plane directions of measurement.

The *through-plane* method of measurement is limited to the electrode distance by the sample thickness, whereby the in-plane measurement will be limited by the geometry of the electrodes.

When measuring through plane, the most common setup used is that described in Figure 2.3.1, using two electrodes. However, an in-plane measurement can be performed using two electrodes and a similar equivalent circuit results due to the capacitive contact of the electrode-electrolyte interface. To eliminate this capacitive part of the circuit, a 4-electrode setup in the in-plane direction can be utilised. In this case the voltage is applied by the two outer electrodes, while the central two electrodes are used as voltage probes only. Theoretically, by using these probes any contact impedances can be eliminated from the circuit. The assumptions are that the potential drops across the voltage probe interfaces are negligible compared with the potential to be measured, and that the current through the probes is negligible compared with the current through the sample. The differences between these 3 types of electrode setup can be seen in Figure 2.4.2.

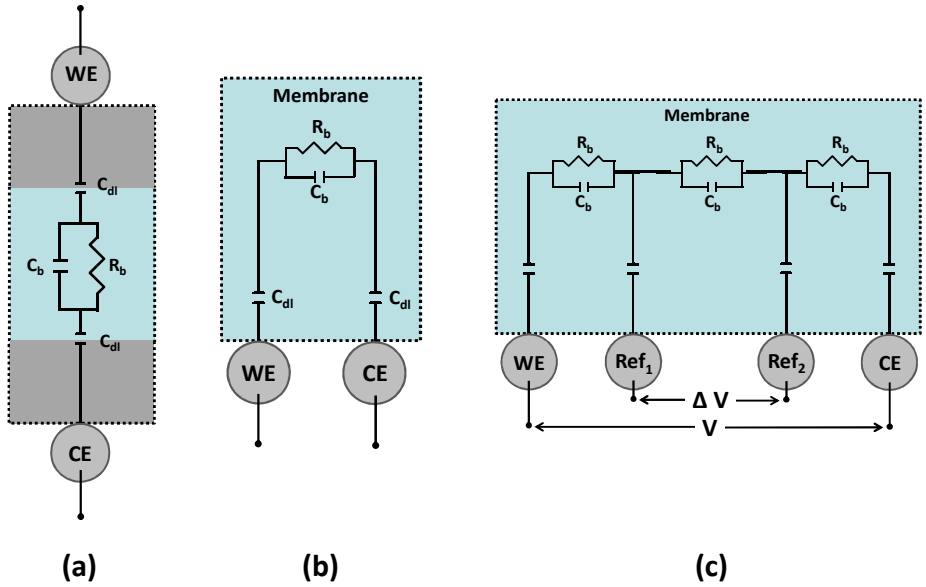

Figure 2.4.2 Schematic of cell geometry, (a) 2-electrode through-plane, (b) 2-electrode in-plane and (c) 4-electrode in-plane.

The Nyquist plots for the 2-electrode through-plane and the 2-electrode in-plane would appear as that of Figure 2.3.3. A Nyquist plot for the 4-electrode in-plane measurement would appear purely as the RC parallel circuit with no low frequency vertical spur. If the sample was purely resistive, only points around the electrolyte resistance would appear around the real axis.

With regards specifically to polymer electrolytes, the 2-electrode through-plane method is particularly suited to lithium ion polymer electrolytes where the conductivity to be measured is in the region of 1×10^{-3} to 1×10^{-8} S cm^{-1}. For a typical 1 cm^2 electrode, the bulk electrolyte resistance would be approximately 100 – 10,000 ohms.

For proton conducting polymer electrolytes, sample have much higher conductivities with a minimum of 1×10^{-2} S cm^{-1}, and are generally cast as films less than 100 am thick meaning the subsequent bulk resistances will be approximately less than 10 ohms an even less than one ohm in some cases. For measurement of such low resistances, an extremely specialised instrument would be needed to resolve the values against the capacitive nature of the electrodes. For these polymer electrolytes, the 2-electrode or 4-electrode in-plane method is more suited.

Extensive studies into the effects of electrode geometry on conductivity measurements of polymer electrolytes have been undertaken. It has been shown using simulation studies, that electrode spacing is a key factor in optimising the measurement techniques. A ratio between the sample thickness, *h*, the distance between the electrodes, *l*, and the width of the electrode, *k*, where $l >> h \sim k$ was found to provide a one dimensional current distribution [8]. In addition, similar experiments have also found that optimisations can be made by using different electrode materials [9] and documented the discrepancies between using two and four electrode measurements.

.

2.4.1 Conductivity Calculations

The current density vector, $\hat{J}$, can be expressed by an electrical field, E_f, and a conductivity tensor σ (Equation 2.4.1).

$$\hat{J} = \boldsymbol{\sigma} E_f$$

Equation 2.4.1

By rewriting Equation 2.4.1 in terms of the dimensions of a sample this leads to Equation 2.4.2,

$$\frac{I}{A} = \sigma \frac{\Delta V}{l}$$

Equation 2.4.2

where *A* is the cross sectional area, and *l* is the distance between electrodes. If this is then rearranged a definition of the bulk conductivity, σ_{bulk}, can be obtained (Equation 2.4.3).

$$\sigma_{bulk} = \frac{I}{\Delta V}\frac{l}{A} = \frac{l}{RA}$$

Equation 2.4.3

In polymer electrolyte measurements, the resistance of a sample is calculated using impedance data. Where a parallel RC component is visible, the extrapolated intercept of the low frequency region of the semi-circle is taken as the bulk electrolyte resistance to give the value of *R*.

The resistivity of a sample can be defined by Equation 2.4.4.

$$\rho = \frac{E}{\hat{\jmath}} = \frac{1}{\sigma}$$

Equation 2.4.4

Sample dimensions are defined by those shown in Figure 2.4.3.

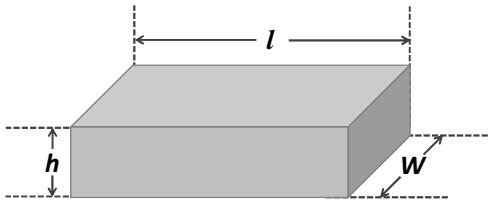

Figure 2.4.3 Sample dimensional layout.

By using these dimensions where the cross sectional area, A = Wh, then the bulk resistivity (measured in Ω cm) can be defined by Equation 2.4.5.

$$\rho = R\,\frac{A}{l}$$

Equation 2.4.5

This applies to conductivities calculated in both through-plane and in-plane directions. In the though-plane direction, surface resistivity is deemed to be negligible. However using an in-plane measurement there is more chance that the conductance path will be along the surface as the sample is generally placed over the electrodes. The surface resistivity can be defined by Equation 2.4.6.

$$\rho = R\,\frac{W}{l}$$

Equation 2.4.6

So when $W = l$, then numerically $\rho = R$, and the surface resistance is give in units of ohms square.

Care must be taken when performing in-plane measurements that a true bulk resistivity is being measured.

This works well with electronically conducting samples, however, in ionic conductors such as polymer electrolytes, the contact is mainly capacitive and some problems have been found which will be discussed in Chapter 6.

2.5 Chapter 2 References

1. G. Blanc, I. Epelboin, C. Gabrielli and M. Keddam, *Electrochimica Acta*, 1975, **Q0**, 599-601.

2. J. R. Macdonald, *Impedance Spectroscopy Emphasising Solid Materials and Systems*, John Wiley & Sons, New York, 1987.

3. R. Claire Greaves, S. P. Bond and W. R. McWhinnie, *Polyhedron*, 1995, **14**, 3635-3639.

4. J. J. Fontanella, M. G. McLin, M. C. Wintersgill, J. P. Calame and S. G. Greenbaum, *Solid State Ionics*, 1993, **66**, 1-4.

5. M. C. Wintersgill and J. J. Fontanella, *Electrochimica Acta*, 1998, **43**, 1533-1538.

6. M. E. Orazem and B. Tribollet, in *Electrochemical Impedance Spectroscopy*, John Wiley & Sons, Inc., Hoboken, New Jersey, 2008, p. 233.

7. P. G. Bruce, in *Polymer Electrolyte Reviews 1*, eds. J. R. MacCallum and C. A. Vincent, Elsevier Applied Science Publishers Ltd, Barking, Essex, 1987, p. 250.

8. A. D. Fitt and J. R. Owen, *Journal of Electroanalytical Chemistry*, 2002, **538-539**, 13-23.

9. Z. Xie, C. J. Song, B. Andreaus, T. Navessin, Z. Q. Shi, J. J. Zhang and S. Holdcroft, *Journal of the Electrochemical Society*, 2006, **153**, E173-E178.

Chapter 3

Lithium Ion Gel Polymer Electrolytes

Chapter 3 Lithium Ion Gel Polymer Electrolytes

The work performed on lithium salt doped polymers was used as an introduction into a class of polymer electrolytes that can conveniently be prepared by combinatorial synthesis methods. Certain types of polymers can easily be combined with lithium salts to make ionically conducting polymer. However these salts require plasticisers to provide a conduction path for the mobile species. The minimum plasticiser content that is required to achieve conductivities high enough for use in battery applications is undefined and usually an excess of the plasticiser-salt solution is used. This section focuses on the category termed gel polymer electrolytes described in Chapter 1, which utilise the presence of a low volatile solvent as a plasticiser to facilitate ionic mobility within the polymer matrix. A complete evaluation of a ternary mixture of polymer, lithium salt and plasticiser was undertaken and analysed with respect to composition specific conductivity values.

3.1 A Ternary Composition System

3.1.1 Starting Materials

Poly (vinylidene co-hexafluoropropylene) (PVdF-HFP), (Aldrich, av. $M_n \approx 130{,}000$, av. $M_w \approx 400{,}000$) and bis (trifluoromethane) sulfonimide lithium salt (LiTFSI), (Aldrich, puriss., ≥ 99.0 %) were dried at 80 °C for 12 hours prior to use. Propylene carbonate (PC), (Aldrich, ReagentPlus™, 99 %), cyclopentanone (CP), (Aldrich, 99 + %) and acetone (Aldrich, Reagent Grade) were used as received.

3.1.2 Preparation Method

Stock solutions of PVdF-HFP in CP and LiTFSI in CP were made up to 7 and 10 % by weight respectively. The actual weight percentage was calculated regularly before each batch of gel electrolytes was prepared by evaporating off all of the CP co-solvent from a known initial weight and recording the mass remaining. This also allowed calculations to be made about the amount of active material per unit volume to be made, which was necessary for preparing the compositions from solutions. The CP co-solvent was used

to dissolve the polymer for two reasons. Firstly, PVdF-HFP dissolved faster and at lower temperature in the co-solvent when compared to the plasticiser. Secondly, experimentally, it would be unlikely that samples with very small weight fractions of plasticiser would have dissolved the mass of polymer that was defined for that composition. The higher volatility of the co-solvent allowed greater volumes to be used in stock solution preparation, while still being easily removable without affecting the plasticiser content.

Before preparation of the samples, the desired weight fraction of each component was pre-determined at intervals of 0.05 as shown in Figure 3.1.1.

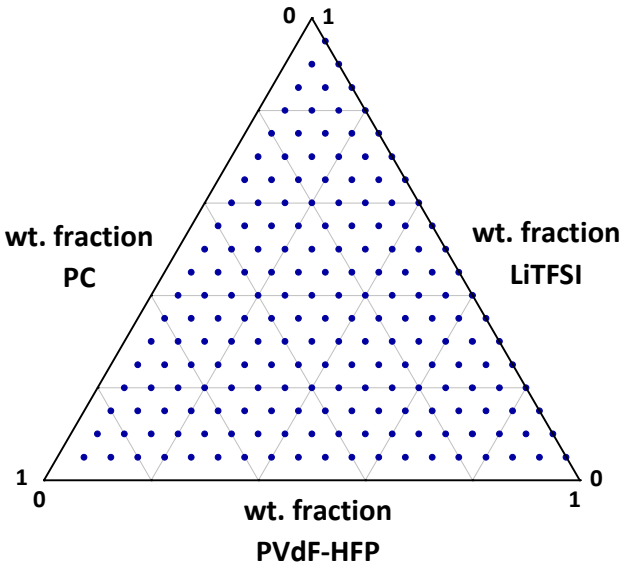

Figure 3.1.1 Ternary plot illustrating weight fraction intervals of each component to be prepared.

The desired amount of each solution was pipetted into an 8 by 8 array of 1 ml vials containing the appropriate fraction of the non-volatile component. The electrochemical cell mirrored the synthesis array plate seen in Figure 3.1.3, and contained 64 individual aluminium electrodes. This meant that 64 different compositions were able to be measured for conductivity at any one time. Repeats of each composition were made on each electrochemical cell so that the number of compositionally different samples changed from 64 to 16. The thickness of each electrode was measured with a micrometer with tolerance values of 1 μm ± 5 μm, before any deposition of the electrolyte and again after the experiment had taken place.

To ensure a homogenous mixture, the vials were placed on a vortex (Fisherbrand, Whirlimixer) mixer before use. For each sample a 20 µl volume was pipetted onto the top of each electrode ensuring an even coverage across the entire electrode area. The co-solvent was evaporated off by enclosing the electrochemical array in a vessel which contained some small holes in the roof. This provided protection of the samples from sudden air movement whilst still allowing enough convection for the evaporation to take place. A benefit of this method is that it also prevented very fast evaporation which leads to samples drying in a "coffee cup" effect. The reason behind this effect is that the edges of the sample will evaporate faster because of an easier diffusion path for the vapour. This leads to a sample that contains a ring near the outside that is thicker than the centre. Elimination of this effect by placing the diffusion restriction away from the sample gave samples of uniform thickness across the electrode. The time necessary for the evaporation of the co-solvent but not the plasticising solvent was determined by using a sample containing known weights of each solvent. Using the same volume of solvent and the same electrode area, the solution was deposited and the weight recorded every minute using an AND GR-202 analytical balance and PC Acquisition software. The results of the weight loss measurements are shown in Figure 3.1.2.

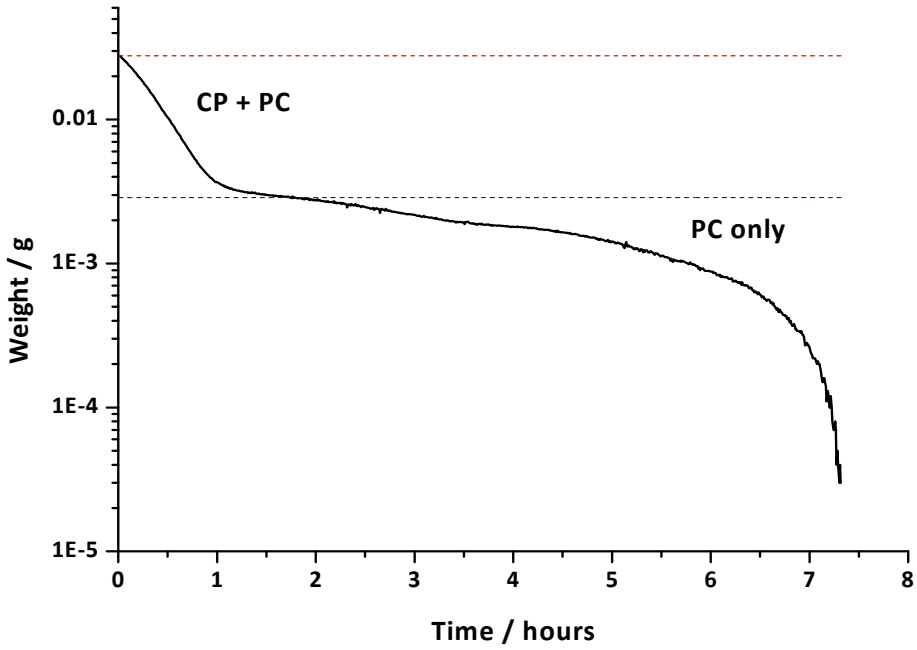

Figure 3.1.2 Evaporation times of a samples containing known weights of CP and PC.

Figure 3.1.2 shows the evaporation time of each component in a plasticiser/co-solvent mixture. It can be seen that the more volatile co-solvent is evaporated off relatively

quickly in comparison to the plasticiser, the specific purpose of the plasticiser being to remain within the system.

This showed that the optimum evaporation time of 1.5 hours allowed complete removal of the CP with a minimum loss of PC. After this time interval had passed, the array plate containing the aluminium electrodes was placed above sprung pin contacts in the combinatorial cell. A flexible carbon loaded rubber sheet was placed above the electrodes on the array plate to ensure a soft contact with the films. A stainless steel current collector was then placed above this and the lid of the combinatorial cell fitted. Previous attempts of construction had been performed with a metallic top electrode instead of the carbon rubber contact. However, variations in the height of the electrodes across the array meant that uneven contacts were formed, and in some cases, short circuits were observed as the metallic electrode was unable to follow the contour of the array. By tightening the screws on the lid, the bottom of the aluminium electrodes touched the sprung contacts underneath. The constructed cell was sealed with parafilm; any further evaporation was deemed to be negligible as there was no gas access to the samples. The high-throughput (HT) process of preparation to deposition on the electrochemical cell is depicted in Figure 3.1.3. The method was repeated a further 15 times to cover all compositions specified in Figure 3.1.1.

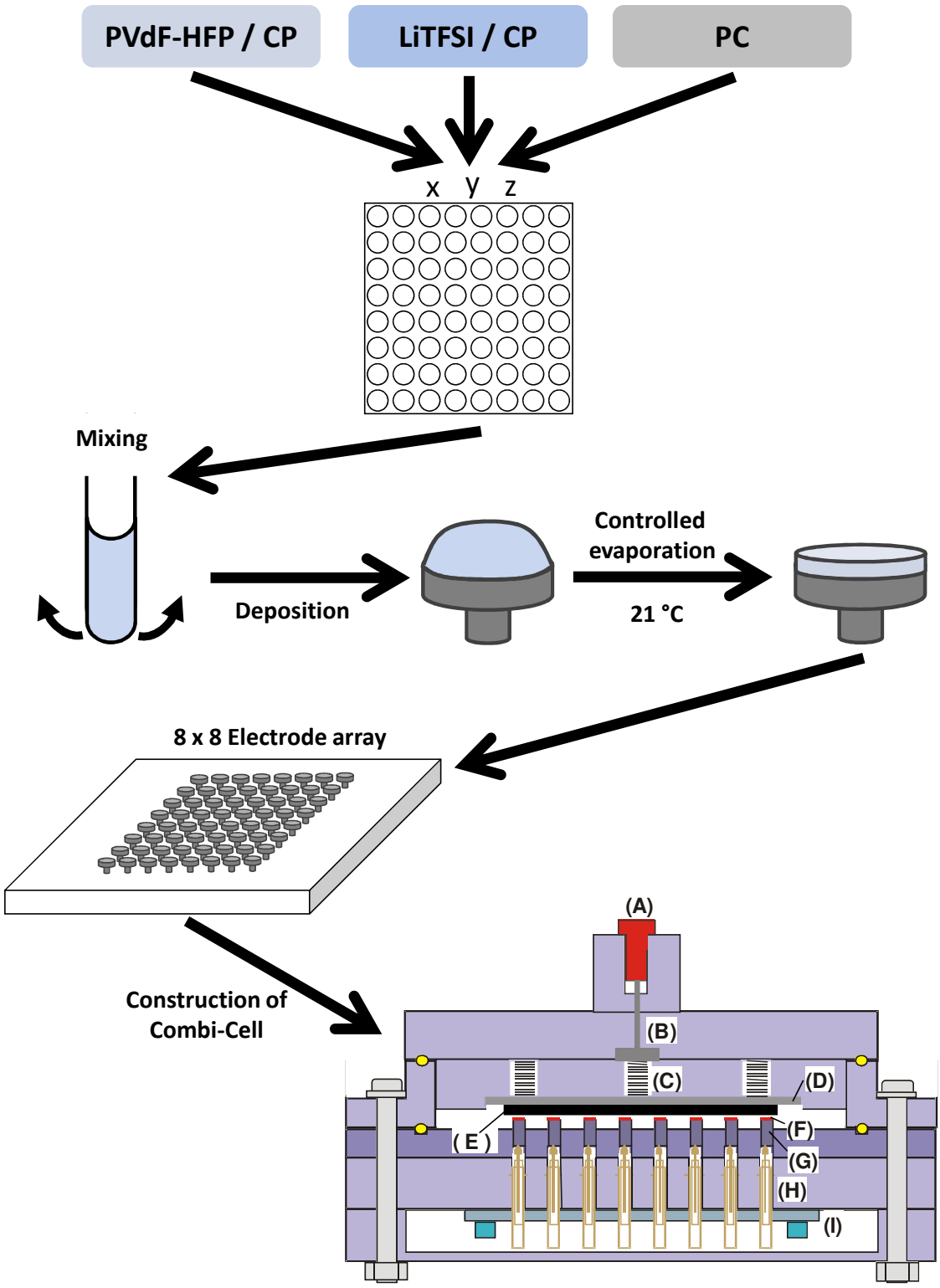

Figure 3.1.3 Schematic showing HT technique of PVdF-HFP / LiTFSI / PC system including the combinatorial cell (A. Negative electrode connector, B. Stainless steel contact, C. Spring contact, D. Stainless steel current collector, E. C-loaded rubber, F. Electrode material, G. Aluminium working electrode, H. spring contact and I. Printed circuit board).

An example of the compositions for one electrochemical array can be seen in Table 3.1.1, which includes 16 different compositions.

Table 3.1.1 Example of compositions of polymer, salt and plasticiser for one electrochemical array.

Sample	PVdF-HFP	wt. fraction LiTFSI	PC
I-1	0.45	0.05	0.5
I-2	0.45	0.1	0.45
I-3	0.45	0.15	0.4
I-4	0.45	0.2	0.35
I-5	0.45	0.25	0.3
I-6	0.45	0.3	0.25
I-7	0.45	0.35	0.2
I-8	0.45	0.4	0.15
I-9	0.45	0.45	0.1
I-10	0.45	0.5	0.05
I-11	0.45	0.55	0
O-1	0.75	0.05	0.2
O-2	0.75	0.1	0.15
O-3	0.75	0.15	0.1
O-4	0.75	0.2	0.05
O-5	0.75	0.25	0

Each of the different compositions was arranged on the electrochemical array as demonstrated in Figure 3.1.4 where the different colours depict the repeated samples. To demonstrate the reproducibility of the results, repeated compositions were prepared in the array of tubes as instead of using the same solution. This gave an indication of the reliability of the preparation method as well as the reliability of the measurement of identical samples.

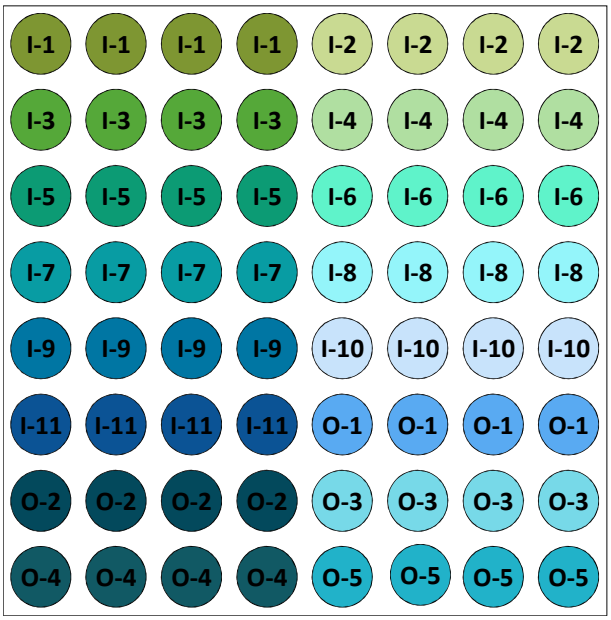

Figure 3.1.4 Schematic example of the layout of different compositions with repeats on the electrochemical cell.

In addition, a complete cell containing only one composition that was prepared from the same solution was made and all electrode channels tested. This was done to reveal any effects of sample deformation due to the applied uniaxial pressure and its non-uniformity across the array as well as any other errors such as insulating films on the electrode surfaces.

3.2 Electrochemical Characterisation

3.2.1 AC Impedance Spectroscopy

The characterisation was performed by using AC Impedance spectroscopy to determine the total ionic conductivity, utilising a though-plane impedance measurement between blocking electrodes. The electrochemical cell containing 64 individual working electrodes and one counter electrode has been detailed elsewhere [1, 2]. Some modifications were made in that carbon loaded rubber was used as a soft top electrode due to the nature of the samples. This ensured a uniform contact across the array. The cell was connected *via* a home made connection box (Figure 3.2.1), to a Solartron 1250 frequency response analyser coupled with a Solartron SI 1287 electrochemical interface via a Solartron 1281 multiplexing device. The multiplexer allowed a sequential measurement of 8 channels.

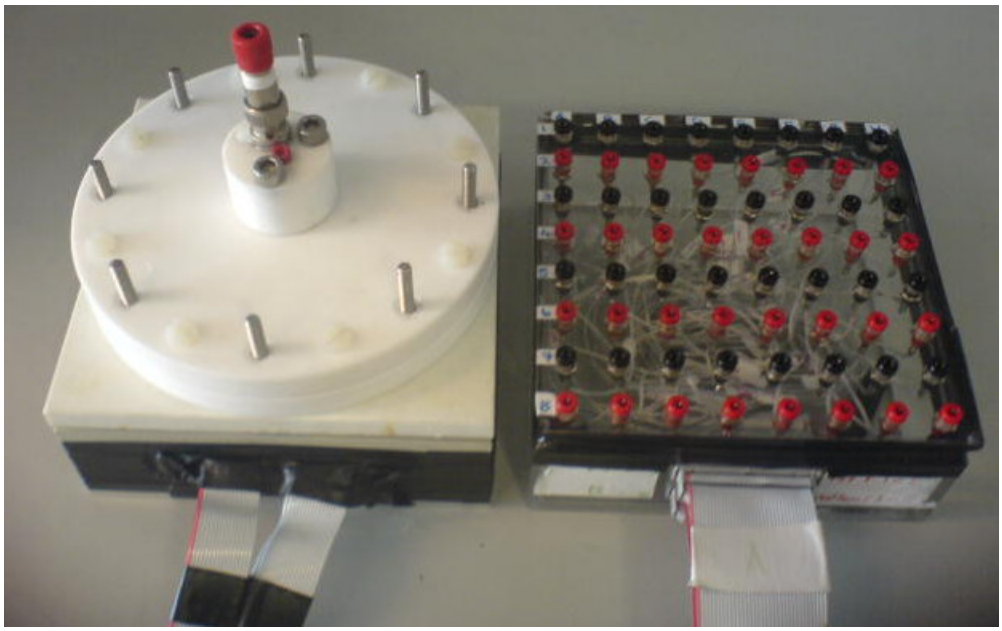

Figure 3.2.1 Combi-cell and connection box for use with a multiplexing device.

Using ZPlot and ZView software packages the impedance experiment was programmed to switch between channels automatically. The settings for the experiments are listed in Table 3.2.1, whereby the limiting current of the potentiostat channel was 1 pA with an

expected noise error of the current values utilised being approximately 1 mA. All experiments were carried out under ambient conditions (21 ± 2 °C).

Table 3.2.1 Impedance settings for all experiments.

Parameter	Symbol	Value	Units
Initial frequency	f_i	65	k Hz
Final frequency	f_f	0.1	Hz
Points per decade	N_d	15	n/a
Peak to peak AC amplitude	V_{pp}	200	mV

The data were displayed as a complex plane Nyquist plot, whereby the bulk electrolyte resistance could be calculated by extrapolating the linear part of the data to the real axis (*Z'*). The data tended towards following two general shapes. Firstly when the sample contained a low weight fraction of lithium salt, the Nyquist plot was characteristic of that in Figure 3.2.2.

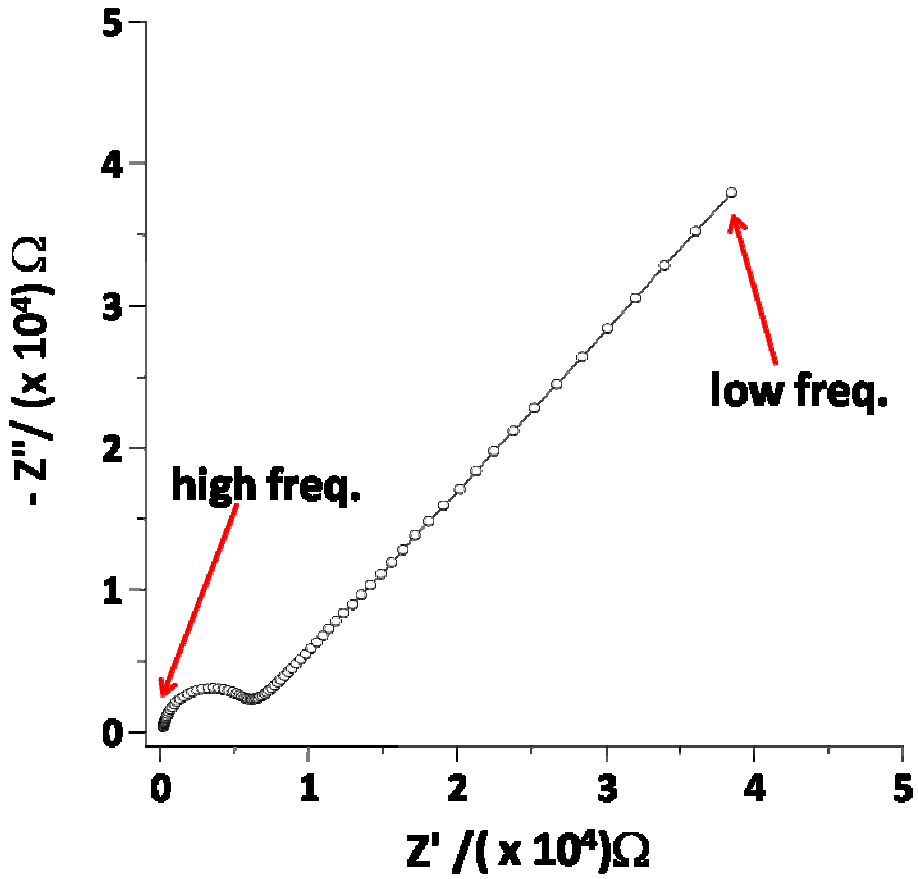

Figure 3.2.2 Nyquist plot of poorly conducting samples.

In this plot the data follows that of a semi-circle at high frequency followed by a spur at an angle of approximately 45 ° at low frequency. In theory, the high frequency intercept may be shifted away from the origin by the resistance of the carbon loaded rubber, while the arc itself originates from the parallel RC component of ionic resistance coupled with the dielectric capacitance of the polymer. As the frequency decreases the low dielectric capacitance of the polymer becomes blocking, so that the resistance of the sample and carbon combine in series to approach a real axis intercept. At still lower frequencies the interface between the ion conducting polymer and the electron conducting carbon presents a constant phase element in series with the sample and carbon bulk resistances to form a final spur in the Nyquist plot. The data are fitted to an equivalent circuit which is represented by Figure 3.2.3.

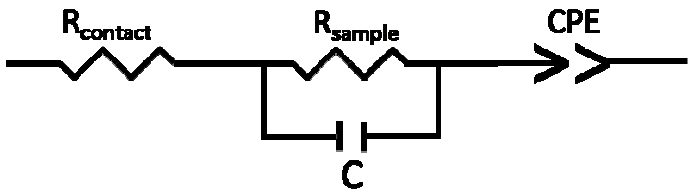

Figure 3.2.3 Representative equivalent circuit for samples with low weight fraction of ionic species.

The constant phase element is a replacement for an ideal capacitor which is rarely seen in single electrochemical reactions. In this setup there is no diffusion as the electrodes used were blocking. The CPE accounts for the double layer capacitance of an electrode that may include some time constant dispersion due to surface roughness.

The second type of Nyquist plot that was seen is illustrated in Figure 3.2.4.

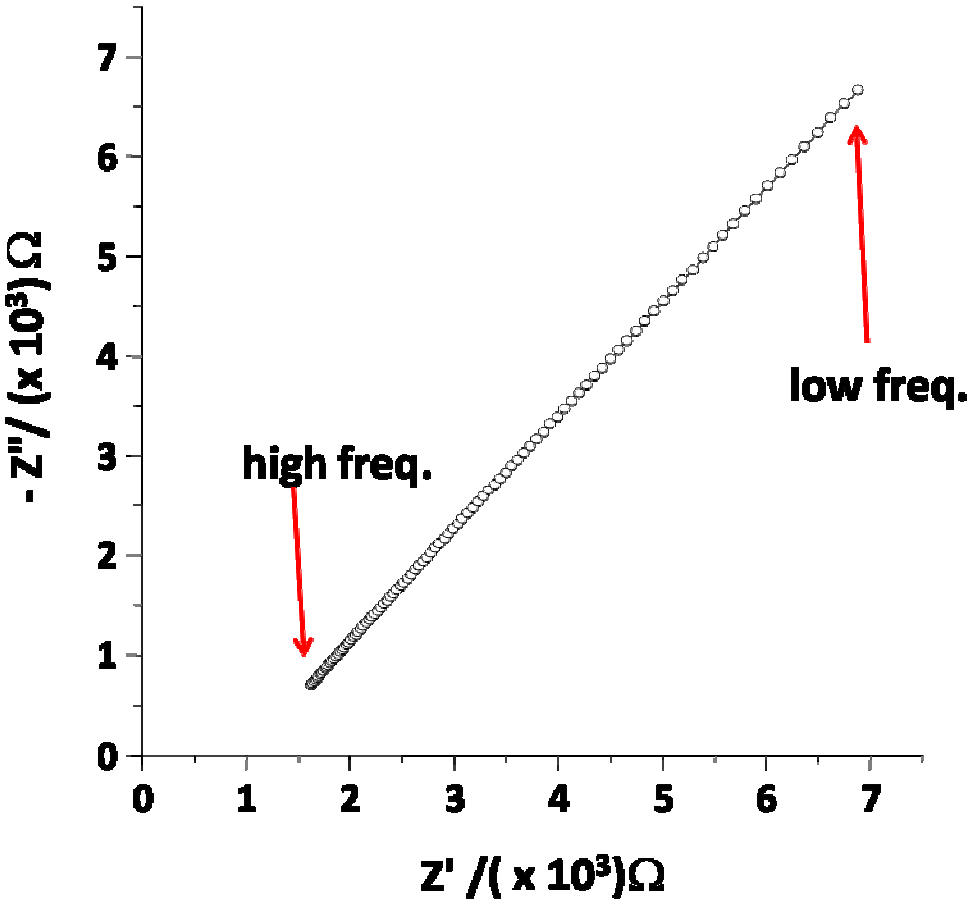

Figure 3.2.4 Representative Nyquist plot of samples with high weight fraction of ionic species.

In this case the high frequency semi-circle is absent. This is explained by a higher ionic conductivity at a higher salt content, resulting in a lower RC time constant and therefore a higher frequency range, typically M Hz, for the semi-circle to appear. Therefore the sample resistance is seen as a series combination with the interface represented by the equivalent circuit in Figure 3.2.5.

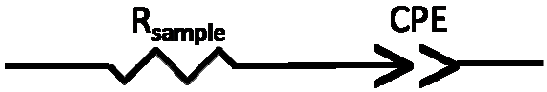

Figure 3.2.5 Representative equivalent circuit for highly conducting samples.

The resistance of the samples was calculated by the extrapolation of the high frequency intercept with the real axis as shown in Figure 3.2.6. The data were plotted so that each graph represented a constant weight fraction of PVdF-HFP while the lithium salt and plasticiser content were varied. The intercept with the real axis was seen to decrease with each subsequent increase of lithium salt content as seen in Figure 3.2.6.

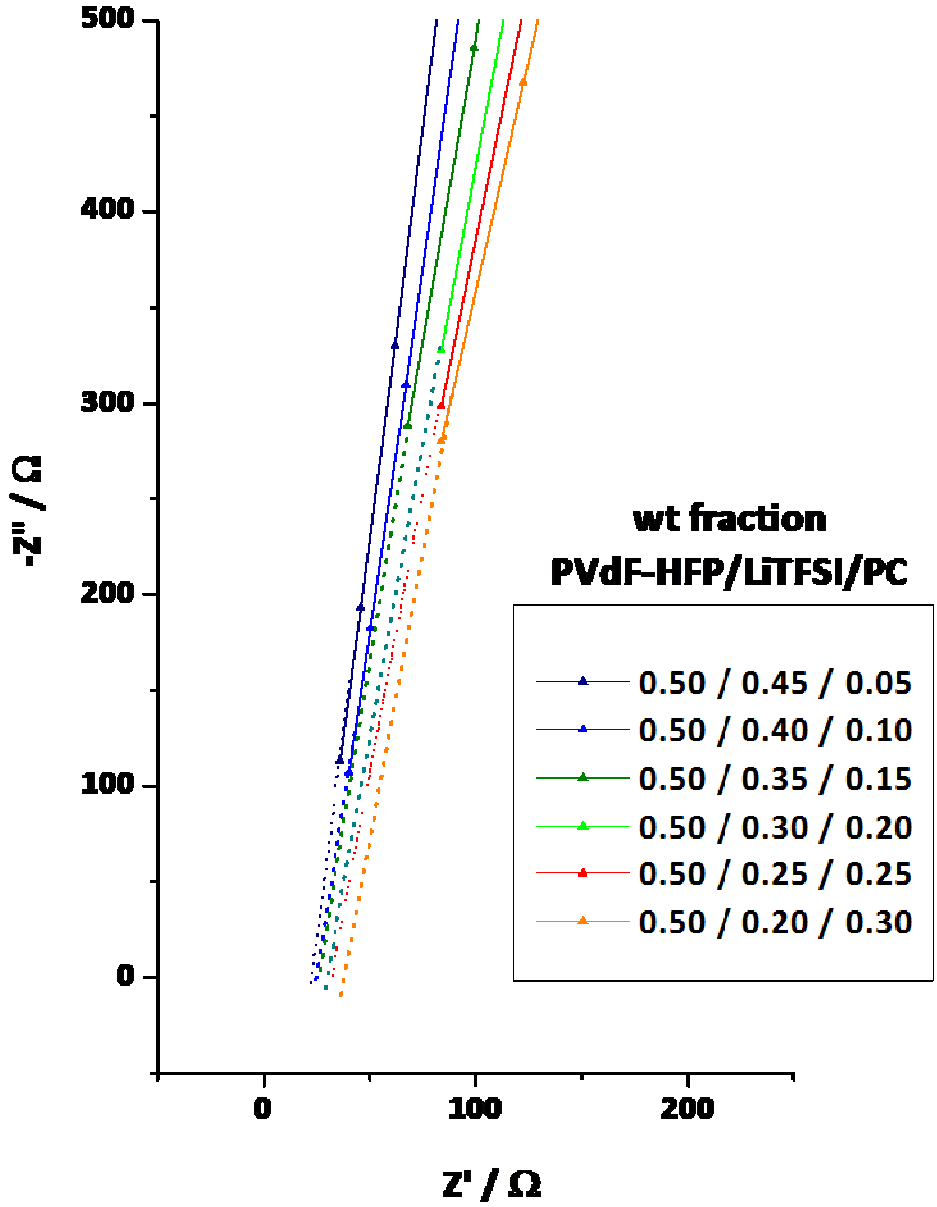

Figure 3.2.6 Part of the Nyquist plot extrapolated to the real axis for samples containing different salt contents at a constant weight fraction of PVdF-HFP.

The final values of the conductivity were obtained using Equation 3.2.1, where l is the sample thickness, R is the sample resistance calculated from the Nyquist plots and A is the geometric area of the electrode.

$$\sigma = \frac{l}{RA}$$

Equation 3.2.1

Since the equation to calculate the conductivity follows the form y = (ka)/b, the propagation of errors in the resistance and thickness values was calculated using Equation 3.2.2.

$$s_\sigma = \sigma \sqrt{\left(\frac{s_L}{Ł}\right)^2 + \left(\frac{s_R}{Ř}\right)^2}$$

Equation 3.2.2

This gave the standard deviation of the conductivity, s_σ, from the average conductivity, σ, the standard deviation of the film thickness s_L, the average thickness, *Ł*, the standard deviation of the resistance, s_R, and the average resistance, Ř. The thickness of the polymer films ranged from 50 – 100 μm, the thicker films being those that contained a higher weight fraction of PVdF-HFP. The error of the film thickness was based upon the degree of error of the micrometer. The average values were based upon the averages of the 4 replica samples. The average conductivity *versus* the weight ratio of lithium salt to plasticiser was plotted with the calculated standard deviation of conductivity, an example of this is shown in Figure 3.2.7.

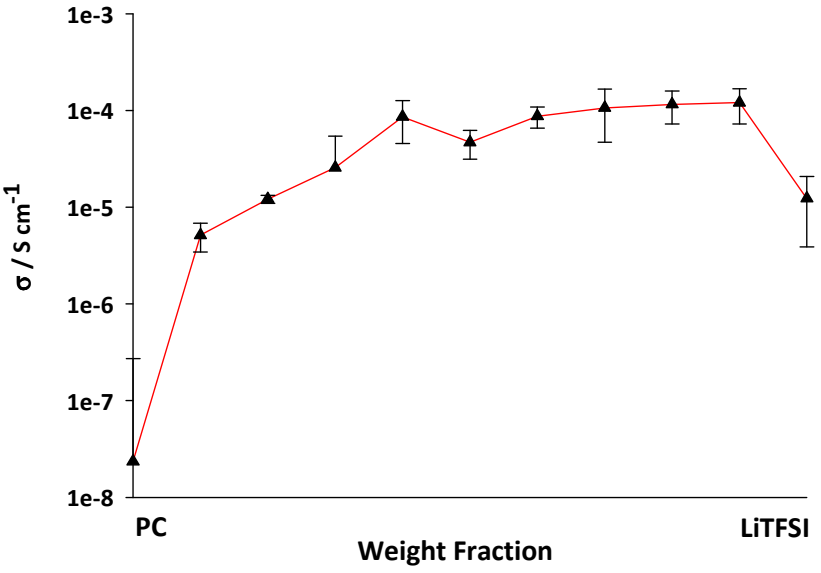

Figure 3.2.7 Average conductivity values with calculated errors for 0.5 weight fraction PVdF-HFP.

The graph more clearly illustrates how the addition of a small amount of salt increased the conductivity by nearly two orders of magnitude. The initial conductivity is attributed purely to impurities when no salt is deliberately added. The value is slightly higher than a representative literature value [3] of PC that is 2.1 x 10^{-9} S cm^{-1}, presumably due to ionic impurities in the polymer. Addition of salt causes a sudden rise in the conductivity followed by a gradual increase with concentration. When there is no solvent present there is a drop in the conductivity value as expected, although the residual conductivity is much higher than expected for a nominally solvent-free and non-solvating polymer. When the different compositions that were prepared are plotted onto a ternary diagram and contour mapped for their respective conductivity values, the trends mentioned previously are more readily defined. This method of viewing the data seen in Figure 3.2.8 shows samples that have similar properties and highlights these "hot-spot" areas with the calculated contours.

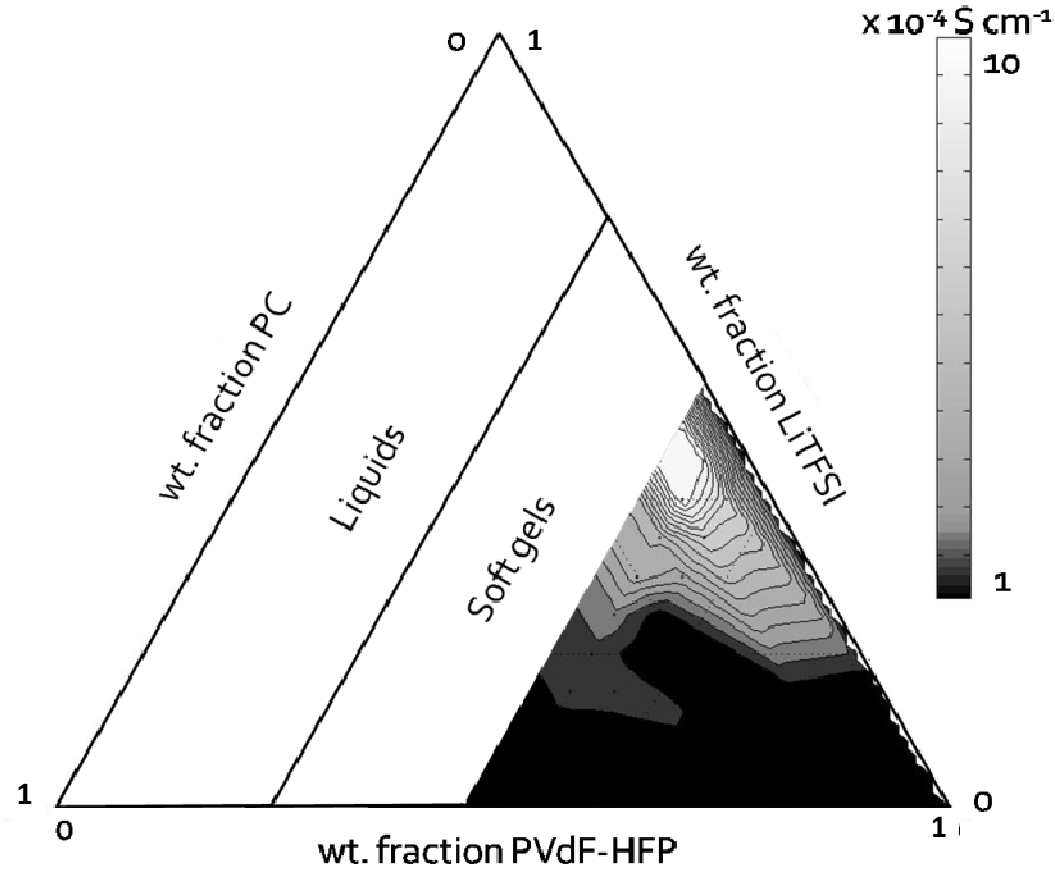

Figure 3.2.8 Ternary plot of different compositions contour mapped for conductivity.

Although all compositions depicted in Figure 3.1.1 were prepared, the results were only considered for approximately half of the samples to be representatively accurate for this method of measurement. The ternary plot is separated into 3 main parts. Firstly at low polymer content, the samples behave according to the "polymer dissolved in solvent" manner, whereby the samples are merely viscous liquids. Secondly, there are the samples that fit into the soft gels category. These samples contain such a weight fraction of solvent that the matrix of the polymer has swelled to near its maximum allowed dimensional expansion limits and that any applied force would unduly cause collapse of the film by "sweating" of the solvent. Thirdly there are the mechanically stable films which have at least 0.45 weight fraction of polymer. After the experiments had taken place and the cell deconstructed, the films were measured and they showed no dimensional instability or solvent loss due to the force applied in the combinatorial cell. In addition, their physical appearance was visibly identical to their pre-experimental conditions.

So, when considering the mechanically stable films only, the maximum conductivity appears at a composition around 0.5 / 0.45 / 0.05, PVdF-HFP / LiTFSI / PC. There is a steep decline in conductivity towards the area of no solvent as mentioned previously. Reasons behind this decrease are that as the solvent content is decreased, there will be a decrease in ion mobility due to the increasing viscosity of the polymer without plasticiser. However, the solvent free conductivity is higher that expected as other studies into solvent free systems have seen values around 3.5×10^{-6} S cm^{-1} [4, 5]. In both cases the lithium salt and polymer were not identical to the ones used in these experiments so the values can only be used as a general comparison.

This observed conductivity may suggest that the polymer has impeded some or all crystallisation of the salt which would normally occur on removal of the plasticising solvent. If this is the case some interaction or solvation of the salt may have occurred within the amorphous regions of the polymer matrix. This possibility is investigated further below.

3.3 Physical Characterisation

To assist in further elaboration of the findings in the previous section, physical characterisation of the samples was performed. Information on both the thermal and crystal structure of the samples can provide information regarding interactions between each component in the system.

3.3.1 Differential Scanning Calorimetry

Thermal properties of the films were investigated using a METTLER model DSC20 oven connected to a METTLER TA4000 controller. The samples were prepared as stated previously with co-solvent evaporation. The sample containing no plasticiser and the pure polymer sample were dried in a *buchi* oven under vacuum to remove any traces of solvent and all samples were then sealed in aluminium cans before being placed in the instrument along with an Indium standard sample. All samples were heated to 200 ° C. They were then cooled to -50 ° C with liquid nitrogen and returned to 200 ° C for a second time. The heating and cooling rate was kept at 10 ° C min^{-1}.

The DSC curve of the pure PVdF-HFP can be seen in Figure 3.3.1 (a). The initial melting point (T_m) can be seen peaking at 145 ° C while on cooling the recrystallisation (T_c) peak is 114 ° C.

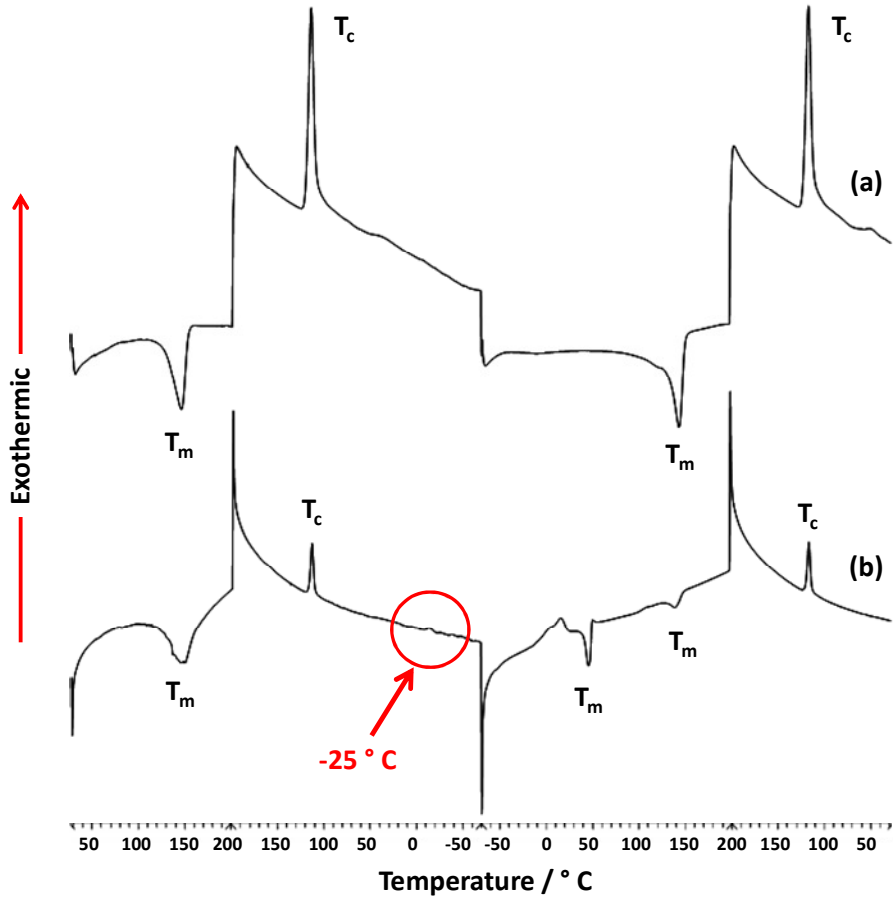

Figure 3.3.1 DSC curves of (a) pure PVdF-HFP and (b) PVdF-HFP / LiTFSI weight fraction 0.6 / 0.4 at a heating rate of 10 ° C min^{-1}.

This is replicated on the second cycle and the enthalpy values also remain the same. When looking at a composite sample that contains 0.6 and 0.4 weight fraction of PVdF-HFP and LiTFSI respectively, Figure 3.3.1 (b), there are some changes that have occurred. The initial T_m remains at 145 ° C and the first T_c at 114 ° C, but the enthalpy of the T_c is considerably less than the T_m. This lack of crystallisation is reflected in the second cooling cycle indicating that not all of the material has recrystallised. In addition to this on the second heating cycle, two T_m peaks are visible as opposed to one previously. The first is at a much lower temperature of 47 ° C, whilst the second remains at the previously seen 145 ° C. The expected T_g of the pure PVdF-HFP is around -25 to -35 ° C. It is often difficult to identify the T_g of a sample unless very slow or very fast scan rates are used, and a clear value cannot be determined in the pure sample (a). The fluctuations around these values in the sample containing the lithium salt (b) could be due to other factors such as bound water. It may be suggested that the

presence of the salt has impeded the crystallisation due to some salt-polymer interaction. However the effect of water absorption on the cooling cycle cannot be eliminated which may also cause a phase separation of salt from the polymer.

3.3.2 X-ray Diffraction

The X-ray diffraction (XRD) patterns of the samples were measured on a specifically designed *Bruker AXS C2* diffractometer seen in Figure 3.3.2. The benefit of this instrument is the completely automated design. The samples were measured directly off the multi-electrode plate where they were prepared. The coordinates of the samples were then programmed into the GADS controlling software and the movable x, y, z stage sequentially moved over each sample in turn. The measurement was accelerated by the use of a general area detector to measure the diffracted rays. This type of instrumentation has previously been used successfully in high throughput experiments of positive battery electrode materials [2, 6], where identical substrate and electrode setups were used. An acquisition time of 5 minutes per sample was used to measure over the whole 2θ range.

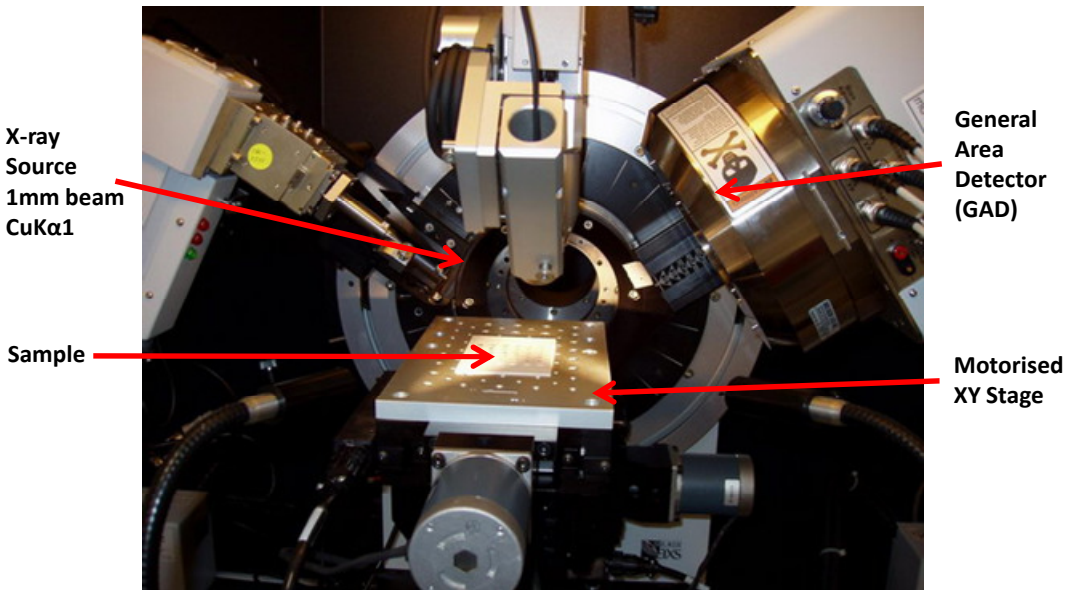

Figure 3.3.2 Bruker AXS C2 diffractometer.

By contrast with PVdF homopolymer which is mainly crystalline, PVdF-HFP polymers are mainly amorphous. The amorphous structures are a key influence on the conductive properties of the material because the mobility of any ionic species due to added salt should depend on whether a salt-polymer interaction causes dissolution (and thus conductivity) of the salt or not. Figure 3.3.3 shows the diffraction pattern of a pure PVdF-HFP sample. When this is compared to the diffraction pattern of a PVdF homopolymer [7], the same characteristic peaks appear at 2θ = 18.4, 20 and 26.7 representing the (100), (020) and (110) reflections. These reflections are known to be typical for the orthorhombic cell of neat PVdF in its crystalline form. The occurrence of the same values for both the homo and copolymers, indicates that the copolymer is indeed semi-crystalline. The intensity of the peaks does fluctuate somewhat indicating that the structures are not identical.

Unfortunately, the instrumentation did not allow water exclusion and it was not possible to encapsulate the samples without attenuating the x-ray output. Therefore the results indicate the effect of both salt and water on the polymer. By contrast with conductivity experiments, however the effect of water is expected to be minimal because of the hydrophobic nature of this polymer.

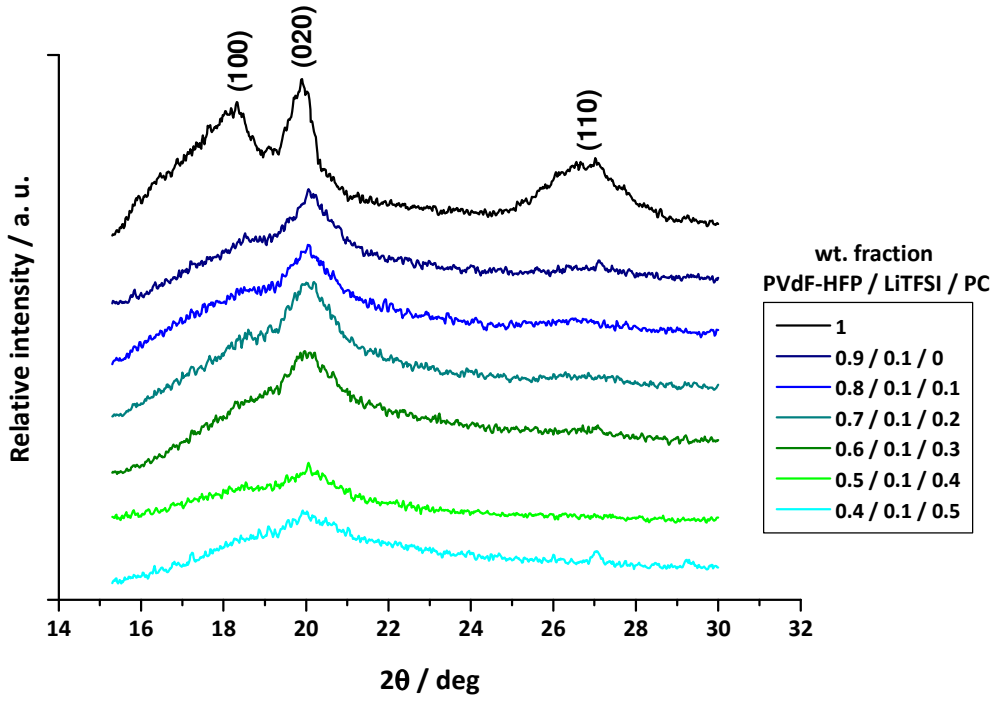

Figure 3.3.3 X-ray diffraction patterns of pure PVdF-HFP and different weight fractions of LiTFSI and PC.

When the LiTFSI salt is added to the polymer the diffraction patterns begin to change. There is a disappearance of the reflections at 2θ = 18.4 and 26.7 along with a broadening of the reflection at 2θ = 20. This would indicate some plasticisation of the polymer by the salt, possibly aided by absorbed water. In addition, when the samples contain PC, the broadening of the reflection at 2θ = 20 is significantly increased. Similar findings have been reported when using PVdF-HFP with ionic liquids [8], but results for gel electrolytes of PVdF-HFP and LiTFSI [9-11] are more pertinent to this work. Studies of crystallinity and morphology of PVdF-HFP with LiTFSI and numerous plasticising solvents have also seen similar salt effects [12]. The findings in [13], when using samples of copolymer, lithium salt and plasticiser presented only one remaining reflection at 2θ = 20, which could be attributed to either of the polar phases I or III. The result is consistent with the expectation that salt would stabilise the polar phases with respect to the non-polar phase II. Similar works have commented on this finding and deduced that the addition of LiTFSI or other ionic species [10, 14] has reduced the crystallinity of the PVdF-HFP and increased the amount of amorphous domains in the sample.

3.4 Chapter 3 Conclusions

- High-throughput methods of preparation for ternary systems using liquid mixing of a polymer, lithium salt and plasticising solvent have been successfully demonstrated using manual pipetting techniques.

- The preparation of a complete compositional spread enabled elimination of unsuitable samples for the measuring technique based on their mechanical properties.

- The HT technique provides general information on the system whilst using much smaller quantities of material than conventional methods would for comparable data.

- Fast sequential impedance measurements have been performed in a combinatorial cell for compositionally different samples.

- Impedance data can be batch fitted to determine sample resistance and conductivity, while the process of sample repeats gives indications into the reliability of the technique.

- Ternary composition plots can be mapped for conductivity allowing trends based on composition to be seen.

- The mulit-electrode array plate can easily be transferred to a combinatorial XRD machine and spectra recorded by machine automation.

- This method has of obtaining conductivity data in this manner is novel and has not been published before on such a system as PVdF-HFP/LiTFSI/PC.

- The results from impedance, DSC and XRD may suggest that PVdF-HFP is able to solvate LiTFSI to some extent.

3.5 Chapter 3 References

1. A. D. Spong, G. Vitins, S. Guerin, B. E. Hayden, A. E. Russell and J. R. Owen, *Journal of Power Sources*, 2003, **119**, 778-783.

2. M. R. Roberts, A. D. Spong, G. Vitins and J. R. Owen, *Journal of The Electrochemical Society*, 2007, **154**, A921-A928.

3. D. Linden, ed., *Handbook of Batteries*, 2 edn., McGraw-Hill, Inc, New York, 1995.

4. A. Manuel Stephan, K. S. Nahm, T. Prem Kumar, M. A. Kulandainathan, G. Ravi and J. Wilson, *Journal of Power Sources*, **In Press, Corrected Proof**.

5. A. K. A. N. S. Mohamed, *physica status solidi (a)*, 2004, **201**, 3096-3101.

6. M. R. Roberts, G. Vitins and J. R. Owen, *Journal of Power Sources*, 2008, **179**, 754-762.

7. Z. Jiang, B. Carroll and K. M. Abraham, *Electrochimica Acta*, 1997, **42**, 2667-2677.

8. S. H. Yeon, K. S. Kim, S. Choi, J. H. Cha and H. Lee, *J. Phys. Chem. B*, 2005, **109**, 17928-17935.

9. A. M. Voice, J. P. Southall, V. Rogers, K. H. Matthews, G. R. Davies, J. E. Mcintyre and I. M. Ward, *Polymer*, 1994, **35**, 3363-3372.

10. A. M. Stephan, K. S. Nahm, M. A. Kulandainathan, G. Ravi and J. Wilson, *Journal of Applied Electrochemistry*, 2006, **36**, 1091-1097.

11. A. M. Stephan, S. G. Kumar, N. G. Renganathan and M. A. Kulandainathan, *European Polymer Journal*, 2005, **41**, 15-21.

12. S. Abbrent, J. Plestil, D. Hlavata, J. Lindgren, J. Tegenfeldt and A. Wendsjo, *Polymer*, 2001, **42**, 1407-1416.

13. A. M. Stephan, K. S. Nahm, T. P. Kumar, M. A. Kulandainathan, G. Ravi and J. Wilson, *Journal of Power Sources*, 2006, **159**, 1316-1321.

14. J.-H. Cao, B.-K. Zhu and Y.-Y. Xu, *Journal of Membrane Science*, 2006, **281**, 446-453.

Chapter 4

Experimental – H^+ Conducting PEM's

Chapter 4 Experimental – H^+ Conducting PEM's

4.1 Nafion

Nafion is the most well known proton conducting polymer membrane to date. As mentioned in the introduction, Nafion is used in the majority of commercial H_2 / air fuel cells, but it still has major drawbacks in its properties. Due to this not only are groups researching new alternatives, but modifications to Nafion are also being considered.

Although it was not possible to any physical modification such as grafting, or a complete synthesis of a Nafion polymer system due to the chemistry involved with fluorinated molecules, commercially available Nafion samples were studied by other methods.

4.1.1 Starting Materials

Nafion 117 (EW 1100, thickness 180 µm), Nafion 112 (EW 1100, dry thickness 50 µm), Nafion perfluorinated ion-exchange resin (20 wt. % in solution of aliphatic alcohols and 20 wt. % H_2O, EW 1100) were purchased from Aldrich. A Nafion 115 (EW 1100, thickness 130 µm) was obtained *en gratis* from other sources. A Nafion alternative was kindly provided by Johnson Matthey in the form of JM N117 and JM N115 with nominal thicknesses of 170 µm and 125 µm, respectively. A Johnson Matthey perfluorosulfonic acid-PTFE copolymer solution (5 wt % in aliphatic alcohols and H_2O,) was purchased from Alfa Aesar. Propan-2-ol (Fisher, Reagent Grade), Acetonitrile (ACN) (Fisher, Reagent Grade), Cyclopentanone (CP) (Fisher, Reagent Grade), Dimethylformamide (DMF) (Fisher, Reagent Grade), ethylene glycol (EG) (Fisher, puriss, 99.5 %), 0.5 M sulphuric acid (H_2SO_4) (Riedel-de-Haen, Volumetric Standard Grade) and 6 % w/v hydrogen peroxide (H_2O_2) (Timstar, Laboratory Grade) were used 'as-received'.

4.1.2 Preparation from solution

Membranes were prepared using the Nafion® solution and the perfluorosulfonic acid solution. Both solutions were initially in proton form. The first experiment involved casting directly from the solution into a glass petri dish before evaporating off the

solvents. In the second experiment, the polymer solutions were concentrated down and then a higher boiling point co-solvent was added before casting. The observations on the membranes that were fabricated can be seen in Table 4.1.1.

Table 4.1.1 Table showing the solvents added and their properties with any visual observations.

Sample	Solvent	Solvent B_{pt} (° C)	Film Appearance	Observations
ALD 1	None	-	-	No film formed, only yellowy agglomerates
ALD 2	Propan-2-ol	80	Clear	Good mechanical strength, poor elasticity
ALD 3	ACN	81	Pale yellow	Good mechanical strength and elasticity
ALD 4	CP	130	Dark brown	Good mechanical strength, poor elasticity
ALD 5	DMF	153	Pale yellow	Good mechanical strength and elasticity
ALD 6	EG	197	Clear	Good mechanical strength and elasticity
JM 1	None	-	Clear	Good mechanical strength and elasticity
JM 2	Propan-2-ol	80	Clear	Good mechanical strength and elasticity
JM 3	ACN	81	Pale yellow	Good mechanical strength and elasticity
JM 4	CP	130	Brown	Good mechanical strength and elasticity
JM 5	DMF	153	Clear	Good mechanical strength and elasticity
JM 6	EG	197	Clear	Good mechanical strength and elasticity

The Aldrich purchased Nafion solution performed less than ideally when it was cast neat. At ambient drying temperatures cracking was clearly visible as the co-solvent evaporated off. The majority of samples after removal of all co-solvent appeared as a brittle shattered mass of material. By comparison, the membranes that were cast with a secondary solvent formed smooth films similar to that of the purchased extruded membrane. The difference in quality of the two types of membranes can be seen in Figure 4.1.1.

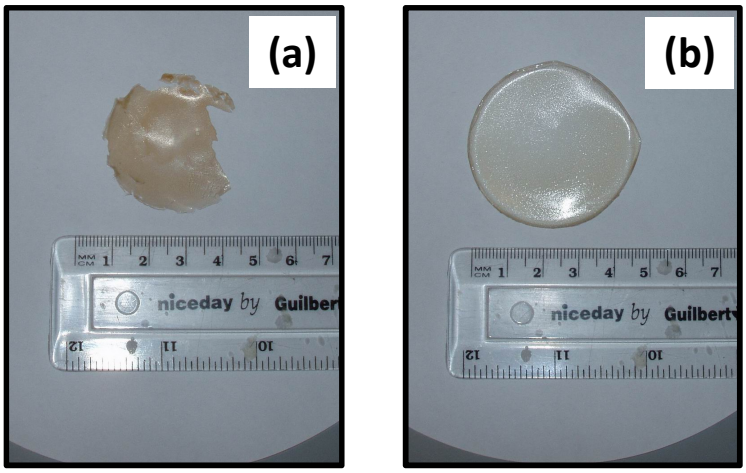

Figure 4.1.1 Image of solution cast Ald Nafion membranes (a) cast from neat solution, (b) cast with DMF.

The first image in Figure 4.1.1 shows a film that was cast directly from solution, while the second shows a recast film using DMF as the co-solvent. The quality of the neat cast membrane is seen to be visibly poor. At this point, by using gravimetric measurements, the film was found to still have retained some of the aliphatic alcohols and water that the polymer was dissolved in. This allowed it to maintain a solid shape and be removed from the Petri dish. After complete evaporation of the solvent, there was no resemblance to the partial film seen above, only small agglomerates. The difference between the two samples in Figure 4.1.1 was initially thought to be due to the volatility of the solvent used, with the less volatile solvent allowing slower and more controlled evaporation. However, the Johnson Matthey samples cast from the neat solution did not suffer from the same film deformation. Since the polymers were processed by the two companies using slightly different methods, the problem encountered with the Aldrich samples was deemed to be a solubility issue. The

characteristics of the Aldrich sample behaved not as true solutions but as suspensions of the Nafion in the alcohol-water mixture.

In addition to the observation just mentioned, from Table 4.1.1 the colour of some of the membranes can be seen to be not of the normal transparency associated with the extruded membranes. The dark brown colour of the cyclopentanone films is possibly attributed to a polymerisation reaction occurring due to the super-acid behaviour of Nafion (pKa = -6) and cyclopentanone is therefore unsuitable for use as a solvent. Other films that exhibited colour change, turned clear upon immersion in concentrated sulfuric acid. This has been described in the literature previously [1] when samples have been annealed above the polymers glass transition temperature (T_g). Before testing the conductivity, the samples were pre-treated, the method of which is described in the following section.

4.1.3 Preparation from Extruded Membrane

The extruded membranes were used 'as-received'. As with all other samples, they were pre-treated before conductivity testing was performed. This is the standard literature procedure for preparing H^+ membranes for use [2]. This involved immersion in boiling H_2O_2 for one hour, boiling in de-ionised (DI) H_2O for one hour, heating in 0.5 M H_2SO_4 at 150 ° C for one hour and then finally boiling in H_2O for 12 hours. This pre-treatment was deemed to remove any organic impurities by H_2O_2, while the H_2SO_4 removed any inorganic impurities and ensured that all ion-exchange sites were protonated.

4.2 Synthesis of Sulfonated Poly(ether ether ketone)

Due to the difficulties in processing Nafion from its solution form, it was decided that another type of proton conducting polymer would be studied. Sulfonated poly (ether ether ketone) belongs to the new group of aromatic polymers that are being investigated as the alternative to the current commercial PEM's. The benefit of this particular type polymer is the ease of synthesis and greater control of the addition of the active sulfonic acid group which facilitates the proton transport within the polymer membrane.

4.2.1 Starting Materials

Poly(ether ether ketone) (PEEK), 450G (average M_W. ≈ 40,000) was kindly provided by Victrex® Plc. and dried under vacuum at 100 °C for 24 hours before use. Concentrated sulphuric acid (H_2SO_4), (Fisher, 98 wt %, Reagent Grade) was used as received. Water used was either DI or purified. For casting of the membranes, Dimethyl Sulfoxide (DMSO) (Alfa Aesar, 99 %), N-methyl-2-pyrrolidinone (NMP), (Aldrich, 99 + % ACS Reagent), *N*,*N*-Dimethyl acetamide (DMAc) (Aldrich, Reagent Grade) and *N*,*N*-Dimethyl formamide (DMF), (Fisher, Reagent Grade) were used as received.

4.2.2 Preparation of Raw SPEEK

The reaction was carried out on a magnetic stirrer plate with constant vigorous agitation. 20 g of dried PEEK powder was added slowly to a beaker containing 500 ml of concentrated H_2SO_4 and was mechanically stirred. The temperature of the initial reactants was 21 ± 1.5 °C, however the solution rose to 37 °C on addition of PEEK to the acid. Upon adding the granules to the acid, the colour of the solution also changed to light orange initially and after full dissolution of the PEEK the colour changed to dark brown as shown in Figure 4.2.1. This is a common colour change for sulfonation reactions involving benzene sulfonation.

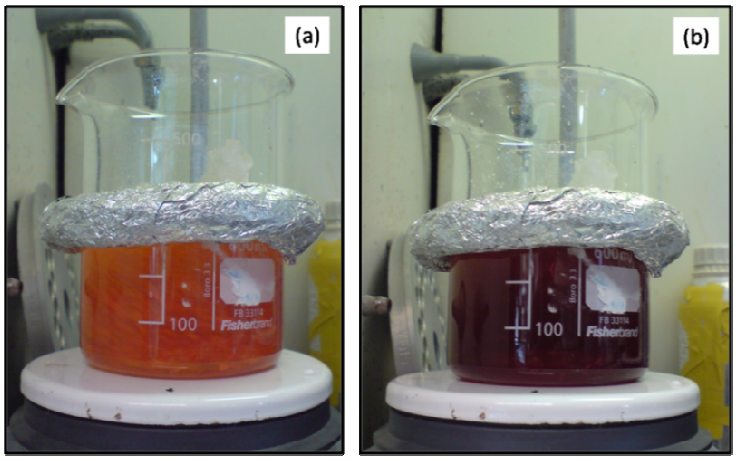

Figure 4.2.1 Solutions from (a) initial addition of PEEK and (b) complete dissolution of PEEK in conc. H_2SO_4.

All times of reaction were measured from the time of addition of the PEEK to the acid. The initial screening of the sulfonation time proceeded by removing 10 ml of solution periodically (*c.a.* 2 hours) and quenching in an excess of mechanically stirred ice cold water. This was necessary due to the exothermic nature of the reaction of the acid with water. This also prevented the precipitate from forming a dense mass at the bottom of the beaker. In addition, the stirring of the water allowed noodle like strands (Figure 4.2.2) of the polymer to form as the acid solution was added. The newly formed precipitate was then filtered and washed in water till the washings were pH neutral. The SPEEK was then stored in pure water until it was cast into a membrane to prevent any acid catalysed cross linking which occurs when the polymer is stored under dry conditions for prolonged periods of time.

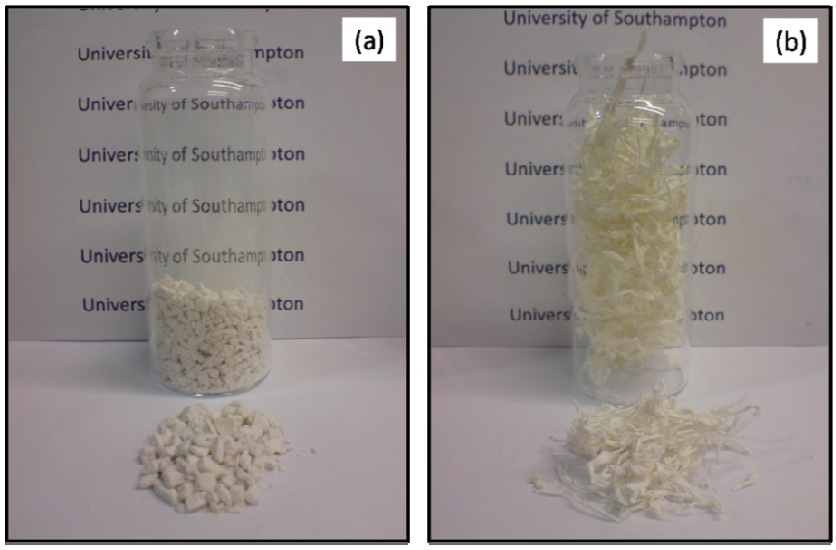

Figure 4.2.2 (a) Granules of PEEK, and (b) SPEEK noodle strands.

The synthesis was also performed using a high-throughput parallel synthesis method. In this case the same quantity (*c.a.* 0.3 g) of raw PEEK was placed in a 2 dram vial on a multi-stirring carousel plate shown in Figure 4.2.3.

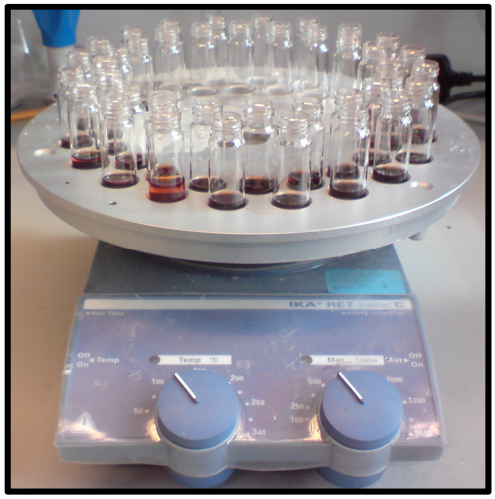

Figure 4.2.3 High-throughput parallel synthesis of SPEEK.

Sulfuric acid was added to make approximately a 3 wt. % solution and the solution was mechanically stirred. At the specified time intervals, a vial was removed and the

reaction quenched as described earlier. This method of preparation was particularly useful for synthesising the samples for testing using ^1H NMR.

The reaction follows that of Figure 4.2.4 whereby PEEK is sulfonated via an electrophilic aromatic substitution.

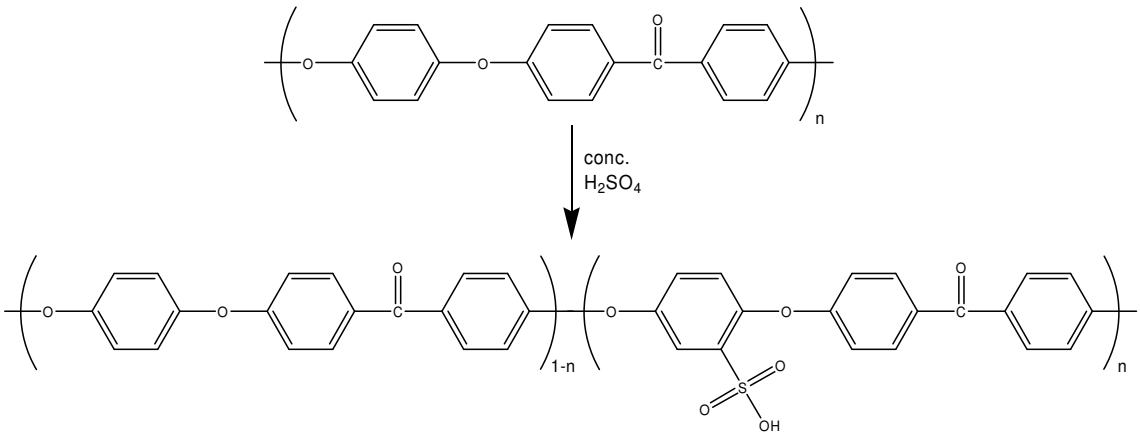

Figure 4.2.4 Reaction scheme of the sulfonation of PEEK to SPEEK.

The sulfonation process provides a maximum of one sulfonic acid group per repeat unit and is located at one of the four chemically equivalent positions of the phenyl ring surrounded by two ether groups. There are two reasons behind this. Firstly the other two phenyl rings are deactivated for the electrophilic substitution by the electron-withdrawing effect of the carbonyl function, and secondly once a sulfonic acid group is introduced, the electron withdrawing nature of the group prevents any further substitution on the same unit. One problem that can arise in this reaction is the crosslinking of the sulfone group which can occur in very concentrated acidic environments. However in this work, no chemical degradation or sulfone crosslinking were observed as the concentration of the acid remained below 100 % as the presence of water drove the equilibrium back to the left. Evidence of crosslinking would have been visible in the brittleness of the dried polymer. This was however observed in samples that were stored in their dry form. In this case any residual acidity would have been concentrated enough to promote the crosslinking reaction, and subsequent preparations were stored in water after the neutralisation process thereafter.

One area of consideration with this reaction is that the starting material is only soluble in concentrated acids. The polymer only becomes soluble in other solvents after a

certain percentage of sulfonic acid groups have been introduced. The reason behind this solubility behaviour is due to the hydrophobic nature of the PEEK. The introduction of sulfonic acid groups adds clusters of hydrophilic domains, increasing the solubility. This phenomenon was seen in samples that were reacted for shorter periods of time in that after quenching and drying they were left insoluble in both casting solvents and deuterated solvents. However, the opposite occurred when reacting the PEEK for longer periods of time. The high level of sulfonic acid groups provided more hydrophilic domains that hydrophobic, and upon quenching of the reaction, no precipitate was formed in the water. Instead a very fine suspension of particles was left which when filtered and on drying formed a hard solid mass and was unsuitable for any further use.

4.2.3 Preparation of SPEEK Membrane

The SPEEK membranes were prepared by using a solution casting technique. The raw SPEEK after being stored in pure water was dried for 24 hours at 80 ° C. Immediately a 5 weight percent solution was prepared in the casting solvent. Initially three casting solvents were used, namely DMF, DMAc and NMP. To remove the solvent, the membrane was dried at 80 ° C for 2 days, and then a further 48 hours at 110 ° C. After this time period it was deemed that all solvent traces had been removed. Before use, the SPEEK membranes were subjected to the same pre-treatment that the Nafion samples were.

Unlike the solution cast Nafion membranes, which had varying properties depending on the casting solvent, the SPEEK samples had very good mechanical properties to the touch and appeared very similar to the extruded Nafion membrane in quality. The samples had different levels of opaqueness which were dependent on the reaction time which was also found by [3] and can be seen in Figure 4.2.5.

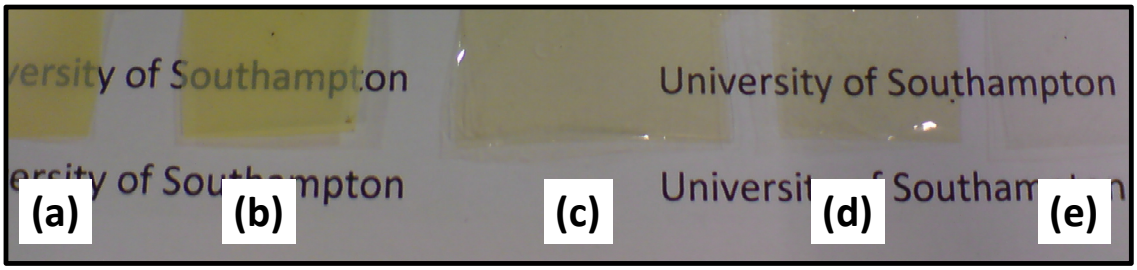

Figure 4.2.5 Appearance of (a) SPEEK-47, (b) SPEEK-57, (c) SPEEK-63, (d) SPEEK-75 and (e) SPEEK-80 membranes.

The image above in Figure 4.2.4 shows 5 different SPEEK samples, (a) being the shortest reaction time and (e) being the longest reaction time at 24 hour intervals. The difference in appearance of the samples is clearly seen and may be due to variation in the morphology.

4.3 Characterisation of SPEEK Polymer

4.3.1 Degree of Sulfonation Determination

The degree of sulfonation (DS) of the polymer gives a percentage of sulfonated groups per repeat polymer unit. This can also be related to a materials ion-exchange capacity (IEC) which is a quantified by the number of fixed ionic groups per unit weight under specific conditions, and the equivalent weight (EW) which is the reciprocal of the IEC. The DS and IEC can be experimentally determined *via* two methods for verification of the results namely proton nuclear magnetic resonance (^{1}H NMR) and titration analysis.

4.3.2 Starting Materials

For the ^{1}H NMR experiments, the deuterated solvent used was Dimethyl Sulfoxide (DMSO-d_6) (Aldrich, 99.9 atom % D). For the titration analysis, sodium chloride (NaCl) (Fluka, 0.1 M Standard Solution), sodium hydroxide (NaOH) (Riedel-de-Haen, 0.1 M Volumetric Standard Grade) and phenolphthalein indicator (Fisher) were used as received.

4.3.2.1 ^{1}H NMR Analysis

The ^{1}H NMR method for the determination of the DS of SPEEK is well documented in the literature as the primary method of analysis [4-7]. The samples were dried at 70 ° C for 24 hours prior to dissolving in DMSO-d_6 to make a 2 - 5 wt % solution. All experiments were carried out on a Bruker AV300/1 spectrometer at a resonance frequency of 300 MHz with tetramethylsiloxane (TMS) used as the internal standard.

The reaction in Figure 4.2.4 shows the expected sulfonated copolymer consisting of n SPEEK units and (1-n) PEEK units. The nomenclature of the aromatic protons in the SPEEK copolymer is shown in Figure 4.3.1.

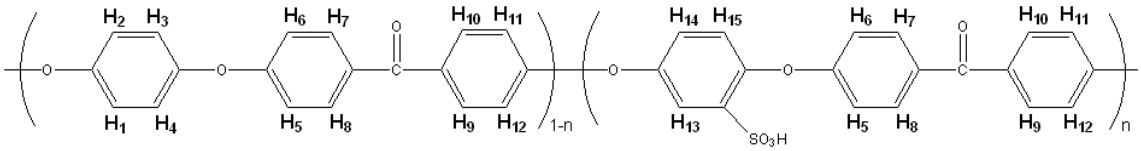

Figure 4.3.1 Nomenclature of the aromatic protons in the SPEEK copolymer.

The number of different protons in each polymer unit can be calculated based upon the protons of particular type in each unit as demonstrated in Table 4.3.1.

Table 4.3.1 Calculation of hydrogen's in each polymer unit.

Unit	H_{13}	H_{other}
(1-n)	0	12(1-n)
n	1	10n
	n	**(12-2n)**

The protons are labelled with respect to their chemical equivalence and environment. The hydrogen atoms, $H_{1,2,3,4}$, contained within the hydroquinone group of the PEEK unit are equivalent to each other. On the other two aromatic rings separated by the carbonyl group, $H_{5,6,11,12}$, on the ether sides of the rings are equivalent, and $H_{7,8,9,10}$, positioned adjacent to the carbonyl group are also equivalent. With the addition of the sulfonic acid group, H_4 is removed. Consequently the three remaining hydrogen's change equivalence to each become separate signals H_{13}, H_{14} and H_{15}.

The DS of the polymer is calculated based on the relationship between the intensity of the alpha hydrogen (adjacent to the sulfonic acid group), and the intensity of all other aromatic hydrogen's. So it follows that the DS may be defined by the integrated peak area of the alpha hydrogen divided by the integrated peak areas of all other hydrogen atoms defined by Equation 4.3.1.

$$\frac{n}{(12-2n)} = \frac{\Sigma H_{13}}{\Sigma H_{1,2,3,4,5,6,7,8,9,10,11,12,14,15}}$$

Equation 4.3.1

Where the DS = n, and $0 \leq n \leq 1$.

The characteristic peaks of each proton may be identified by a typical SPEEK sample as shown in the spectra of Figure 4.3.2.

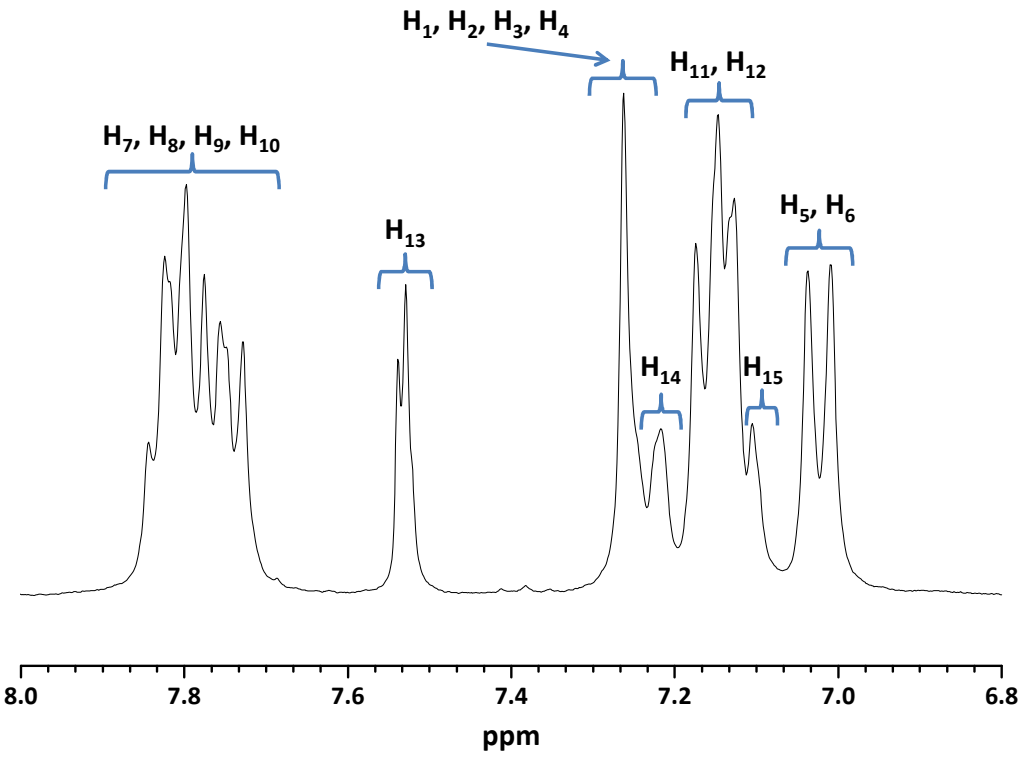

Figure 4.3.2 ^{1}H NMR spectra of a typical SPEEK sample in DMSO-d_6.

When the DS is low the majority of polymer remains as PEEK units. The H_1, H_2, H_3 and H_4 on these PEEK units show their characteristic singlet at around 7.25 ppm, while H_7, H_8, H_9 and H_{10} appear at low field due to the deshielding from the carbonyl group. In the units that contain the sulfonic acid group, a number of protons are affected by the electron rich property of the group. H_5 and H_6 are a doublet which is shifted upfield to 7.05 ppm due to the proximity of the group, but H_{11} and H_{12} remain unaffected at 7.15 ppm. On the hydroquinone ring, the presence of the sulfonic acid group causes a down-field shift of approximately 0.25 ppm of H_{13} to ≈ 7.5 ppm compared with the other hydrogen atoms. This results in a distinct signal for the proton adjacent to the sulfonic acid group which is equivalent to the sulfonic acid content and increases in intensity as the DS increases. Subsequently the other two protons change where H_{14} is a doublet of doublets due to its interaction with H_{13} through four bond coupling as well as with H_{15}

through three bond coupling [8]. The DS of a range of samples which were calculated using Equation 4.3.1 can be seen in Table 4.3.2.

Table 4.3.2 Calculation of DS from integrated values of SPEEK samples from ^{1}H NMR.

Reaction time / h	H_{13}	H_{other}	DS
24	0.12	2.81	0.47
48	0.15	2.72	0.57
72	0.16	2.69	0.63
96	0.19	2.63	0.75
122	0.2	2.61	0.80

The above table shows how upon increasing the reaction time leads to an increase in the DS. The effect can be more prominently seen in Figure 4.3.3, which shows five representative spectra with experimental times ranging from 24 – 122 hours. The peak ratio between the H_{13} proton and the other peak signals is seen to increase with reaction time.

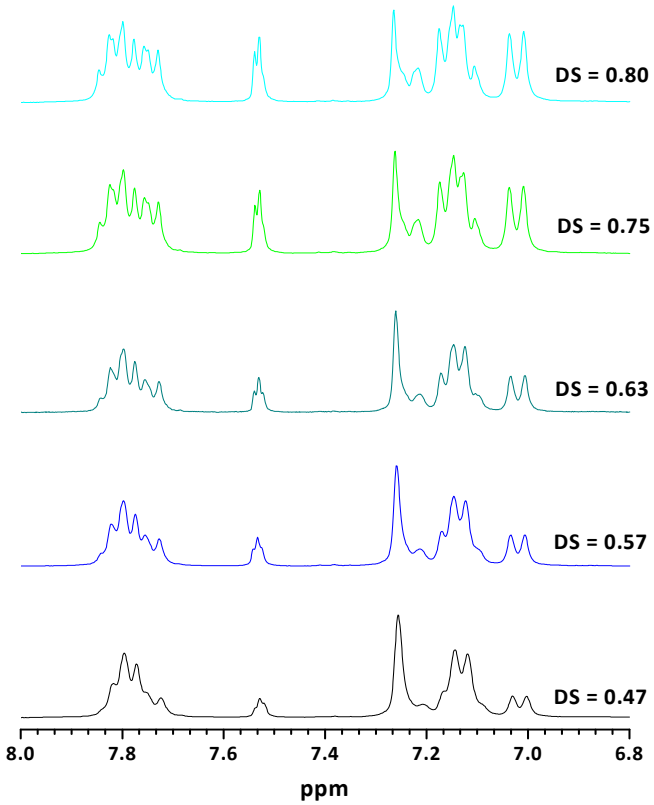

Figure 4.3.3 ^{1}H NMR spectra of SPEEK samples in DMSO-d_6.

4.3.2.2 Titration Analysis

When the IEC was determined by titration analysis, the sample was firstly immersed in dilute H_2SO_4 to ensure it was fully protonated. The removal of any traces of acid was performed by soaking and repeatedly rinsing in H_2O before drying at 110 ° C for 24 hours. Approximately 0.5 g of dried SPEEK was weighed before immersing into a known volume of 0.1 M NaCl. The solution was mechanically stirred for 48 hours which was considered enough time for complete ion exchange of the material [9]. If the material is assumed to have all sulfonic acid protons present available for ion exchange, then the reaction follows that of Equation 4.3.2.

$$SPEEK_H + NaCl \rightarrow \mathrm{SPEEK_{Na}} + \mathrm{HCl}$$

Equation 4.3.2

The solution was then back titrated against 0.1 M NaOH using phenolphthalein as the indicator to determine the neutral point [10-12]. By measuring the amount of NaOH consumed in the titration, the molar quantity of the sulphuric acid groups contained in the $SPEEK_H$ can be determined by Equation 4.3.3,

$$N'_{SPEEK_{Na}} = (c\ x\ V')_{NaCl} - (c\ x\ V')_{NaOH}$$

Equation 4.3.3

where *N'* is the number of moles, *c* is the molar concentration and *V'* is the volume of solution used. Using the value of $N'_{SPEEK\text{-}Na}$, where $N'_{SPEEK\text{-}Na}$ equals $N'_{SPEEK\text{-}H}$, then the IEC can be estimated using Equation 4.3.4, where *W'* is the sample weight.

$$IEC = \frac{N'_{SPEEK_H}}{W'_{sample}}\ x\ 1000\ (meq/g)$$

Equation 4.3.4

So in 1 g of $SPEEK_{Na}$ sample there are N'_x number of moles of $SPEEK_{Na}$ and N'_Y moles of PEEK. Using Equation 4.3.5 and Equation 4.3.6, N'_x and N'_y can be determined where $Mw_{SPEEK\text{-}Na}$ and Mw_{SPEEK} are the molecular weights of $SPEEK_{Na}$ and PEEK being 390 and 288 respectively.

$$N'_x = 0.001\ x\ IEC$$

Equation 4.3.5

$$N'_y = \frac{1 - \left(0.001\ x\ IEC\ x\ M_{W_{SPEEK_{Na}}}\right)}{M_{W_{PEEK}}}$$

Equation 4.3.6

The DS is defined as the number of individual polymer repeat units which have been sulfonated as a percentage of the total number of polymer repeat units available in the

reaction mixture solution containing the reacting polymer. In this case the DS can be defined by Equation 4.3.7.

$$DS = \frac{N'_x}{N'_x + N'_y}$$

Equation 4.3.7

By substituting Equation 4.3.5 and Equation 4.3.6 into Equation 4.3.7, the DS can be written as Equation 4.3.8.

$$DS = \frac{288(IEC)}{1000 - 102(IEC)}$$

Equation 4.3.8

If the DS is at 100 % then the maximum IEC would be 2.56 meq/g.

The titration was performed on samples with the same reaction time that were tested using ^{1}H NMR. The calculated IEC from the titrations is shown in Equation 4.3.3.

Table 4.3.3 Calculated IEC and DS from titration values of SPEEK samples.

Reaction time / h	IEC	DS
24	1.30	0.43
48	1.65	0.57
72	1.90	0.66
96	1.99	0.72
122	2.19	0.81

4.3.3 Comparison of DS Determination Methods

The difference between the ^{1}H NMR and the titration results was very small. The IEC calculated from the ^{1}H NMR data using Equation 4.3.8 gave values of 1.42, 1.67, 1.79, 2.01 and 2.16 for the reaction times 24, 48, 72, 96 and 122 hours respectively. A comparison of the DS for both techniques can be seen in Table 4.3.4.

Table 4.3.4 Comparison of DS from ^{1}H NMR and titration analysis.

Reaction time / h	$DS_{1H\ NMR}$	$DS_{Titration}$
24	0.47	0.43
48	0.57	0.57
72	0.63	0.66
96	0.75	0.72
122	0.80	0.81

With only a few DS % error between the two methods, the calculations based upon data from the ^{1}H NMR experiments was taken as the true result. This was partially due to time constraints, as if any further samples needed to be tested, the ^{1}H NMR experiments were performed a lot quicker than the titration experiments. The values that were obtained corresponded with literature calculations in that at around 120 hours an IEC of approximately 2.1 meq/g should be found [6].

It should be noted that all samples will be referred to by their degree of sulfonation which is listed below in Table 4.3.5.

Table 4.3.5 SPEEK sample naming system based upon DS.

Reaction time / h	IEC	DS	Sample name
24	1.40	0.47	SPEEK-47
48	1.65	0.57	SPEEK-57
72	1.79	0.63	SPEEK-63
96	2.05	0.75	SPEEK-75
122	2.18	0.80	SPEEK-80

4.4 Comparison of Nafion and SPEEK Membranes

4.4.1 EDX Analysis

The samples were studied using energy dispersive x-ray spectroscopy (EDX) analysis for the distribution of the ion-exchange sites. The calculations in the previous sections have provided a numerical comparison between the two polymer membranes in the form of the IEC. The Nafion samples had an IEC value of 0.91 meq/g while the SPEEK samples ranged from 1.20 to 2.05 meq/g. While the distribution of the proton sites in the Nafion is assumed to be uniform across the sample as the manufacturing process has been optimised, the uniformity of the proton sites in the SPEEK is unknown. By mapping a known area of each sample for sulfur sites, the distribution could be compared.

The images obtained can be seen in Figure 4.4.1.

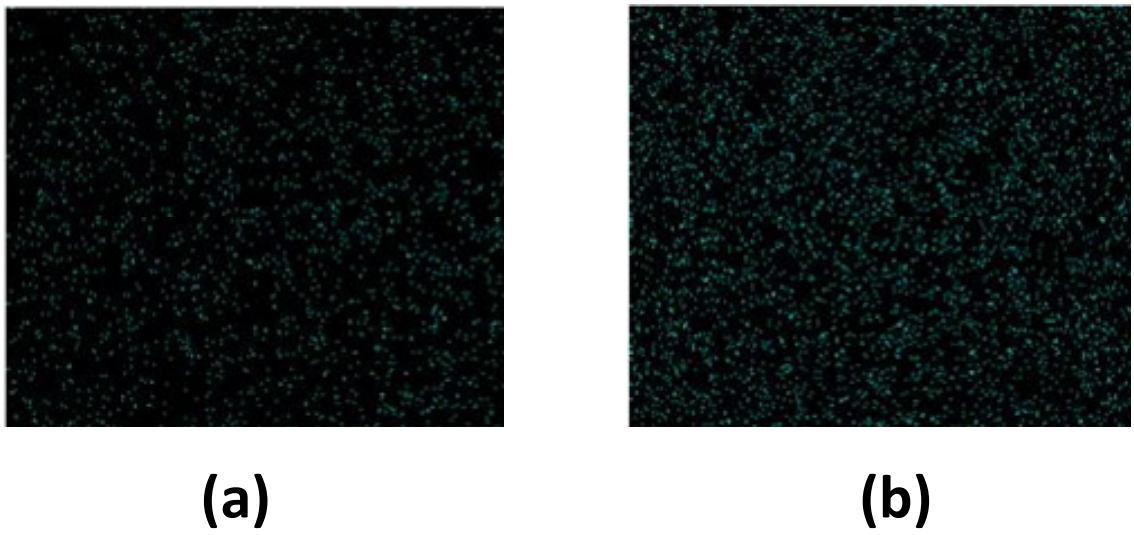

Figure 4.4.1 EDX images of (a) Aldrich Nafion 117 and (b) SPEEK-75.

There is a clear uniformity in both samples with regards to the distribution of sulfur, and it is also recognised that there is a greater quantity of sulfur sites in the SPEEK than the Nafion. These images confirm that no aggregation has occurred in the SPEEK samples, and the denser distribution can be assumed to be from the higher IEC value of the SPEEK.

4.5 Chapter 4 Conclusions

- Nafion samples were cast directly from Aldrich and Johnson Matthey supplied solutions. Using the Aldrich solution, freestanding films were not able to be formed after casting. The Johnson Matthey solution did allow a mechanically stable freestanding film.

- By concentrating the as received solutions and adding a co-solvent, improved films were produced in both cases.

- SPEEK was successfully synthesised from PEEK with a number of different reaction times.

- Characterisation of the SPEEK using ^1H NMR and titration analysis ascertained that the DS could be markedly altered by extending the reaction time of the synthesis step. The two methods also gave close agreement of their DS and IEC values.

4.6 Chapter 4 References

1. G. Alberti, M. Casciola, A. Donnadio, R. Narducci, M. Pica and M. Sganappa, *Desalination*, 2006, **199**, 280-282.

2. V. Basura, P. Beattie and S. Holdcroft, *Journal of Electroanalytical Chemistry*, 1998, **458**, 1-5.

3. P. Xing, G. P. Robertson, M. D. Guiver, S. D. Mikhailenko, K. Wang and S. Kaliaguine, *Journal of Membrane Science*, 2004, **229**, 95-106.

4. H.-L. Wu, C.-C. M. Ma, F.-Y. Liu, C.-Y. Chen, S.-J. Lee and C.-L. Chiang, *European Polymer Journal*, 2006, **42**, 1688-1695.

5. H.-Y. Jung and J.-K. Park, *Electrochimica Acta*, 2007, **52**, 7464-7468.

6. S. M. J. Zaidi, S. D. Mikhailenko, G. P. Robertson, M. D. Guiver and S. Kaliaguine, *Journal of Membrane Science*, 2000, **173**, 17-34.

7. S. Kaliaguine, S. D. Mikhailenko, K. P. Wang, P. Xing, G. Robertson and M. Guiver, *Catalysis Today*, 2003, **82**, 213-222.

8. G. P. Robertson, S. D. Mikhailenko, K. Wang, P. Xing, M. D. Guiver and S. Kaliaguine, *Journal of Membrane Science*, 2003, **219**, 113-121.

9. E. B. Easton, T. D. Astill and S. Holdcroft, *Journal of The Electrochemical Society*, 2005, **152**, A752-A758.

10. D. Daoust, J. Devaux and P. Godard, *Polymer International*, 2001, **50**, 917-924.

11. R. Jiang, H. R. Kunz and J. M. Fenton, *Journal of Power Sources*, 2005, **150**, 120-128.

12. S. Kaliaguine and S. D. Mikhailenko, *New Materials for Electrochemical Systems IV. Extended Abstracts of the Fourth International Symposium on New Materials for Electrochemical Systems*, 2001, 350-351.

Chapter 5

Multi-electrode Cell Design and Calibration

Chapter 5 Multi-electrode Cell Design & Method Validation

A portion of the research was dedicated to lithium ion gel polymer electrolytes. This utilised a multi-electrode cell design, which was addressed in Chapter 3. The main research concentrated on proton conducting polymers. This involved more highly conducting systems which required the conductivity to be measured *via* the *in-plane* method.

5.1 Single Cell Prototype

Before designing a multi-electrode cell, a singular 4 electrode cell was designed which could be tested with a commercially available sample. The cell was designed so that a sample could be placed across the 4 electrodes but still allow the sample gas access so it could participate in water uptake from the environment. The single cell can be seen in Figure 5.1.1.

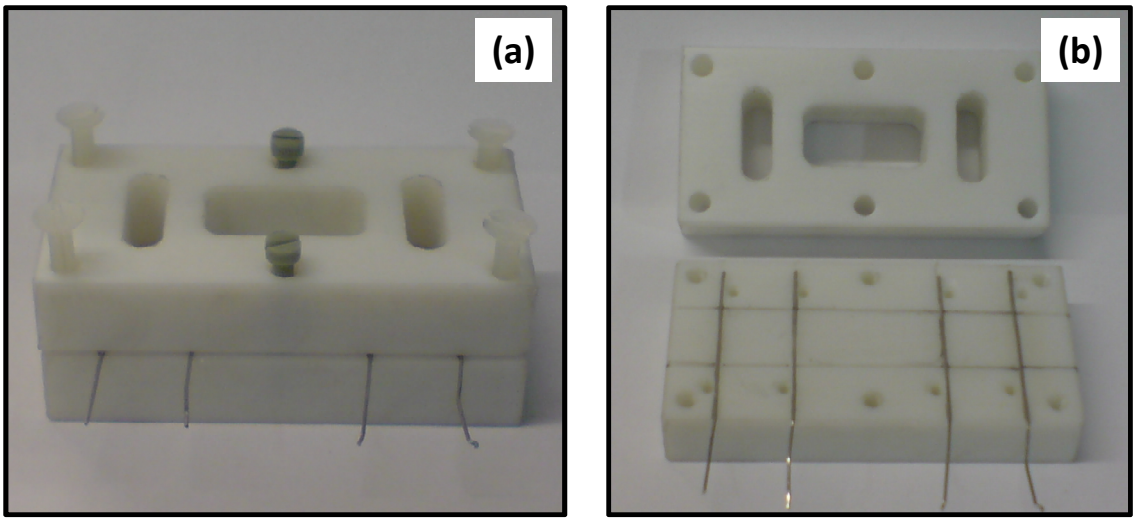

Figure 5.1.1 Image of the prototype single 4 electrode cell, (a) closed, (b) open.

The cell utilised 50 µm diameter 99.99 % platinum wires which were glued to a Teflon base plate. The Teflon lid provided the gas access over the voltage probe spacing and the counter-voltage probe spacing. The cell was tested with Nafion samples over a

range of different temperatures and reproducible conductivity values were obtained. Before a multi electrode cell was constructed, a number of problems needed to be addressed. It was initially thought that there would be some amount of difficulty in fabricating a cell which had many wires placed on a substrate. The prototype cell simply used the platinum wire adhered to the base plate, but since the tests performed with it were only short term, a better solution to gluing was needed. In addition, to ensure no corrosion reactions would occur at the sample-electrode interface, the electrodes could only be made from inert metals.

5.2 Multi-electrode Cell Design 1

This problem of electrode material was resolved by using gold which was evaporated onto the substrate *via* an inter-digitated track design. Teflon could not be used as the substrate as the surface was too rough, so a machinable glass ceramic (MACOR) substrate was used as the alternative. A mask was micro-machined so that the tracks were approximately 50 μm thick. This was then attached to the MACOR base plate and gold was evaporated onto it as seen in

Figure 5.2.1. Twenty individual electrodes can be seen, which gave a maximum of 5, 4-electrode cells, or 19, 2-electrode cells.

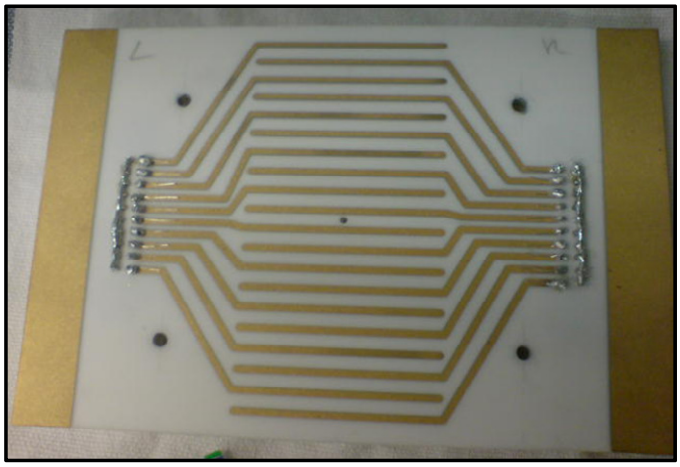

Figure 5.2.1 Image of gold plated multi-electrode cell.

Holes were drilled through the plate allowing the pins from an IDE header to be pushed through from underneath. The gold tracks were connected to the IDE pins using aluminium wire and solder so that the base plate was of similar style to a PCB board. To ensure gas access for this cell, a thin piece of meshed polypropylene was used as a lid. This did however limit the maximum working temperature to around 100 ° C for continuous usage. The connections then ran *via* ribbon cable to a connector box (Figure 5.2.2) which mirrored the layout of each connection on the plate.

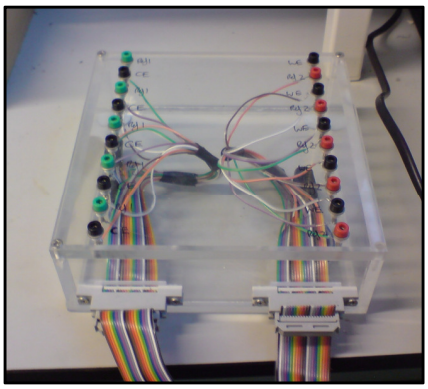

Figure 5.2.2 Connection box from multi-electrode cell to instrument.

From this box, the instrument could be connected with ease to the specific track on the cell. This particular cell proved initially very good, and it was found that using another mask, polymer membranes could be directly cast onto the substrate. However casting directly onto the plate meant that on removing the polymer, the gold was removed also. Under normal procedure of casting the membrane first and then transferring into the plate, the tracks were good for at best 5 experiments. After this time they would become worn and adhesion was lost in some places due to general wear and tear. Since only a small amount of gold was required in the evaporation process, the cost was relatively low, making it possible to re-evaporate after every 5 experiments or so. However, reapplication after every 5 experiments was deemed to be more of a hindrance as the connections would need to be removed, and so another design had to be conceived.

5.3 Multi-electrode Cell Design 2

The focus was turned back to the original prototype cell using the wire design. The wires needed to be held in place by some means other than glue to make it more durable. It was found that by feeding the wire through holes from the bottom of a Teflon plate to the top where the contact with the membrane would be, that the wire would stay in a fixed position. Using some high temperature ceramic glue in the holes and at the end of the wire, the tautness could be increased to a satisfactory level before affixing to the IDE pins. The same design as the gold plated cell was retained in that the 20 individual electrodes were present (

Figure 5.3.1).

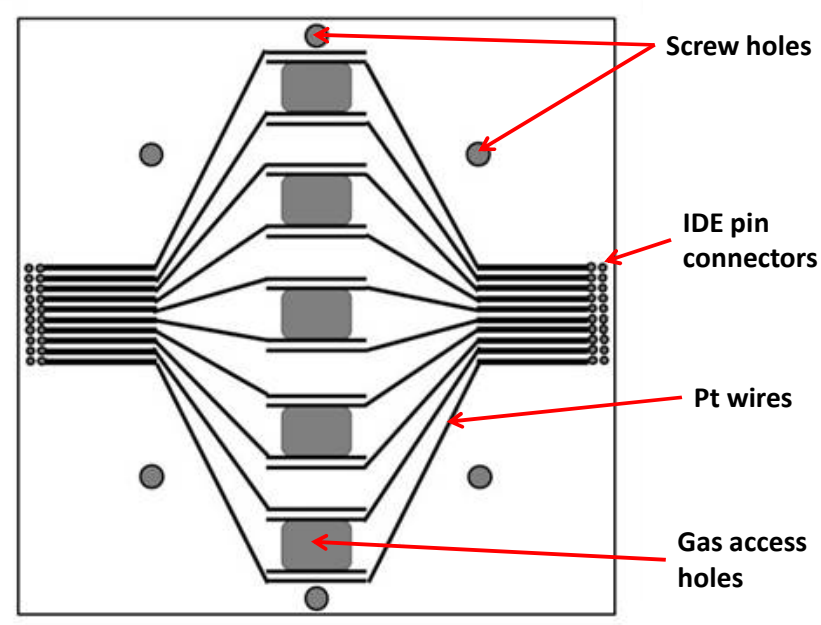

Figure 5.3.1 Schematic of the Pt wire multi-electrode cell base plate.

Another major difference is that the number of gas access holes had increased. Not only did the lid which was also constructed of Teflon have larger holes, but the base plate had holes between the two voltage probe electrodes. This can be seen in more detail in the image in Figure 5.3.2.

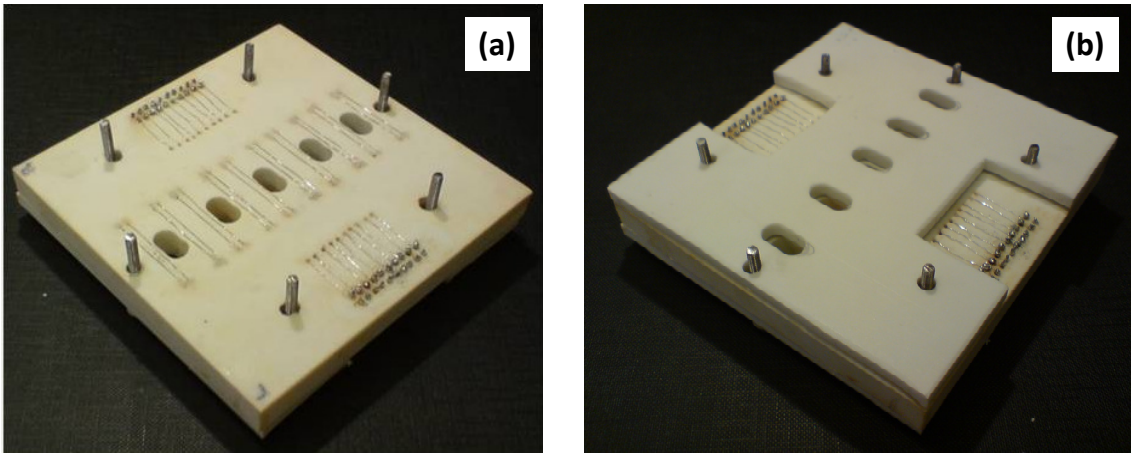

Figure 5.3.2 Image of the Pt wire multi-electrode cell, (a) base plate, (b) complete cell.

This second multi-electrode cell was only successful after many changes to the design as time progressed. Some specific problems that were encountered with multi-electrode cells included uniform contact which could be maintained throughout a complete experiment. This was partially due to the type of lid being used. Initial trials utilised a perforated PP lid to allow gas access, but the flexibility meant that equal pressure was not applied across the cell. Additionally, at higher temperatures the material became soft and was deemed unsuitable. It was found that using a Teflon lid provided the required rigidity with this being reinforced by a second Teflon plate under the base plate. This spread the pressure evenly across the cell and no contact problems were encountered thereon.

Other alterations to the setup included the application of aluminium foil around the cables to reduce noise. Due to the length of cabling from the instrument to the environmental chamber, the impedance data was often affected by noise. This addressed the problem to a satisfactory standard.

5.4 Calibration of WKL Chamber

The experiments that will be detailed in Chapter 6 using the Pt wire multi-electrode cell, were carried out in an environmental chamber (Weiss-Gallenkamp , WKL 34/+10) seen in Figure 5.4.1 and will hereon in be referred to as the *WKL* chamber. The chamber is able to function from 10 – 95 ° C with a 10 – 98 % relative humidity range ± 3 %

relative humidity. Above these temperatures the relative humidity is limited to ± 5 %. The maximum temperature is 160 ° C with a constancy of ± 0.5 K.

Figure 5.4.1 Picture of the WKL environmental chamber used to control temperature and relative humidity.

The *WKL* chamber was controlled using the accompanying "*Simpat!*" software. Programs were created that ramped the temperature from ambient to a higher temperature whilst keeping the relative humidity constant, and also performed relative humidity ramps whilst keeping the temperature constant. Two such programs can be seen in Figure 5.4.2 and Figure 5.4.3.

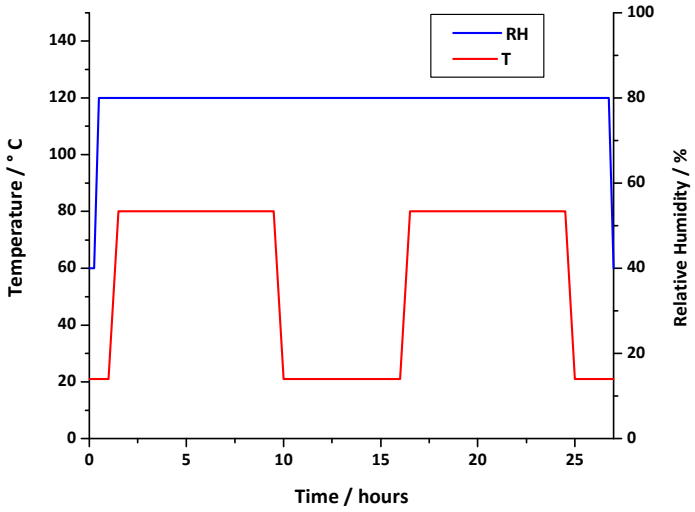

Figure 5.4.2 Temperature ramped profile at constant humidity.

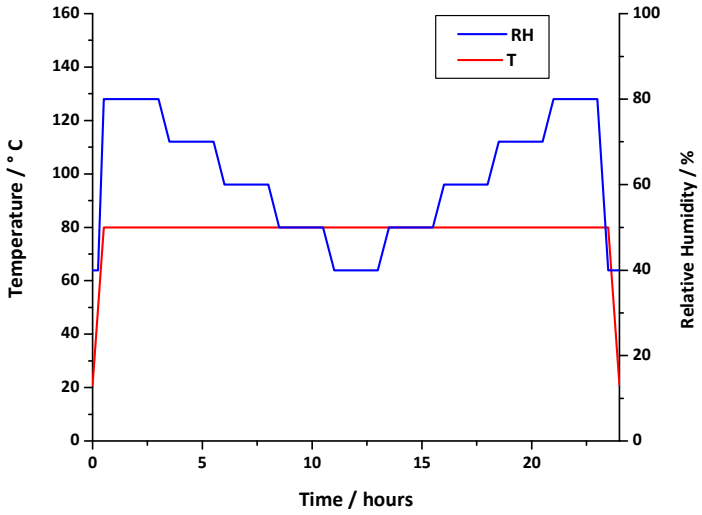

Figure 5.4.3 Relative humidity ramped profile at constant temperature.

The two graphs above are just examples of the software's abilities that were used in this work, although more complicated programs can be developed. The software also logs the data from the commencement of the profile until the experiment has finished so that the exact time, along with respective temperature and relative humidity values may be cross referenced to the electrochemical experiment times.

To initially calibrate the *WKL* chamber, a range of set constant temperatures and relative humidities were programmed into the software and run. An external thermocouple and relative humidity sensor were inserted through the access port for independent measurements. Over the complete range of set values, the instruments sensor values were consistent with the external values.

To calibrate programs that involved a ramping profile, experiments were designed with fast ramping rates. The actual values that were logged by the instrument showed that when ramping the temperature at a fast rate, an overshoot occurred from the set value. This subsequently caused the relative humidity to deviate significantly away from its constant value. The ramping rates were decreased until no detrimental effects were seen on both the temperature and relative humidity. A maximum ramp rate of 1.8 °C min^{-1} resulted in no overshoot of temperature or fluctuation of the relative humidity.

5.5 Calibration of Multi-electrode Cell

To ensure that the multi-electrode cell performs the function it was designed for a calibration test was necessary. The problem with measurement made using *in-plane* cells is ensuring that the bulk conductivity is actually measured and not the surface conductivity which was addressed in Chapter 2. In a through-plane measurement the surface conductivity is insignificant, with mainly contact and bulk resistances being seen. In *in-plane* measurements the surface resistance and bulk resistance may appear in a parallel circuit as seen in Figure 5.5.1.

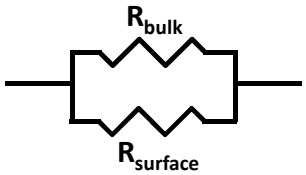

Figure 5.5.1 Equivalent circuit of resistances in an *in-plane* measurement.

The conductance and resistance equations given in Chapter 2 can be used to determine the bulk and surface resistances. These can be adapted to Equation 5.5.1 when the layout of the sample orientation is defined by that in Figure 5.5.2.

$$R = \frac{1}{\sigma}\frac{l}{Wh}$$

Equation 5.5.1

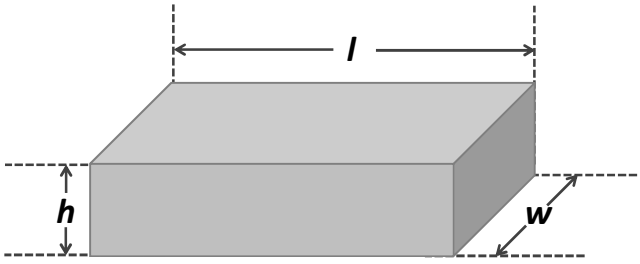

Figure 5.5.2 Sample orientation layout.

Surface resistance is measured in ohms per square while bulk resistance is measured in ohms. It follows from Equation 5.5.1 that the surface resistance, $R_{surface}$, and bulk resistance, R_{bulk}, may be defined by Equation 5.5.2 and Equation 5.5.3.

$$R_{surface} = \frac{l}{\sigma_s W}$$

Equation 5.5.2

$$R_{bulk} = \frac{l}{\sigma_b W h}$$

Equation 5.5.3

By expressing Equation 5.5.2 and Equation 5.5.3 in terms of conductance, (where the conductance $G = 1/R$), the surface conductance, $G_{surface}$, and bulk conductance, G_{bulk}, can be defined by Equation 5.5.4 and Equation 5.5.5.

$$G_{surface} = \frac{\sigma_s W}{l}$$

Equation 5.5.4

$$G_{bulk} = \frac{\sigma_b W h}{l}$$

Equation 5.5.5

The total conductance of the parallel sample can be defined by substituting Kirchhoff's Current Law with Ohm's Law to get a total conductance in Equation 5.5.6.

$$G_{total} = G_{surface} + G_{bulk}$$

Equation 5.5.6

Therefore in expanded terms the total conductance can be written as Equation 5.5.7.

$$G_{total} = \frac{\sigma_s\, w}{l} + \frac{\sigma_b\, w\, h}{l}$$

Equation 5.5.7

In a series of samples with the same identical bulk conductivity, but of varying thickness the conductance will be proportional to the thickness of the sample. The gradient of a plot of thickness *versus* conductance can be defined by Equation 5.5.8,

$$gradient = \frac{\sigma_b\, W}{l}$$

Equation 5.5.8

while the intercept can be defined by Equation 5.5.9.

$$intecept = \frac{\sigma_s\, W}{l}$$

Equation 5.5.9

5.5.1 Experimental Determination of Conductance

To determine the relative magnitude of the surface conductance, a series of Nafion samples of varying thickness were examined. The preparation of which was described in Chapter 4, and a more in depth analysis of measurement techniques will be described later in Chapter 6. The samples although from varying sources had the same ion exchange capacity (IEC) and equivalent weight (EW). Table 5.5.1 shows the dry thickness and origin of the samples.

Table 5.5.1 Physical properties of Nafion calibration samples.

Sample	Company	IEC & EW	Dry thickness / µm
ALD N112	Aldrich	0.91 / 1100	55
JM N115	Johnson Matthey	0.91 / 1100	125
ALD N115	Aldrich	0.91 / 1100	130
JM N117	Johnson Matthey	0.91 / 1100	170
ALD N117	Aldrich	0.91 / 1100	180

The conductivity value was taken at a constant plateau when the sample was subjected 80 ° C and 95 % relative humidity. Conductance values were calculated and plotted against the sample thickness as seen in Figure 5.5.3.

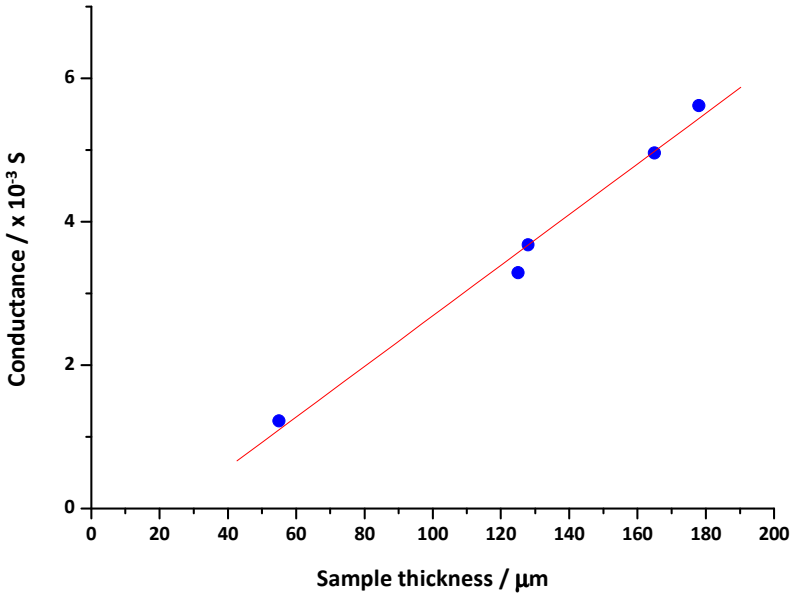

.

Figure 5.5.3 Conductance plot of varying thickness Nafion samples.

The graph shows an almost direct proportionality between the conductance and the thickness of the samples. When a linear fit of the data is made, the intercept is shown to be at -0.08 x 10^{-3} S. The unexpected negative value can be explained by experimental errors. The value of the intercept is within the standard deviation of the data series. This allows the value to be deemed as insignificant as it falls below the standard deviation and subsequently the surface effect can be said to not interfere with the true bulk measurement.

The cell was verified and used for all further experiments dealing with proton conducting membranes.

5.6 Chapter 5 Conclusions

- A multi-electrode cell has been constructed to utilise an *in-plane* conductivity method.

- The multi-electrode cell has been calibrated with commercially available samples to determine that the true bulk conductance of the samples is measured.

- The cell provides gas access so that the samples may be subjected to humidified air whilst the conductivity is being measured allowing relative humidity effects to be investigated.

- The environmental chamber that will be used for future experiments has also been calibrated with the temperature and relative humidity response times being documented. The multi-electrode cell can be placed inside the chamber and programs run with a degree of accuracy such that samples will be kept at the set values.

Chapter 6

Temperature and Relative Humidity Effects on H^+ Membranes

Chapter 6 Temperature and Relative Humidity Effects on H^+ Membranes

In current PEM's used in fuel cell applications, the stability of the membrane is an important restriction on the maximum operating temperature of the fuel cell system. Typically the cells with operate at 80 ° C and greater than 80 % relative humidity. Perfluorosulfonic acid polymers such as Nafion have a very high water dependence, and that deviation away from high humidity values can decrease the bulk conductivity by orders of magnitude. The resulting effect is that using lower temperatures affects the efficiency of other components of the fuel cell as mentioned previously. Studies into the effects of both increasing and decreasing the relative humidity on the conductivity of PEM's as well as changes in the temperature with different humidities were studied. The investigations may provide information that could lead to improvements in the overall efficiency of fuel cell systems.

6.1 The WKL Environmental Chamber

The experiments detailed in this chapter were carried out in the *WKL* chamber described in Chapter 5. The programs were designed based on the findings of the calibration tests. The ramping rate of both temperature and relative humidity were programmed in order that no overshooting of each value occurred.

6.2 Relative humidity and Water Uptake

The relative humidity, *RH*, of air is defined as the ratio of the partial pressure of water vapour in the air, p_W, to the maximum partial pressure of water termed the saturation vapour pressure, p_{WS}, at the same temperature. It is calculated using Equation 6.2.1.

$$RH = \left(\frac{p_W}{p_{WS}}\right) x\ 100\ \%$$

Equation 6.2.1

For temperatures above 100 ° C, the maximum relative humidity that can be achieved is limited by the pressure of the environment which is usually one atmosphere. Numerous equations have been developed to describe how the water saturation pressure changes with temperature. The Arden Buck equation [1] is based upon more recent experiments than the previous models [2] and follows that of Equation 6.2.2.

$$p_{WS} = 6.1121 \exp\left(\frac{\left(18.678 - \frac{T}{234.5}\right) x\, T}{257.14 + T}\right)$$

Equation 6.2.2

This equation for which the data are plotted in red in Figure 6.2.1 shows that at a temperature of 100 ° C, the saturation vapour pressure is equal to one atmosphere. Since the relative humidity cannot be greater than 100 % without precipitation, for temperatures below 100 ° C, p_W, is always less than one atmosphere. Above 100 ° C, p_{WS} is greater than one atmosphere and would therefore need a p_W greater than one to obtain high humidities. However, at normal atmospheric pressure and temperatures above 100 ° C, the total pressure will remain at one atmosphere leading to the relative humidity being calculated by Equation 6.2.3.

$$RH = \frac{1}{p_{WS}}$$

Equation 6.2.3

The data relating to this equation is seen in blue in Figure 6.2.1, whereupon increase of temperature above this point a fairly high relative humidity can still be attained. For the experiments performed in this work, significant ambient relative humidity is still possible at 150 ° C.

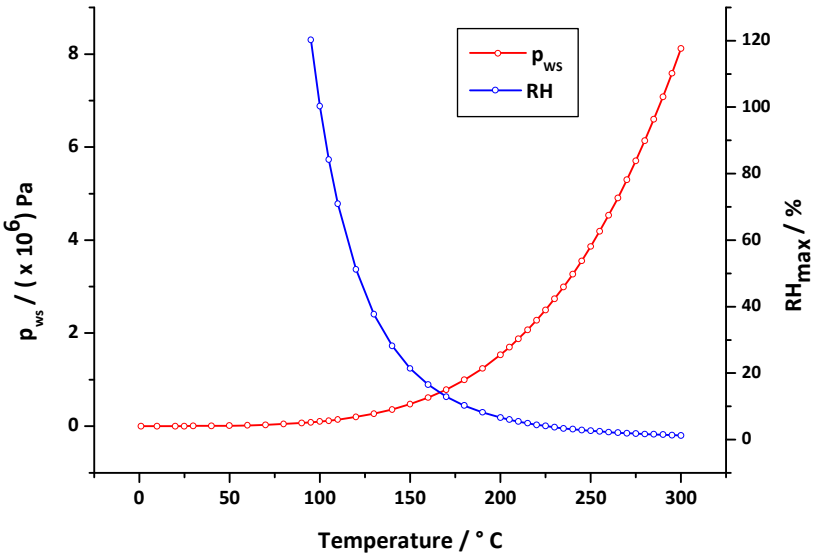

Figure 6.2.1 Saturation vapour pressure and relative humidity at different temperatures.

Therefore, in experiments above 100 ° C the set humidity should be restricted appropriately to avoid precipitation. In addition, the sensors used in the WKL chamber have a lower accuracy when calculating the relative humidity above 100 ° C so when creating the programme the relative humidity values should be set below the maximum value that can be realised.

When a polymer sample is subjected to water, whether it is in the liquid or gaseous state, there can be two states of equilibrium. It has been shown [3] that there are two meta-stable states of polymer. The polymer can exist in either of these two states that can be inter-converted by hydration and dehydration.

Firstly there will be water molecules that are strongly associated with the ions of the sulfonic acid group. These molecules correspond to uptake of "waters of solvation" of the proton and sulfonate ions and will be bound within the structure. The minimum amount of water necessary for solvation only will then remain inside the pores. The number of water molecules per ionic group, λ, is expected to be around 4 in the case of Nafion.

Within the structure of the polymer there are forces repelling any water due to the elastic forces of the matrix. These forces form a resistance against swelling of the

structure, and along with the repelling forces due to any hydrophobic domains, there will always be a tendency for the polymer to exclude any water.

The second state, corresponds to much higher water contents and can be achieved under extreme hydrating conditions. Some of the elastic and hydrophobic forces will be overcome and swelling of the polymer matrix occurs. In the near fully hydrated state of a Nafion membrane, $\lambda \approx 20$ [4]. At this point, the water molecules are free to exhibit similar local mobility to water molecules in liquid water as they are in excess and will create channels for proton conduction to occur. These two states can be described as meta-stable equilibria that can respond to the water vapour pressure with each having an equilibrium between the composition and vapour pressure. By contrast with the small variations in the water vapour pressure within each state which are kinetically fast, the conversion between the two states is kinetically slow because it involves breaking of strong hydrogen bonds, and relaxation of the polymer structure itself. Due to the energies involved, it may be assumed that this second state is unlikely to occur unless the sample is subjected to relative humidities near 100 %.

The water content of a sample gives important information which relates to the conductivity. Understanding of these processes will enable more detailed analyses of the state of the membrane at different conductivities and consequently should always be considered.

In polymer electrolyte membranes such as SPEEK and Nafion, water effectively acts as a plasticiser enabling conductivity through processes such as the Grotthus mechanism, mentioned previously in Chapter 1. The method for water content determination is defined by Equation 6.2.4.

$$Water\ Uptake\ \% = \frac{\left(M_{wet} - M_{dry}\right)}{M_{dry}}\ x\ 100$$

Equation 6.2.4

M_{dry} is the dry weight of the membrane, M_{wet} is the weight of the membrane after it has been either immersed in water or equilibrated at a set relative humidity for at least 24

hours. Subsequently, the number of moles of water per mole of sulfonic acid group can be calculated by knowing these parameters also as shown in Equation 6.2.5.

$$\lambda = \frac{\left(\frac{(M_{wet} - M_{dry})}{18}\right)}{\left(\left(\frac{1}{EW}\right) x\, M_{dry}\right)}$$

Equation 6.2.5

The lambda value will correspond to the swelling state of the membranes which have been detailed in Chapter 1 using the Gebel representation.

6.2.1 Experimental Procedure

To ensure that all samples were fully dry before performing the measurements they were dried under vacuum at 110 ° C for 24 hours. A 1.65 cm by 1.25 cm piece was cut out and each sample was then weighed three times to ensure a constant weight was achieved. For the samples that were to be immersed in liquid water, the water was conditioned in the WKL chamber in a sealed vessel to the required temperature for 4 hours prior to the sample immersion. For the samples that were to be subjected to gaseous state water, the WKL chamber was conditioned to the required relative humidity for 4 hours before placing the samples situated on a plastic mesh into the chamber. The samples remained in the liquid water or under a constant humidity for 24 hours to ensure complete equilibration. On removal from the WKL chamber the samples were immediately blotted dry with Whatman® tissue paper to remove any excess surface water and weighed. The thickness of the hydrated membranes was recorded along with any dimensional changes that had occurred. All samples had been subjected to the same pre-treatment procedure described in Chapter 4.

6.2.2 Results of Water Uptake Experiments

Since the water uptake was occurring through both liquid and gaseous phase water, it is prevalent to group water uptake from the same phase together. The data shown in Table 6.2.2 illustrates the dry thicknesses of some Nafion samples from both Aldrich (Ald) and Johnson Matthey (JM).

Table 6.2.1 Nominal dry thicknesses of Nafion membranes.

Sample	Dry thickness / μm
Ald Nafion 112	55 ± 5
JM Nafion 115	125 ± 5
Ald Nafion 115	128 ± 5
JM Nafion 117	170 ± 5
Ald Nafion 117	178 ± 5

The water uptake percentages and lambda values of the same membranes can be seen in Table 6.2.2 whereby the samples were immersed in water at different temperatures.

Table 6.2.2 Water uptake and lambda values of varying thicknesses of extruded Nafion immersed in water at varying temperatures.

		Aldrich Nafion 112	JM Nafion 115	Aldrich Nafion 115	JM Nafion 117	Aldrich Nafion 117
20 ° C	**WU %**	10.8	16.2	14.3	15.6	16.2
	λ	7.9	9.9	8.7	9.5	9.9
50 ° C	**WU %**	17.8	23.4	24.5	23.1	23.8
	λ	10.9	14.7	14.5	14.1	14.5
80 ° C	**WU %**	23.4	29.6	29.0	29.2	29.6
	λ	15.7	18.1	17.7	17.8	18.1

The data shows a general trend that as the water temperature increases the water uptake and subsequently the λ values increase also. The lambda values that are seen at 80 ° C correspond to a near practically obtainable maximum water content without subjected the samples to the peroxide and acid pre-treatment which is suggested to force a greater volume of water in through the pores [3]. This step has also been associated with irreversible changes to the structure which will be dealt with later on in the chapter.

When viewed in graphical form, (Figure 6.2.2), there is a second trend visible at every temperature that the samples were subjected to. The thicker the membrane, the greater the water content in comparison to the thinner membrane. The IEC of all samples was identical being 0.91 meq/g. However due to the shorter diffusion path in the thinner membranes, more water may be lost between the water environment and the balance where the samples were weighed. This experimental error may form a possible explanation of the differing water contents across the thickness range.

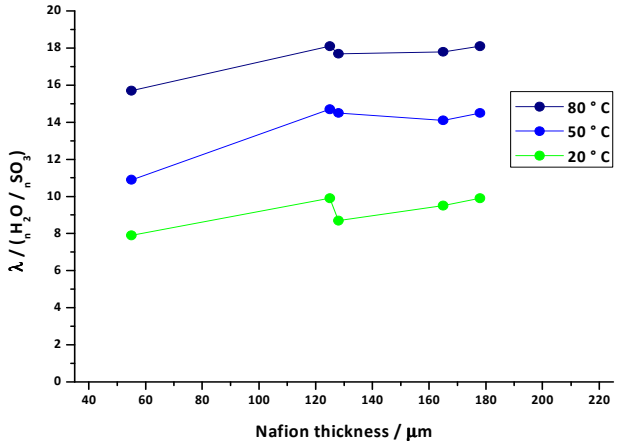

Figure 6.2.2 Plot of the water content for varying Nafion samples when immersed in water at different temperatures.

If this data is now compared with that of *Ald* and *JM* Nafion samples that were still subjected to a relative humidity of 95 % instead of being immersed in water at the same temperatures as seen in Table 6.2.3, the water content is seen to be considerably less.

Table 6.2.3 Water uptake and lambda values of varying thicknesses of extruded Nafion at 95 % relative humidity and at varying temperatures.

		Aldrich Nafion 112	JM Nafion 115	Aldrich Nafion 115	JM Nafion 117	Aldrich Nafion 117
20 ° C	**WU %**	4.9	6.4	6.7	6.2	6.1
	λ	3.0	3.9	4.1	3.8	3.7
50 ° C	**WU %**	2.3	1.58	1.6	1.3	1.6
	λ	2	1.2	1.0	0.9	1.0
80 ° C	**WU %**	2.3	1.9	1.4	1.4	1.19
	λ	1.5	1.0	0.9	0.9	0.7

At low temperatures the water content resembles that of the solvated water with *lambda* values of around 4. However, when the temperature is increased the water content decreases.

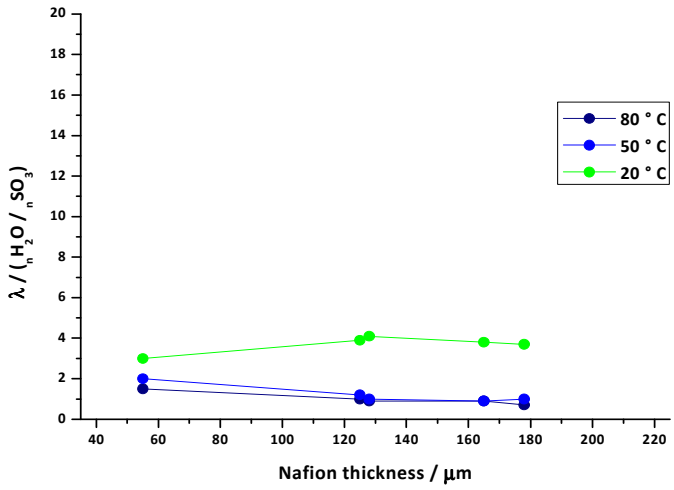

Figure 6.2.3 Plot of the water content for varying Nafion samples when subjected to 95 % relative humidity at different temperatures.

To get a clearer picture of the processes it is also practical to look at the results from the SPEEK polymer. Although this polymer is not fluorinated it still possesses hydrophobic domains, but unlike the Nafion structure there is not the same ionic cross-linking from pendant side chains, so one would expect the elastic forces to be weaker in this case. The data in Table 6.2.4 shows the SPEEK samples subjected to the same conditions as the immersed Nafion.

Table 6.2.4 Water uptake and lambda values of varying DS % SPEEK immersed in water.

		SPEEK (DS %)				
		47	**57**	**63**	**75**	**80**
20 ° C	**WU %**	22.1	30.4	48.2	74.5	91.0
	λ	8.2	11.2	17.2	20.6	25.1
50 ° C	**WU %**	27.0	41.2	58.5	88.1	115.0
	λ	11.1	14.5	18.7	24.6	30.4
80 ° C	**WU %**	53.2	65.1	76.0	156.8	177.2
	λ	21.0	22.6	24.7	42.8	47.9

The data in Table 6.2.4 shows a significant increase in water content when compared to the Nafion samples. By looking at the data displayed graphically in Figure 6.2.4, a steady increase in water content can be seen as the DS increases at each specific temperature. This can be accounted for due to the increase in ion exchange sites and hydrophilic domains.

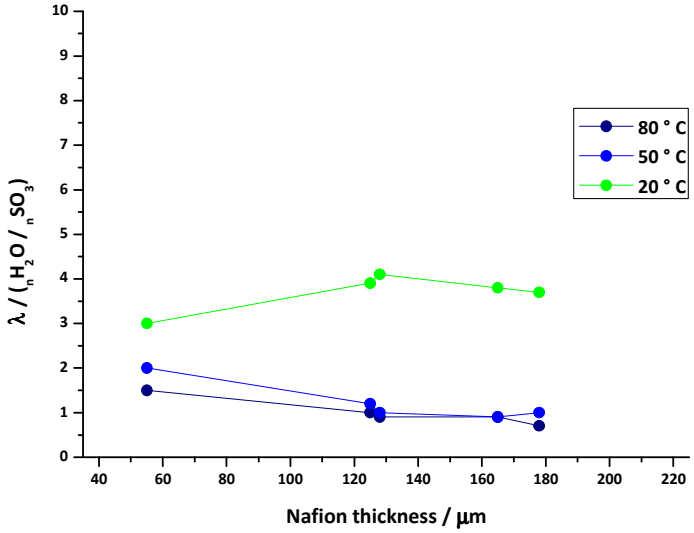

Figure 6.2.4 Plot of the water content for varying DS SPEEK samples when immersed in water at different temperatures.

With regards to temperature effects on the water uptake, at low DS the difference is relatively small. This trend continues until the sample DS reaches 63 %. At the sample DS of 75 and 80 %, water temperature has a much more profound effect. In particular at 80 °C, the water content almost doubles its values from 50 °C.

The water uptake values for samples subjected to vapour phase water at 20, 50 and 80 °C can be seen in Table 6.2.5. As with the Nafion samples there is a clear decrease in the lambda value at all temperatures compared with the samples that were immersed in water at the same temperatures.

Table 6.2.5 Water uptake and lambda values of varying DS % SPEEK at 95 % relative humidity.

		SPEEK (DS %)				
		47	**57**	**63**	**75**	**80**
20 ° C	**WU %**	14.9	18.2	19.5	56.2	72.0
	λ	5.3	5.9	6.2	16.6	19.8
50 ° C	**WU %**	8.7	15.8	23.6	50.5	65.2
	λ	3.4	5.0	9.1	13.7	15.7
80 ° C	**WU %**	6.0	8.1	13.7	18.4	19.6
	λ	1.8	2.3	4.2	8.5	9.0

When the data can be seen graphically as in Figure 6.2.5, at lower temperature, all samples are able to retain more water than at high temperature.

For both Nafion and SPEEK when immersed in water, high temperatures favoured greater water uptake, while the reverse occurred for both polymers under water vapour conditions.

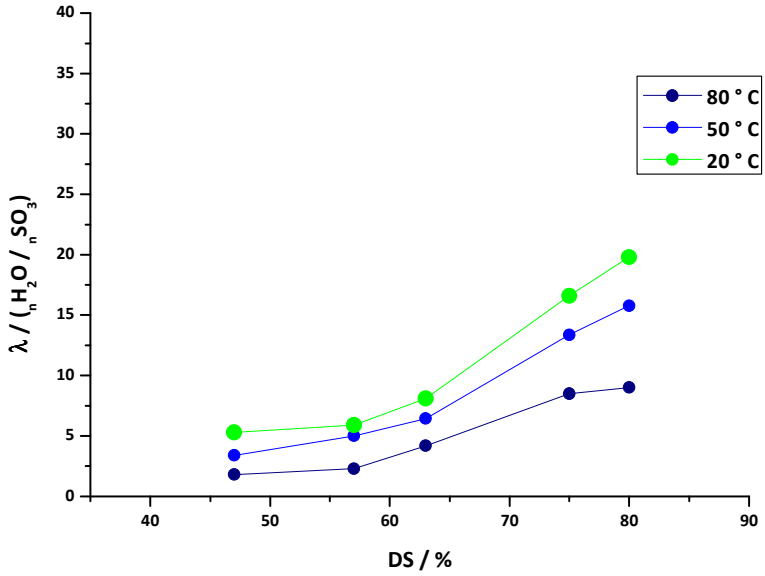

Figure 6.2.5 Plot of the water content for varying DS SPEEK samples when subjected to 95 % relative humidity at different temperatures.

In both polymer systems there is a significant difference between the water uptake values that have arisen from water vapour and liquid water at the same temperature. Although the relative humidity used in the experiments was not at 100 %, at 95 % relative humidity there is less than a tenth of the water content than when immersed. The phenomenon of varying water content with uptake from vapour and liquid phases has been observed as early as 1903 [5]. The phenomenon known as Schroeder's Paradox found that the uptake of water into gelatine films from 100 % water vapour was less than water uptake from liquid water. The result of this was surprising since the chemical potential of both states of water are identical. Publications on studies of water transport in proton conducting membranes have also now come across this irregularity in water content [6, 7]. More recently in attempts to model the different swelling states of Nafion, some explanations have been suggested [8-10]. As mentioned previously, there are two distinct types of water in the membrane. There are the strongly bound waters $\lambda_W{}^B$ and the free waters $\lambda_W{}^F$. This leads to the total water uptake by the molecule being that of Equation 6.2.6.

$$\lambda = \lambda_W^B + \lambda_W^F$$

Equation 6.2.6

If the general chemical potential, μ, for the water species W in any phase α is defined similarly to [11], as a function of the temperatures, T, pressures, P, partial molar volume, $\tilde{V}$, activities, a_W, and other potentials, Ψ_W, then it may be represented as shown in Equation 6.2.7.

$$\mu_{W\alpha} = \mu^o_W(T, P^o) + \int_{P^o}^{P} (\tilde{V}_{W\alpha})\, dP + RT \ln a_{W\alpha} + \Psi_{W\alpha}$$

Equation 6.2.7

In the above equation, the water is considered to be the solvent component of the membrane, and the equation describes the change in the chemical potential of water with its activity or concentration as it is diluted by the membrane from its pure standard state, and its change with pressure.

Thermodynamic conditions that describe phase equilibrium between water in the membrane, μ_{WM}, and that of the external liquid phase, μ_{WL} may be defined as in Equation 6.2.8.

$$\mu_{WM} = \mu_{WL}$$

Equation 6.2.8

With the case of water systems, the solvent is said to incompressible, and Equation 6.2.8 may be simplified to that of Equation 6.2.9 for the case of a liquid – membrane phase equilibrium, where the osmotic pressure due to the stretching of the polymer network, Π_M, $\Pi_M = P_{WM} - P_{WL}$, where P_{WM} is the pressure from water in the membrane and P_{WL} is the pressure from water in the liquid.

$$\ln \frac{a^F_{WM}}{a_{WL}} = -\left(\frac{\tilde{V}_W}{RT}\right) \Pi_M$$

Equation 6.2.9

When considering the vapour – membrane phase equilibrium there is an additional interface between any condensed water and the vapour phase. The pressure within the polymer will then not only change due to the stretching of the network but due to the pressure brought about by the curved vapour – liquid interface, Π_ξ. The activity of the vapour phase activity is defined by Equation 6.2.10 similar to equation governing the relative humidity.

$$a_{WV} = \frac{p_W}{p_{WS}}$$

Equation 6.2.10

Subsequently the equilibrium is represented by Equation 6.2.11,

$$\ln \frac{a_{WM}^F}{a_{WV}} = -\left(\frac{\tilde{V}_W}{RT}\right)\left(\Pi_M + \Pi_\xi\right)$$

Equation 6.2.11

where Π_ξ is calculated from the Young – Laplace equation to give the secondary pressure value (Equation 6.2.12).

$$\Pi_\xi = -\frac{2\xi \cos\theta}{r_p}$$

Equation 6.2.12

This equation takes into consideration the surface tension of the interface, ξ, the contact angle of the condensed phase, θ, and the pore radius, r_p and would mean that as the radius of the curvature becomes infinite, the difference in pressure would decrease to zero. A schematic of the possible behaviour of the polymer structure and the liquid – vapour interface can be seen in Figure 6.2.6.

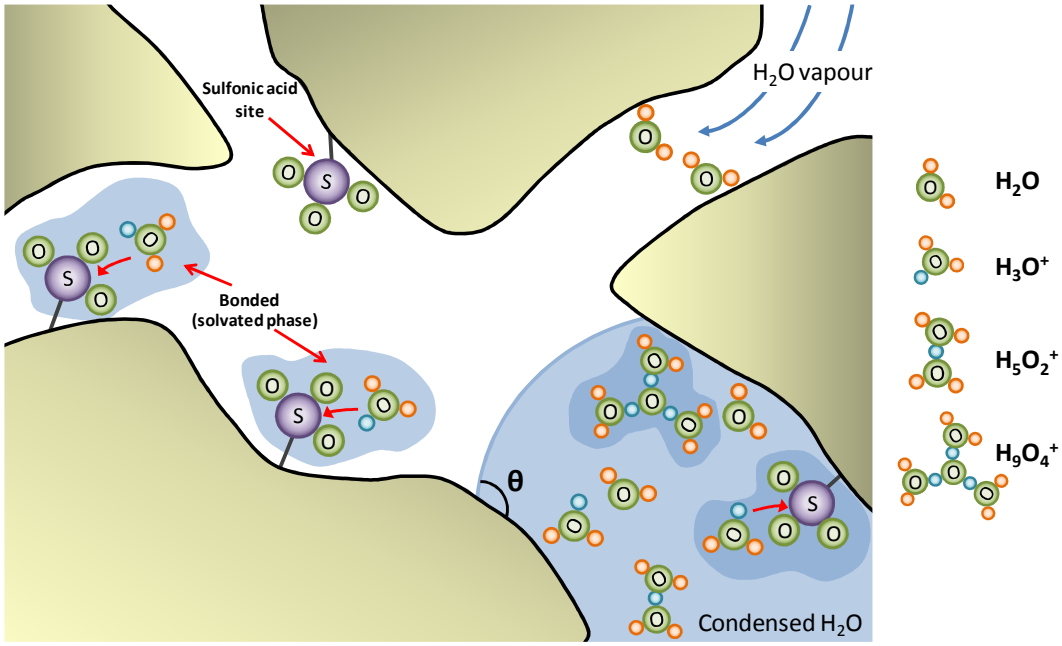

Figure 6.2.6 Schematic of Nafion pores in the presence of water vapour.

This diagram shows how the vapour phase water bonds with the sulfonic acid sites forming small groups that are solvated. The condensed phase, where a number of these solvated groups join to form a cluster can also be seen with the formation of a convex meniscus due to the hydrophobic nature of the polymer.

When considering water vapour, with an activity of 1, when $p_W = p_{WS}$, Equation 6.2.9 becomes Equation 6.2.13.

$$\ln a_{WM}^{F} = -\left(\frac{\bar{V}_W}{RT}\right) \Pi_{\mathrm{M}}$$

Equation 6.2.13

However, Equation 6.2.11 becomes that of Equation 6.2.14.

$$\ln a_{WM}^{F} = -\left(\frac{\bar{V}_W}{RT}\right) \left(\Pi_{\mathrm{M}} + \Pi_{\xi}\right)$$

Equation 6.2.14

This modification to the equation relating to the vapour phase may go some way to elucidate the ambiguity between experimental values of water uptake from liquid and vapour phases.

As experimentally found, this behaviour of water uptake is not exclusive to Nafion. SPEEK is not as hydrophobic as Nafion due to its lack of fluorinated groups, but the main chain is hydrophobic to some degree. In comparison, SPEEK has a much greater IEC, with subsequently more sites for solvated water than Nafion. Models have been suggested that depict the pore channels in Nafion being relatively large and of uniform size as seen in Figure 6.2.7.

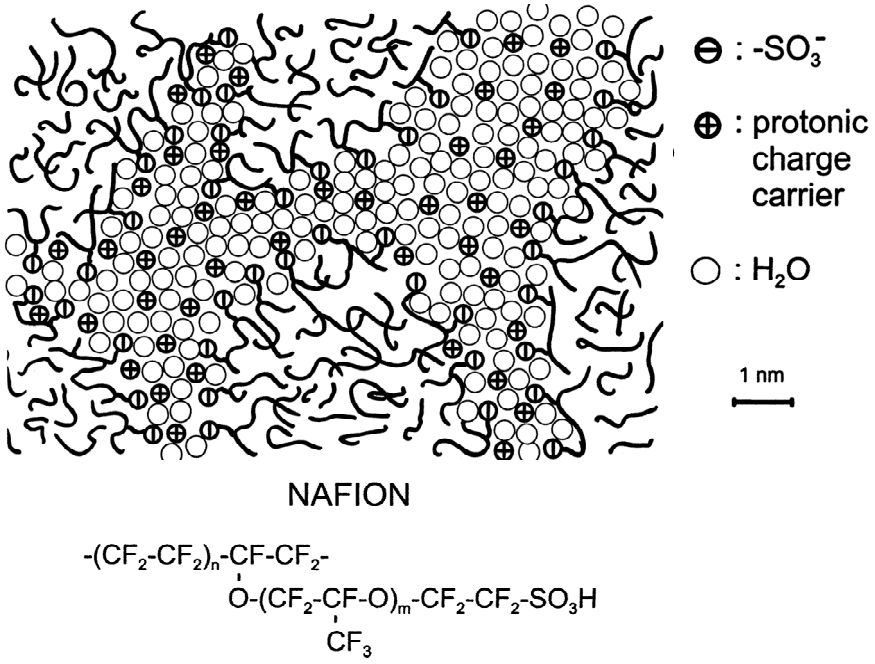

Figure 6.2.7 Schematic model of Nafion pore channels [12].

In comparison, models based on the sulfonated aromatic polymers such as SPEEK, have been presented showing many more pore channels per unit area than Nafion as seen in Figure 6.2.8.

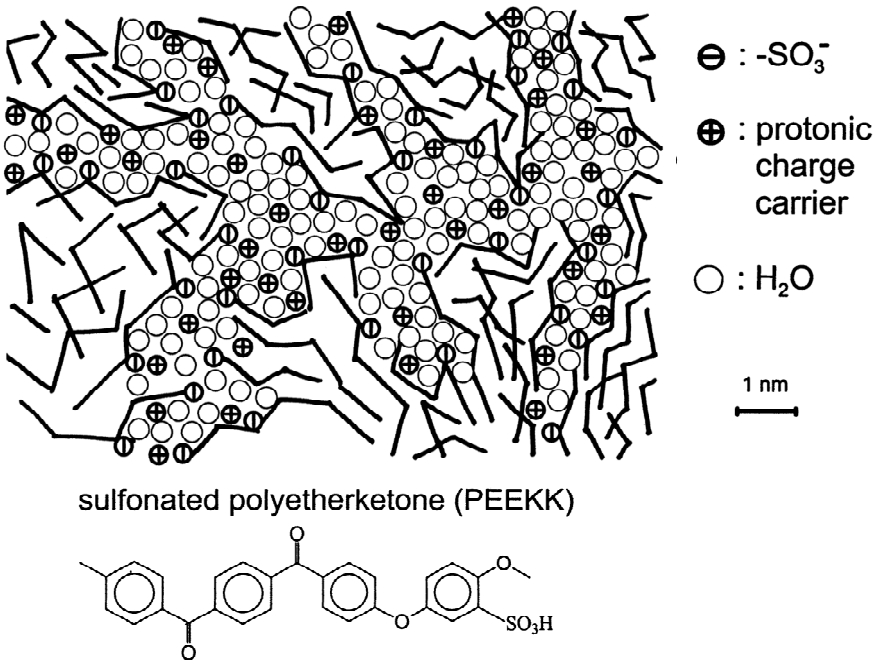

Figure 6.2.8 Schematic showing SPEEKK pore channels [12].

The effect of channel size in the membrane could also play an important part in governing the water content of the membrane. For water to enter into the polymer matrix, a pore would need to begin or end at the membrane environment interface or an ionic group would need to be located on the surface. Only a single point of contact would theoretically be needed for water to enter the matrix. If the model of SPEEKK shown in Figure 6.2.8 is accurate, then the number of pore channels in SPEEK would most likely be higher than that of Nafion samples. The probability of water molecules entering the membrane would be much greater in SPEEK than Nafion and could well be a contributing factor in the equilibration water content values. However, should both samples possess the same number of pore channels that reach the surface, it could be expected that due to the highly fluorinated structure of Nafion, any water close to the membrane surface would suffer a greater repelling force than from the hydrocarbon chain of the SPEEK. This would also mean that it would be energetically more favourable for water molecules to enter a SPEEK sample.

However, the possible benefits of more ionic channels in SPEEK could also lead to detrimental effects on the conductivity of the sample. If the sample possesses more pore channels, then an arrangement of the chains different to Nafion will occur. This

increase in the number of pore channels could lead to instances of dead-end channels. If this is the case then on an individual sample basis, conductivity could be decreased if such orientation was to occur.

When considering the effect of temperature on the water content on both Nafion and SPEEK there are two areas of consideration. Firstly, there is the situation where the sample is exposed to humidified air. The results showed that lower temperatures at the same relative humidity had greater water contents than those at higher temperature. This behaviour may be compared to that of salt hydrates, whereby the tendency to absorb water decreases as the temperature is increased in a humid atmosphere. The reaction of these types of salts with water is exothermic due to bond formation between the molecules and is, therefore, enthalpy driven. This would mean that all but the most strongly bound waters would be lost due to evaporation

The second situation is the samples being immersed in liquid water. Here, the opposite effect is seen whereby at higher temperatures, more water is contained within the structure of both Nafion and SPEEK samples. Possible reasons behind this may be that when samples are in contact with liquid water, the uptake is direct and all the pores are filled [4]. The mobility of the polymer chains also increases at higher temperature and so the diffusion of the water molecule into the membrane becomes faster. This in turn creates more free volume inside the polymer allowing more water to be stored in the membrane.

6.3 HT Impedance Measurements Whilst Changing Temperature and Relative Humidity

6.3.1 HT Experimental Procedure

The impedance of samples was measured using the multi-electrode cell detailed in Chapter 5. The cell was placed inside the *WKL* chamber and connected *via* IDE cable to a control box (Figure 6.3.1) which connected to a *Variable Multi-Channel Potentiostat* (*VMP*), (Princeton Applied Research; Biologic-Science Instruments) as shown in Figure 6.3.2. The *VMP* is a 16 channel potentiostat, to which 5 channels were used for the 5 individual samples in the multi-electrode cell.

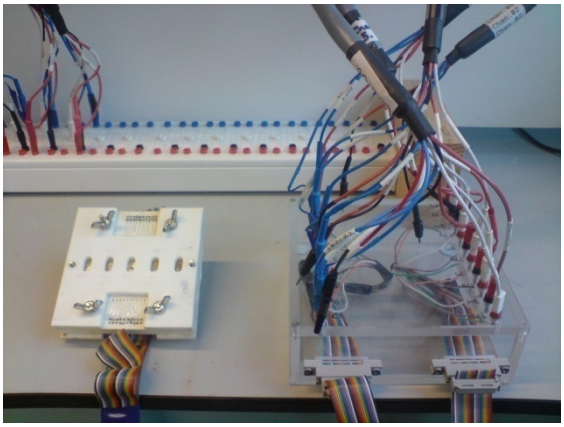

Figure 6.3.1 Cell and connector box to VMP.

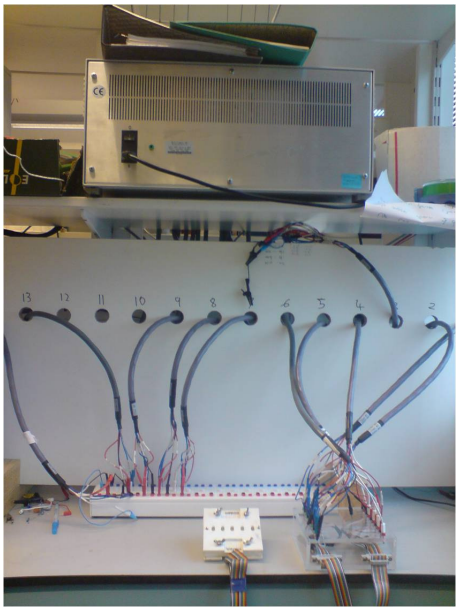

Figure 6.3.2 VMP with cell and connector box.

The *EC Lab* software was programmed to perform an impedance experiment, wait for a specified time and then loop back to the impedance experiment again indefinitely, the settings of which are detailed in Table 6.3.1.

Table 6.3.1 VMP settings for multi-electrode cell impedance experiments.

Parameter	Symbol	Value	Units
Initial frequency	f_i	100	k Hz
Final frequency	f_f	0.1	Hz
Points per decade	N_d	20	n/a
Peak to peak AC amplitude	V_{pp}	300	mV
Number of frequencies	N_f	101	n/a
Single experiment time	T_{exp}	18	s
Wait period	T_{wait}	2	min

The time of each impedance experiment was also logged using the software so this could be referenced to the temperature and relative humidities throughout the experiment. At time zero, both the *VMP* and the *WKL* chamber programs were started and left to run until the *WKL* chamber program had completed its cycle. Observation on the condition of the samples was noted before and after the experiment to ensure there was no sample decomposition. The logged temperature and relative humidity from the *WKL* chamber were exported to a PC where the data could be converted and processed. The impedance data was exported from the *VMP* whereby a program was created in *Visual Basic* (*VB*) to split the continuous file into individual files for each experiment.

The *VB* program was necessary due to the sheer volume of files. For a typical profile in the *WKL* chamber over a 26 hour period, the *VMP* would collect around 800 files for each sample; 4000 impedance files total. The *WKL* chamber would log 1600 temperatures and 1600 relative humidity values. The data files were then examined using *ZView* software and the Nyquist plots were batch fitted to a relevant equivalent circuit model. The *VB* program then performed a secondary fitting of the low frequency points which would be equal to the sample resistance, and compared this to values from the batch fitting data. If the values were within a 5 % error margin of each other then they were deemed acceptable, if not, for instances such as noise interference, then the fitting was performed in *ZView* manually. The *VB* program then recombined the data in a suitable format whilst matching the individual calculated resistance values and times of that experiment with the temperature and humidity from the *WKL* chamber data. The conductivity was then calculated at each specific time, temperature and relative humidity.

The impedance results will be represented in numerous ways. Firstly, Nyquist plots will be shown for illustrative purposes for the shape of the graph. Secondly, the data will be exhibited in the form a conductivity profile that follows the temperature and relative humidity profile set from the *WKL* chamber. Thirdly data will be tabulated describing the maximum and minimum conductivities achieved.

6.3.2 Initial Testing - Calibration of Multi-electrode Cell

6.3.2.1 Experiment 1 - T_{max} = 80 ° C and 80 % Relative Humidity

The initial test that was used to calibrate the multi-electrode cell described in Chapter 2 utilised Nafion membranes of varying thicknesses. The experimental conditions were T_{max} = 80 ° C and 80 % relative humidity as seen in the profile (WKL Program 1) in Figure 6.3.3.

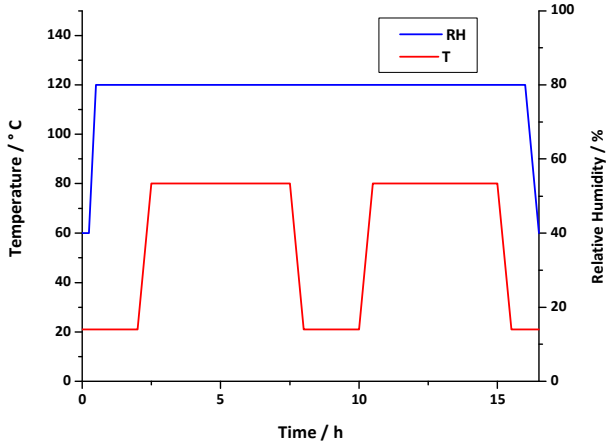

Figure 6.3.3 WKL Program 1 – Temperature and relative humidity profiles used for calibration of multi-electrode cell with Nafion samples.

Actual fuel cell stacks that use Nafion as the PEM, generally operate at 80 ° C and 100 % relative humidity. By considering the conductivity data in Figure 6.3.4, the reasons for such high operating relative humidities is visible. The conductivity once at 80 ° C is unsustainable and the membrane suffers from dehydration before reaching its equilibrium plateau.

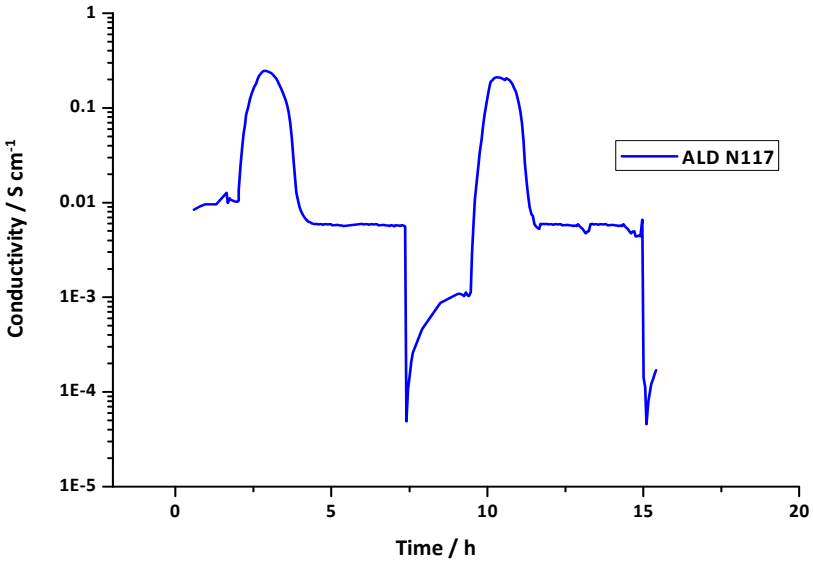

Figure 6.3.4 Experiment 1 - Conductivity trace of Aldrich N117 Nafion sample using WKL Program 1.

The same type of decay was seen for all membranes of varying thicknesses from 50 to 180 µm in the dehydrated state. The values that were used for the purposes of the conductance calibration were taken at the plateau region for every sample.

6.3.2.1 *Experiment 2 - T_{max} = 80 ° C and 80 % Relative Humidity*

As a comparison, the SPEEK membranes were also tested under the same conditions. The samples all had the same DS but had different casting solvents. An example of a conductivity trace can be seen in Figure 6.3.5.

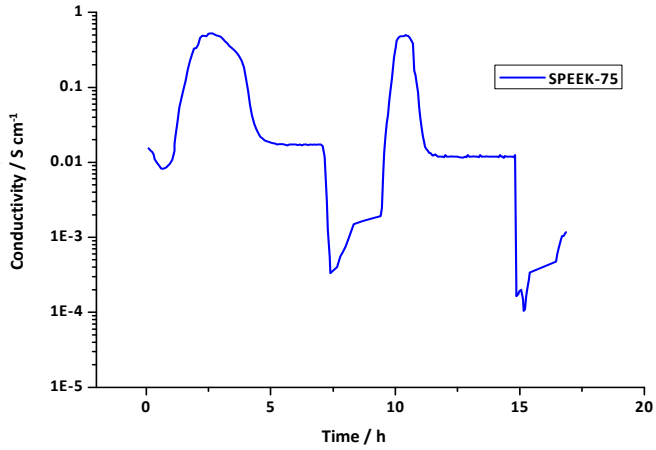

Figure 6.3.5 Experiment 2 - Conductivity trace of SPEEK-75 using WKL Program 1.

It was found that the casting solvent did have some effect on the conductivity plateau at T_{max}. The solvents which had higher boiling points had a higher conductivity plateau. The mechanical properties of the films were also greatly reduced when being cast in DMF and DMAc taking on a more brittle nature. Other studies have used these casting solvents in their experiments [13, 14], though a range of solvents was not investigated, and no comment was made on the properties. It is unclear why this solvent effect may have occurred, although some studies have reported casting solvent-polymer interactions [15, 16]. In these cases it has been documented that through ^{1}H NMR analysis, hydrogen bonding between the amide of DMF occurred at temperatures around 60 ° C. The amide of DMAc did not form bonds until around 100 ° C, but both solvents are prone to thermally activated decomposition which could be assisted by the

highly acidic environment within the polymer. The resulting dimethylamine decomposition product is thought to strongly associate with the sulfonic acid groups in the SPEEK. If this is the case, then a reduction in the number of available acid sites would cause a lowering in the ionic conductivity, while the semi-crosslinking would result in an increased in brittleness. To obtain data that was more comparable to fuel cell conditions the relative humidity was altered for the first main experiment.

6.3.3 HT Impedance Testing and Results

6.3.3.1 *Experiment 3 - Nafion at T_{max} = 80 ° C and 95 % Relative Humidity*

The first experiments were performed with Nafion samples since these were already accessible and had been used as the standard test sample for designing the cell. The temperature and relative humidity values in this experiment were used as a comparison to the values used in an actual fuel cell. Although the relative humidity was slightly less than fuel cell conditions, it was the maximum achievable to a high level of accuracy in the *WKL* chamber and deemed to be comparable. The relative humidity was kept constant at 95 % at all times throughout the experiment, whilst the temperature was ramped from 21 ° C to 80 ° C, kept constant for a set period and ramped back to 21 ° C, the cycle being repeated twice as shown in the profile (WKL Program 2) in Figure 6.3.6.

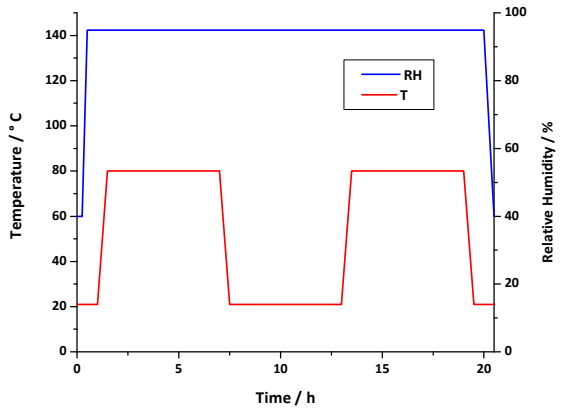

Figure 6.3.6 WKL Program 2 – Temperature and relative humidity profiles – T_{max} = 80 ° C and RH=95 %.

A Nyquist plot of the impedance data for the complete experimental time span can be seen in Figure 6.3.7.

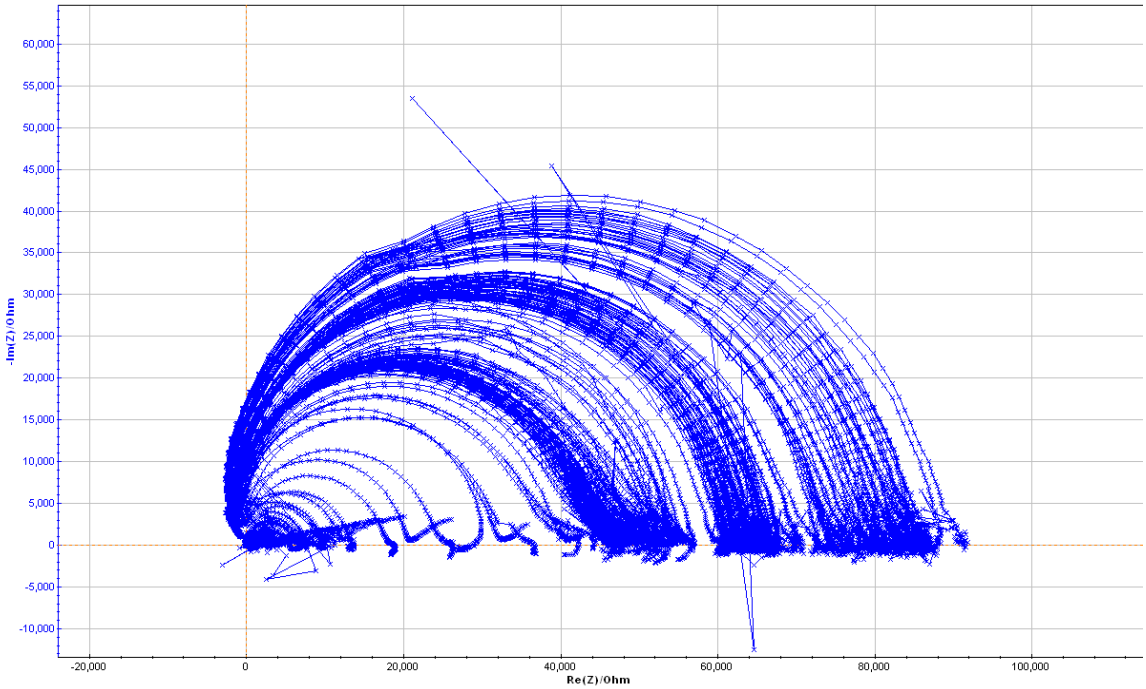

Figure 6.3.7 Screenshot from the VMP of the impedance data of a complete experimental cycle of an Ald Nafion 117 sample under WKL Program 1 conditions.

The impedance plot shows data that is characteristic of a parallel RC component. The scale of the largest semi-circles spans to around 100 kΩ. When the experiment commenced, the semi-circles were quite pronounced, but as it progressed through the temperature profile (*ie*; the temperature increased) the high frequency portion of the semi-circle disappeared. At this point, the low frequency intercept also decreased until at the maximum temperature only a cluster of points on the real axis were seen. The Nyquist plot in Figure 6.3.8 depicts this more clearly with the real axis scale reduced to 2000 Ω. The rogue point seen in the data in Figure 6.3.8, corresponds to instrumental noise at 50 Hz. This could be eliminated by altering the points per decade frequencies, though in this case a greater number of points was desirable and the settings were not altered.

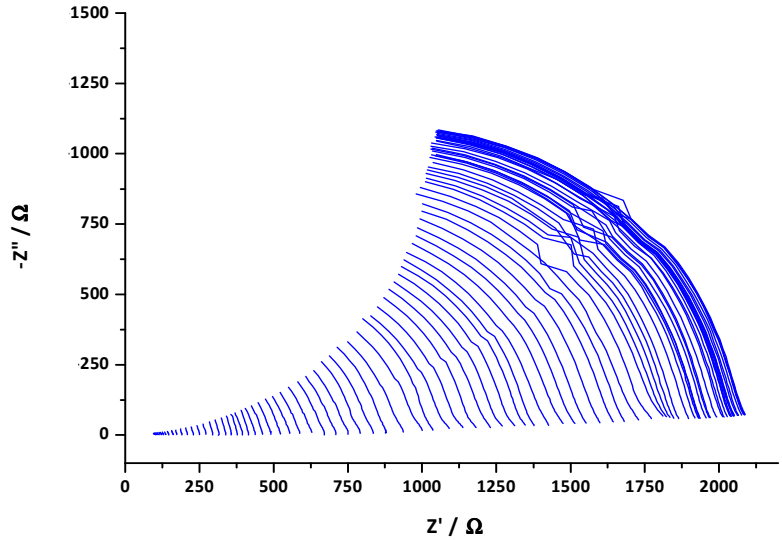

Figure 6.3.8 Representative Nyquist plot of a low resistance Nafion sample.

The complete Nyquist plot also shows some low frequency inductive loops when the sample was more resistive which were absent as the sample resistance decreased. This is thought to be an artefact which may be due to the length of cabling from the *VMP* to the *WKL* chamber. The equivalent circuit that was used for calculation of the bulk resistance values can be seen in Figure 6.3.9.

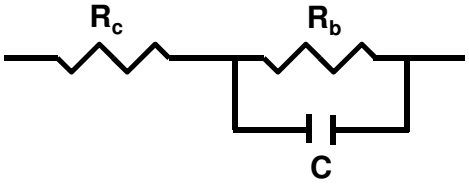

Figure 6.3.9 Equivalent circuit used for fitting the data from temperature and relative humidity profiled experiments.

There is an initial contact resistance which shifts the semi-circle away from the origin, followed by a bulk resistance depicted in parallel with a capacitance. The origin of the capacitance was initially thought to be the bulk capacitance of the polymer, however there is still some ambiguity whether this is correct.

The bulk electrolyte capacitance is related to the dielectric constant of the polymer as defined in Chapter 2. Usual approximations of the dielectric constant of conducting

polymer membranes are at values of around 10. This would lead the calculation of the bulk capacitance to give a value around 9.8 x 10^{-10} F. This value is approximately two orders of magnitude off the expected value. To obtain a value closer to, the dielectric constant would need to be in the order of 100 – 1000.

Studies on the dielectric of Nafion in various states of hydration have been undertaken. Using frequencies of 10 MHz to 5 GHz, the dielectric was indeed found to be in the region of 10. However when the frequency was decreased into the high kHz region, a sharp increase in the dielectric constant was observed [17, 18]. The value increased by several orders of magnitude. Although lower frequencies as used in these experiments were not investigated, this may indicate that the dielectric is in fact higher than expected. An earlier study into the dielectric properties of Nafion documented that to frequencies in excess of 1 MHz were needed to see the bulk capacitance of the polymer [19, 20].

An experiment was performed to further investigate the origin of the capacitance. A model circuit was constructed firstly with a series of three resistors, and secondly with a series of three parallel RC components. The values of the resistors and capacitors was chosen to closely match the values obtained in the data. The *VMP* was connected in the same manner as the 4-point *in-plane* cell. The parallel RC series of components produced a Nyquist plot with a characteristic semi-circle where the resistance and capacitance were calculated to be the values of the components. However, the series of resistors produced a similar semi-circle to that in Figure 6.3.7. The origin of the capacitance may now be attributed to a small current leakage at the voltage probes. While this is undesirable, the true resistance value is unaffected by this stray capacitance.

The time of each impedance measurement was cross referenced to the *WKL* data file and the specific temperatures and relative humidities found as mentioned previously. A conductivity trace that followed the profile was then plotted for each of the 5 samples that were tested simultaneously. In Figure 6.3.10, a trace can be seen of Nafion 117 (thickness = 190 μm).

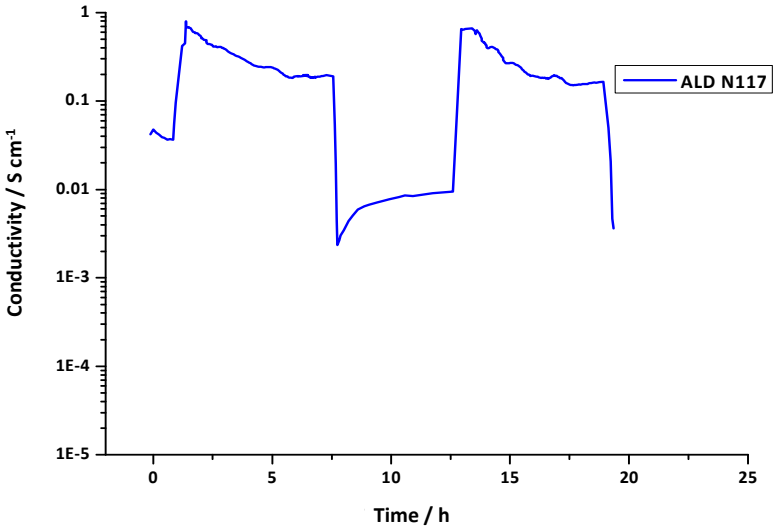

Figure 6.3.10 Experiment 3 (T_{max} = 80 °C, RH = 95 %) - Conductivity trace of Aldrich N117 Nafion sample using WKL Program 2.

The conductivity is seen to begin at an initially high value of approximately 5 x 10^{-2} S cm^{-1}. As the temperature is increased there is a sharp rise in the conductivity which then begins to decay away before reaching a plateau. After this point there is a temperature decrease and subsequently the conductivity decreases before rising to a plateau. These changes associated with the temperature rising and falling can also be seen on the second cycle.

To explain this behaviour a number of considerations must be taken into account. Firstly, when the sample is placed into the multi-electrode cell, it had previously been stored in DI water after the pre-treatment stage. The membrane is therefore water saturated. If the lambda values determined in Section 5.2 are used as approximate values then it can be assumed that at the offset, the membrane has a lambda value of 18. Secondly, due the difference in water content from applied water vapour and that of applied liquid water, the membrane will therefore be loosing water as soon as it is removed from its storage container. This will mean that the rise in conductivity will not be at constant membrane water composition. Thirdly, the water uptake values determined previously showed that even at the same relative humidity, the temperature has a considerable effect. If the membrane had sufficient time to equilibrate itself before the temperature rise then the lambda value after the rise would be in the region of 5 which accounts for the waters of solvation. This would mean that the decay at 80 ° C

to the constant plateau would be the equilibration between lambda of 5 and a lambda of around 1. However, once the sample has reached equilibrium at 80 ° C and 95 % relative humidity, the drop is conductivity due to a constant composition Arrhenius drop from 80 ° C to 21 ° C. This can be deduced since at the lower temperature another rise is seen. This is accounted for by the membrane returning to its solvated state ($\lambda = 5$) at 21 ° C. The time for the water uptake at low temperature is seen to be around three hours at this relative humidity. Since the membrane has now equilibrated at 21 ° C, the second temperature rise results in an increase in conductivity at constant composition. As the maximum temperature is reached for the second time, water is lost into the surrounding environment and the lambda value reaches 1.

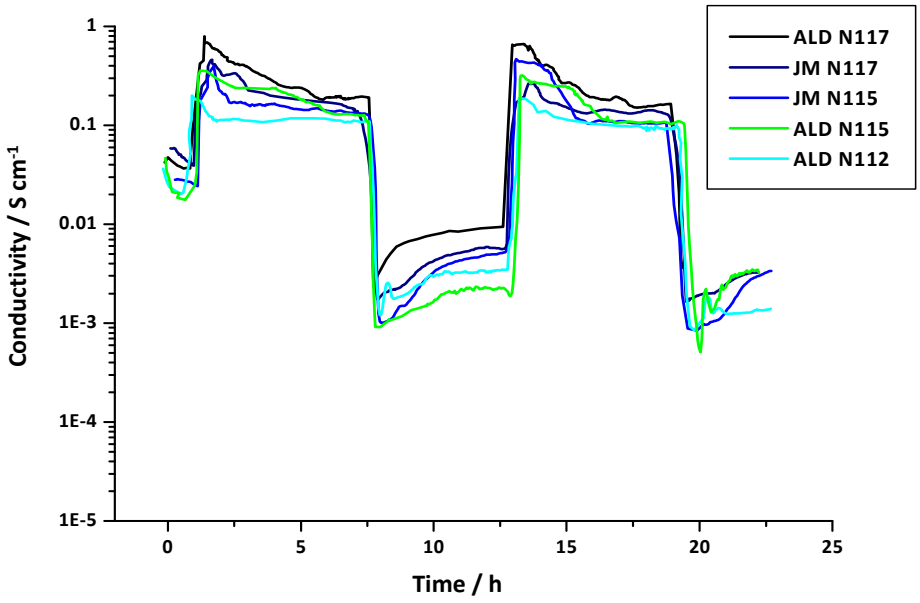

Figure 6.3.11 Experiment 3 (T_{max} = 80 °C, RH = 95 %) - Conductivity traces of all JM Nafion samples using WKL Program 2.

The conductivity traces of the 5 Nafion samples that were tested simultaneously in the multi-electrode cell can be seen in Figure 6.3.11. The samples generally follow the same trends commented on previously, though as with the water uptake experiments, the thicker membranes tended to take up slightly more water than the thinner ones.

6.3.3.2 *Experiment 4 – SPEEK at T_{max} = 80 ° C and 95 % Relative Humidity*

The SPEEK samples that had different DS, namely 0.47, 0.57, 0.65, 0.73 and 0.80 were subjected to the environmental profile conditions shown in WKL Program 2 (Figure 6.3.6), identical to the Nafion samples in Experiment 3. The Nyquist plots returned similar results to Figure 6.3.7 and Figure 6.3.8, in that a parallel RC component type semi-circle was seen at high sample resistance which disappeared as the resistance decreased. However, the conductivity trace was somewhat different in that the water management properties of the SPEEK appeared more advanced than the Nafion samples. A single conductivity trace for a SPEEK sample can be seen in Figure 6.3.12.

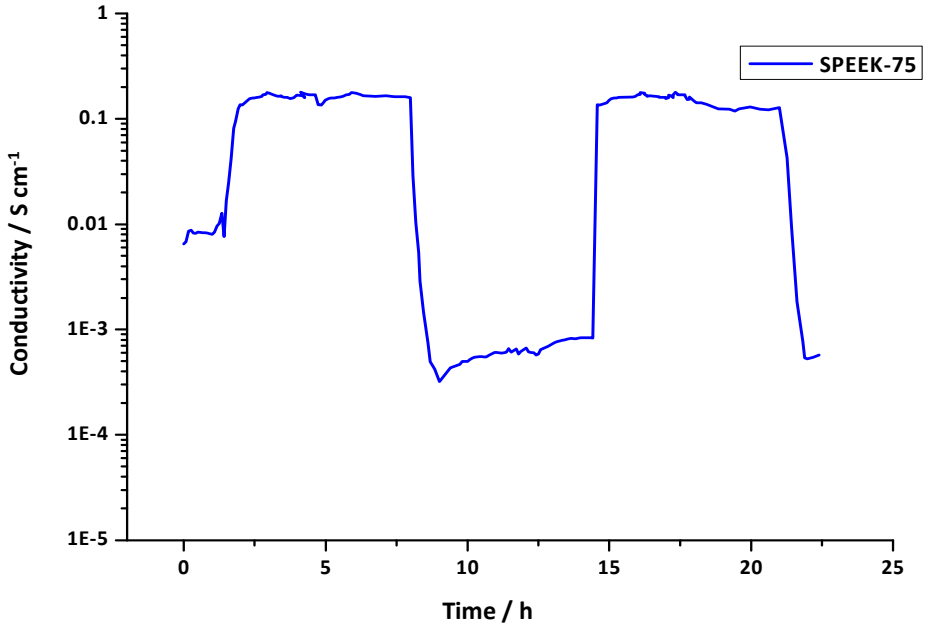

Figure 6.3.12 Experiment 4 (T_{max} = 80 °C, RH = 95 %) - Conductivity trace for an SPEEK-75 sample using WKL Program 2.

As illustrated in Figure 6.3.12, the conductivity has a gradual decrease at the offset due to water loss from being saturated when stored. When the temperature is increased, the conductivity also increases, but unlike the Nafion samples there is no decay from the maximum conductivity and the beginning of the T_{max} plateau. This would indicate that the water retention ability in the SPEEK samples is more efficient than the Nafion samples.

If a plot of different DS SPEEK samples is examined as in Figure 6.3.13, there is also a variation in the maximum conductivity achieved depending on the DS of the SPEEK samples.

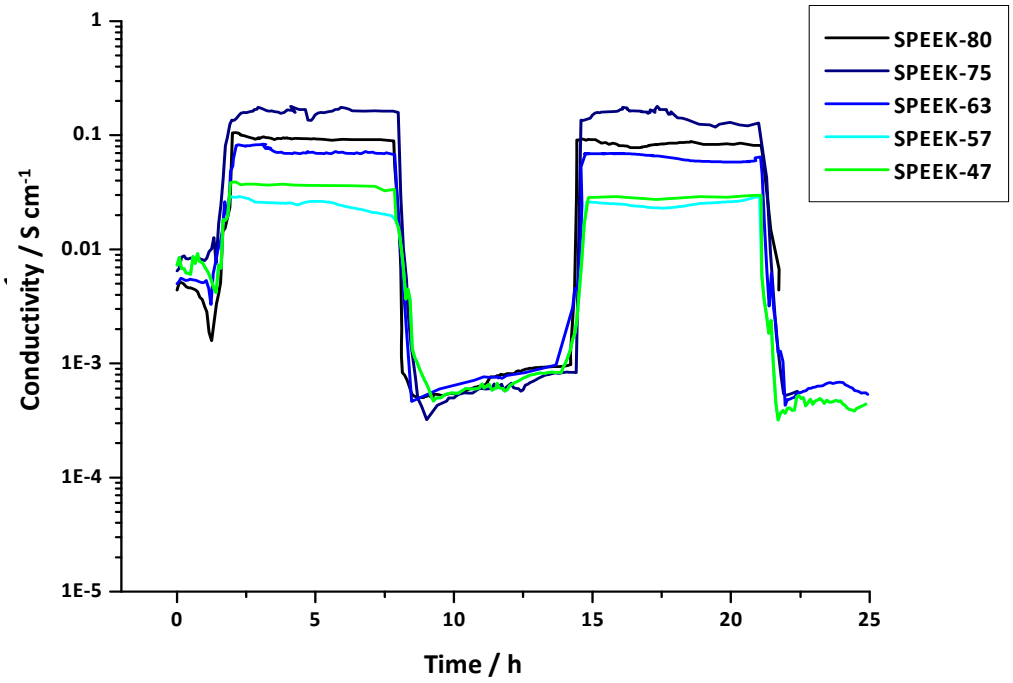

Figure 6.3.13 Experiment 4 (T_{max} = 80 °C, RH = 95 %) - Conductivity traces of all SPEEK samples using WKL Program 2.

The general trend shows that as the DS increases the maximum conductivity also increases. The membrane that had the highest DS (DS = 0.8), had reduced mechanical stability in comparison to the other membranes. The high level of sulfonation was on the boundary of the polymer becoming completely water soluble which was found in the initial synthesis stage. This property led to some extreme dimensional variation in the pre-treatment stage due to the excessive water content it was able to hold. Theoretically, this should have made the sample the most conductive, however this was not the case and the reason behind this is unclear at present. The membrane that had DS of 0.75 was also able to hold a large volume of water, but was not as affected by the dimensional expansion. However, at the end of the experiment when the samples were examined, it appeared much more elastic than samples with a lower DS.

The SPEEK samples showed better performance with relation to their conductivity than Nafion samples at lower humidities, appearing less sensitive to environmental changes.

Since the SPEEK samples were more stable it was deemed acceptable to progress to experiments that had elevated temperatures and reduced relative humidities.

6.3.3.3 *Experiment 5 – SPEEK at 105 ° C and 75 % Relative Humidity*

The environmental profile that was used for Experiment 5 involved keeping the relative humidity at a constant 75 % at all times throughout the experiment, whilst the temperature was ramped from 21 ° C to 105 ° C, kept constant for a set period and ramped back to 21 ° C, the cycle being repeated twice as shown in the profile (WKL Program 3) in Figure 6.3.14.

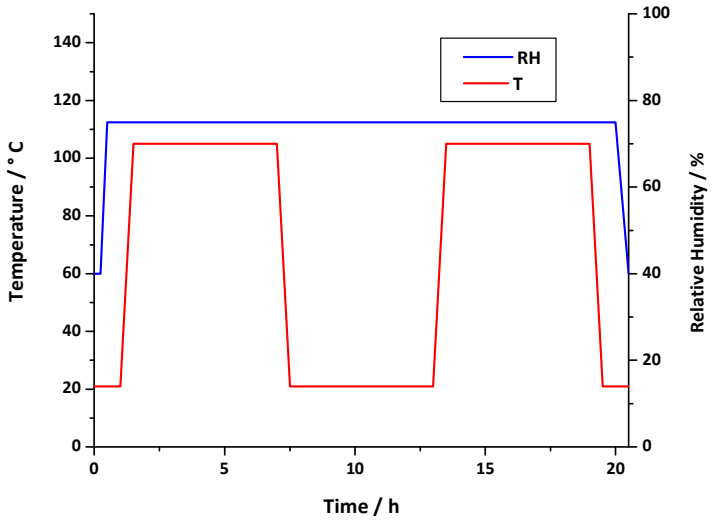

Figure 6.3.14 WKL Program 3 – Temperature and relative humidity profile – T_{max} 105 ° C and RH 75 %.

The relative humidity value was chosen as such due to the restraints of the *WKL* chamber and to ensure the minimal amount of fluctuations would occur. The SPEEK samples were pre-treated as mentioned in Chapter 4 before testing commenced. As the experiment progressed, the Nyquist plots appeared the same as in the previous experiments in that a semi-circle was visible with occasional low frequency inductive loops. When the conductivity data was calculated and plotted in the form of a trace that followed the profile seen in Figure 6.3.14, the graphs seen in Figure 6.3.15 were obtained.

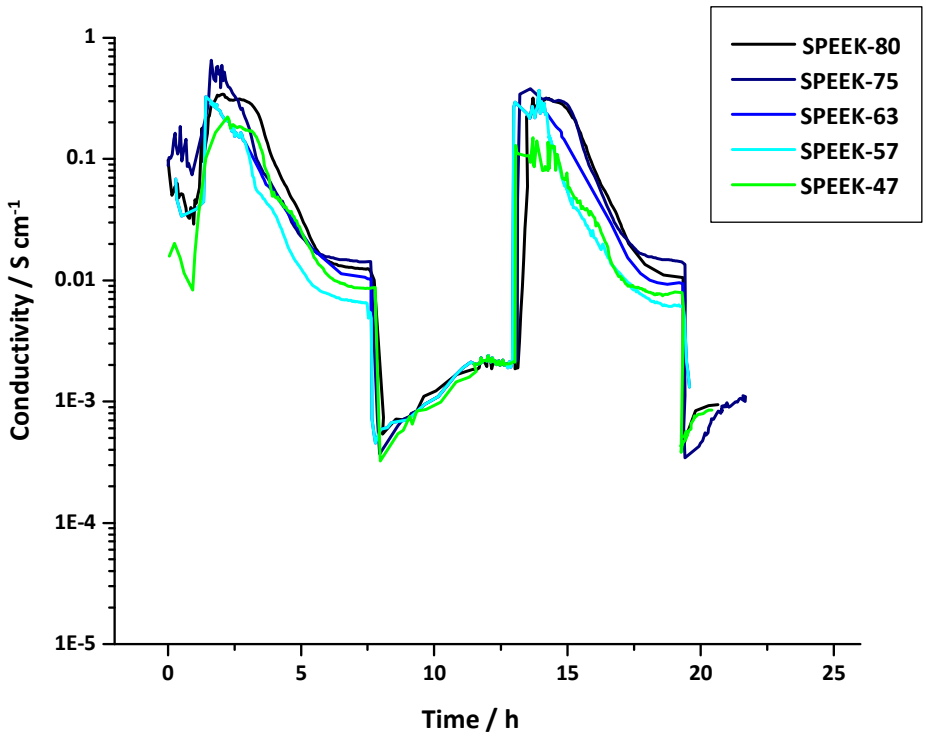

Figure 6.3.15 Experiment 5 (T_{max} = 105 °C, RH = 75 %) - Conductivity trace for all SPEEK samples using WKL Program 3.

Similarly to the experiments used for calibration purposes which the relative humidity was kept at 80 %, the decay in conductivity was seen in Experiment 4 also. Here it was found that the conductivity decay was much more severe, though the maximum conductivity peak was slightly higher. This maximum value will have increased due to the temperature increase as would be expected, and as the samples were initially water saturated, on the second temperature cycle the conductivity max is lower.

When the samples from Experiment 5 were removed from the *WKL* chamber, the mechanical properties of some of the films were found to have suffered. In particular, the higher DS films were unable to withstand the low relative humidity at the higher temperature of the WKL Program 3. The SPEEK-75 and the SPEEK-80 were the samples most affected by the conditions as seen in Figure 6.3.16.

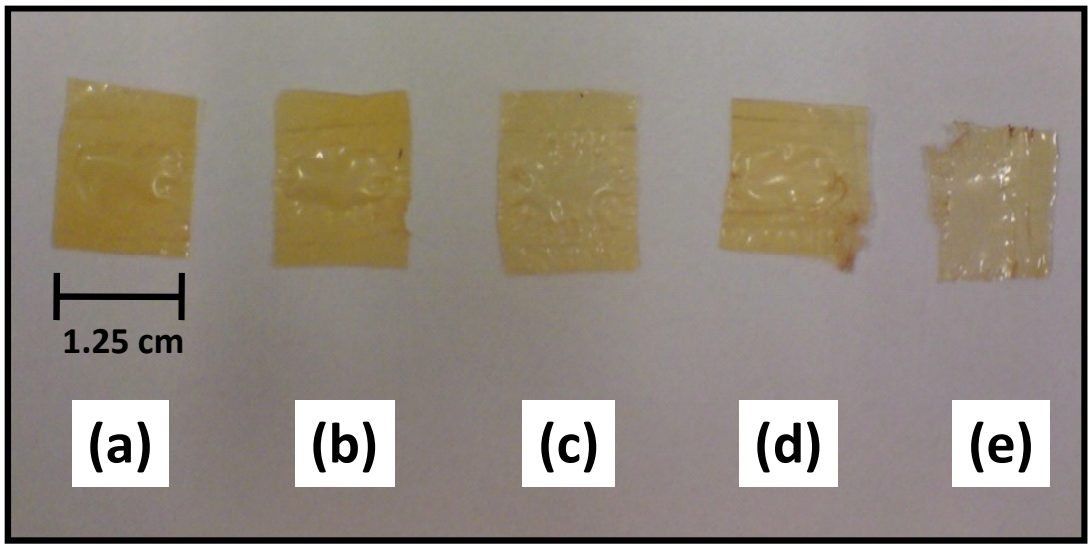

Figure 6.3.16 Physical condition of (a) SPEEK-47, (b) SPEEK-57, (c) SPEEK-63, (d) SPEEK-75 and (e) SPEEK-80 membranes after Experiment 5 had finished.

6.3.3.4 *Conductivity Data Summary*

In order to easily perceive any obvious effects of temperature and humidity, the data values from the previous experiments needs to be collated. The values for the maximum conductivity, σ_{MAX}, achieved after a temperature increase was applied, and the conductivity plateau, σ_P, occurring after equilibration, can be seen in Table 6.3.2.

Table 6.3.2 Collated conductivity data for all samples at varying temperatures and relative humidities.

Sample	Temperature / ° C	Relative Humidity / %	σ_{MAX} / S cm^{-1}	σ_P / S cm^{-1}
Ald N117	80	80	0.125	0.00087
SPEEK-75	80	80	0.335	0.012
Ald N117	80	95	0.7962	0.1964
JM N117	80	95	0.4258	0.1410
JM N115	80	95	0.4114	0.1336
Ald N115	80	95	0.3233	0.1298
Ald N112	80	95	0.1785	0.11673
SPEEK-80	80	95	0.0906	0.0906
SPEEK-75	80	95	0.1767	0.1767
SPEEK-63	80	95	0.0698	0.0698
SPEEK-57	80	95	0.0363	0.0363
SPEEK-47	80	95	0.0243	0.0243
SPEEK-80	105	75	0.3380	0.0125
SPEEK-75	105	75	0.5912	0.0142
SPEEK-63	105	75	0.2867	0.0105
SPEEK-57	105	75	0.1974	0.0085
SPEEK-47	105	75	0.1790	0.0065

6.3.4 Temperature and Conductivity Relationships

When the conductivity of a material is studied at varying temperatures, it is normal to relate the conductivity values to the temperature by the Arrhenius equation shown in Equation 6.3.1,

$$\sigma = \text{Ä}\, exp\left[\frac{-E_a}{\text{R}\dot{}T}\right]$$

Equation 6.3.1

where σ is the conductivity, $\ddot{A}$ is a pre exponential factor, E_a is the activation energy, $\dot{R}$ is the gas constant and T is the temperature.

Data was obtained from the constant composition temperature increase of the second thermal cycle at a constant relative humidity value of 95 %. The results of the Arrhenius plot can be seen in Figure 6.3.17 for an Aldrich Nafion 117 sample and three varying DS SPEEK samples.

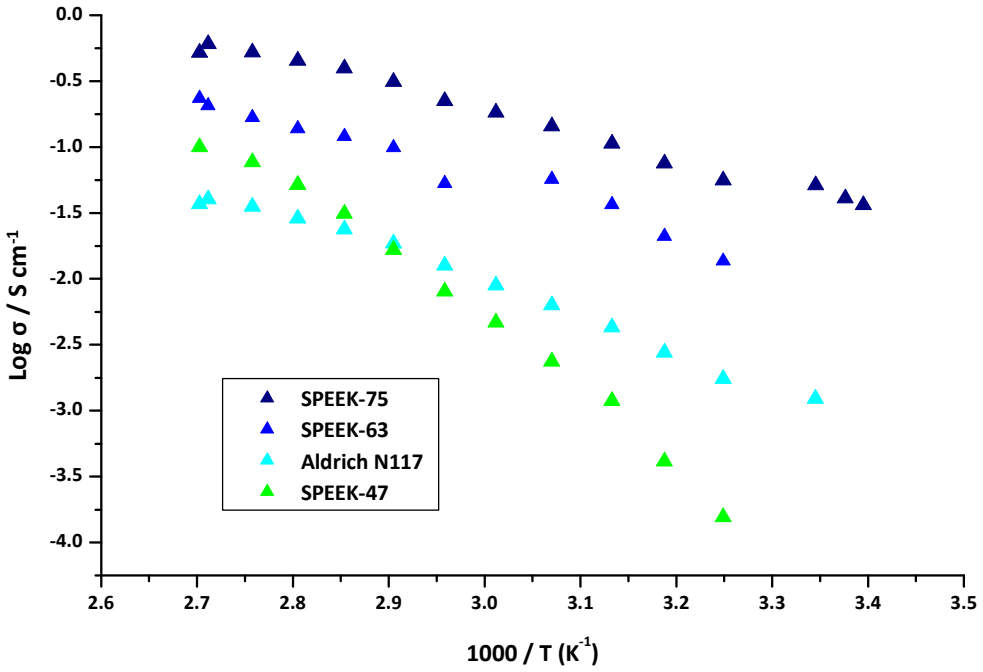

Figure 6.3.17 Arrhenius plots for SPEEK-75, SPEEK-63, Nafion 117, and SPEEK-47 at 95 % relative humidity.

The data in Figure 6.3.17 shows that for all samples the relationship is not entirely linear across the temperature range and for some samples, the relationship is curved over the temperature range. In cases like this when studying polymer electrolytes, the temperature dependence of the conductivity may also obey the Vogel-Tamman-Fulcher (*VTF*) [21] relationship shown in Equation 6.3.2,

$$\sigma = \text{Ä}\, T^{-\frac{1}{2}} \exp\left[\frac{-B}{(T - T_o)}\right]$$

Equation 6.3.2

where, *Ä* is a pre-exponential factor that is proportional to the number of charge ions, *B* is the pseudo-activation energy and T_o is a reference temperature.

The temperature dependence of conductivity with regards to polymer electrolytes has been documented to show a number of different behaviours [22]. The following are the most commonly seen behaviours –

- Arrhenius behaviour at lower *T* and *VTF* at higher *T*.
- *VTF* behaviour throughout the thermal range.
- Arrhenius behaviour throughout, but with two different activation energies, high E_a closer to T_g and smaller E_a at higher *T*.
- *VTF* behaviour for *T* slightly greater than *Tg*, but Arrhenius behaviour at higher *T*.
- Behaviour unlike Arrhenius or *VTF* at all values of *T*.

In these cases, the non-linearity may be due to slight changes in composition with respect to lambda values, as the temperature is changed. The activation energies that were calculated from the data in Figure 6.3.17 were 23 kJ mol^{-1} for the Ald Nafion 117 sample and 13 – 19 kJ mol^{-1} for the SPEEK samples. It can be assumed that a reason for the higher activation energy of the Nafion 117 sample is due to it possessing a lower IEC than the SPEEK samples.

6.4 Chapter 6 Conclusions

By considering both the water uptake data and the conductivity data, some interpretations of the processes involved can be made about the conductivity traces.

- At the initial point of measurement, all samples are water saturated, in that they have a lambda value similar to that of being immersed in water at 20 °C (Table 6.2.2 and Table 6.2.4). The initial temperature rise in the *WKL* profile occurs before the samples have equilibrated at the relative humidity value. The water uptake data shows that at the same temperature, membranes will have less water content when exposed to water vapour than liquid water. This would mean that the samples are loosing water whilst the kinetic effect of temperature increase begins.

- The increase in temperature has a greater effect on the conductivity than the water loss due to equilibration, so the conductivity rises. However, the conductivity reaches a maximum value for the set temperature and water content. At this point the water loss to equilibration at the set temperature and relative humidity becomes apparent, and the conductivity decays. The water loss equilibration occurs over several hours till a plateau is reached, which corresponds to a water content similar to that seen in Table 6.2.3 and Table 6.2.5. As the temperature then decreases, a constant composition drop in conductivity occurs. At the ambient temperature the conductivity again begins to increase. This second increase is not now due to temperature effects, but to water uptake. The data in Section 6.2.2 of this chapter showed that at low temperatures and a constant relative humidity, membranes were able to retain more water than at a high temperature with the same relative humidity. This conductivity rise is resulting from the lambda increase. At the second temperature rise, the conductivity increase due to temperature is also at constant composition, whereby the same water loss effect on the conductivity occurs once the temperature effect has reached its maximum.

- It may seem in this instance that although the SPEEK samples behaved more favourably than Nafion samples at high humidities as seen in Experiment 2 and

Experiment 3, and that the conductivity plateau in Experiment 1 was also higher, SPEEK is still limited to operating under similar conditions to Nafion, and further experiments will be needed for a greater understanding of its limitations.

6.5 Chapter 6 References

1. A. L. Buck, *Journal of Applied Meteorology*, 1981, **20**, 1527-1532.
2. J. A. Goff and S. Gratch, *Transactions of the American Society of Heating and Ventilating Engineers,*1946, **52**, 95-121.
3. G. Alberti, R. Narducci and M. Sganappa, *Journal of Power Sources*, 2008, **178**, 575-583.
4. T. A. Zawodzinski, T. E. Springer, J. Davey, R. Jestel, C. Lopez, J. Valerio and S. Gottesfeld, *Journal of The Electrochemical Society*, 1993, **140**, 1981-1985.
5. P. Schroeder, *Z. Phys. Chem.*, 1903, **45**, 57.
6. L. M. Onishi, J. M. Prausnitz and J. Newman, *J. Phys. Chem. B*, 2007, **111**, 10166-10173.
7. A. Z. Weber and J. Newman, *Journal of The Electrochemical Society*, 2003, **150**, A1008-A1015.
8. P. H. Choi and R. Datta, *Journal of The Electrochemical Society*, 2003, **150**, E601-E607.
9. M. Bass and V. Freger, *Polymer*, 2008, **49**, 497-506.
10. M. Bass and V. Freger, *Desalination*, 2006, **199**, 277-279.
11. T. A. Davies, J. D. Genders and D. Pletcher, The Electrochemical Consultancy, Romsey, UK, 1997, p. 83.
12. K. D. Kreuer, *Journal of Membrane Science*, 2001, **185**, 29-39.
13. J. Wootthikanokkhan and N. Seeponkai, *Journal of Applied Polymer Science*, 2006, **102**, 5941-5947.
14. P. Xing, G. P. Robertson, M. D. Guiver, S. D. Mikhailenko, K. Wang and S. Kaliaguine, *Journal of Membrane Science*, 2004, **229**, 95-106.
15. S. Kaliaguine, S. D. Mikhailenko, K. P. Wang, P. Xing, G. Robertson and M. Guiver, *Catalysis Today*, 2003, **82**, 213-222.
16. G. P. Robertson, S. D. Mikhailenko, K. Wang, P. Xing, M. D. Guiver and S. Kaliaguine, *Journal of Membrane Science*, 2003, **219**, 113-121.
17. S. J. Paddison, G. Bender, K. D. Kreuer, N. Nicoloso and T. A. Zawodzinski, *Journal of New Materials for Electrochemical Systems*, 2000, **3**, 291-300.
18. S. J. Paddison, D. W. Reagor and T. A. Zawodzinski, *Journal of Electroanalytical Chemistry*, 1998, **459**, 91-97.

19. J. J. Fontanella, M. G. McLin, M. C. Wintersgill, J. P. Calame and S. G. Greenbaum, *Solid State Ionics*, 1993, **66**, 1-4.

20. M. C. Wintersgill and J. J. Fontanella, *Electrochimica Acta*, 1998, **43**, 1533-1538.

21. J. F. Le Nest, F. Defendini, A. Gandini, H. Cheradame and J. P. Cohen-Addad, *Journal of Power Sources*, 1987, **20**, 339-344.

22. M. A. Ratner, in *Polymer Electrolyte Reviews - 1*, eds. J. R. MacCallum and C. A. Vincent, Elsevier, 1987, p. 173.

Chapter 7

SPEEK Blends and SPEEK-$Zr(HPO_4)_2$

Chapter 7 SPEEK Blends and SPEEK-$Zr(HPO_4)_2$

SPEEK samples of varying DS were tested for conductivity at different temperatures and relative humidities as detailed in the previous chapter. It was found that conductivities comparable to that of commercially available membranes could be achieved. Samples with a high DS generally had a higher σ_{MAX} than the lower DS samples. However, in samples with a high DS, the mechanical properties after the tests were complete were less than desirable. This included loss of elasticity and flexibility. The dimensional expansion due to excessive water uptake and subsequent water loss in testing led to severe crinkling of the sample during the test procedure, along with mechanical instability. In order to address these problems two further methods were used in an effort to enhance the mechanical stability of the samples.

Firstly, the use of additives was explored in the form of TiO_2, SiO_2 and $Zr(HPO_4)_2$, some of the benefits of which have been discussed in Chapter 1. The samples that were used with additives had DS values of 47, 57, 63, 75 and 80 %. Secondly a blend of a high and low DS polymer was performed in the pre-casting stage of the experimental process. Blending using the same type of polymer is deemed an acceptable way to alter the properties of a polymer. Due to the structure being near identical, bar the number of sulfonic acid groups, there should be no phase segregation between the two different DS polymers [1]. As the lowest DS samples possessed the most ideal mechanical properties, it was decided that this should be blended with the DS of 75 %. The highest DS polymer was not chosen due to its excessive water uptake and dimensional expansion problems.

7.1 Experimental

7.1.1 Starting Materials

SPEEK, the synthesis of which was described in Chapter 4 was used after being stored in DI water. 1-Methyl-2-pirrolidinone (NMP), (Aldrich, 99 + % ACS Reagent) and phosphoric acid (H_3PO_4), (Aldrich, 85 % wt, ACS Reagent) were used as received. Titanium dioxide (TiO_2), (Aldrich, nanopowder, < 25 nm powder), silicon dioxide (SiO_2), (Aldrich, nanopowder, 10-20 nm (TEM)) were dried at 100 °C prior to use. Zironcium oxychloride octahydrate ($ZrOCl_2.{}_8H_2O$), (Aldrich, 99.5 % puriss) was used as received.

7.1.2 SPEEK with Additives

There were two ways that the additives were incorporated into the polymer membrane. Firstly there was the direct method in the casting stage. The additive was mixed by determined weight ratios with the dry polymer and casting solvent, NMP. The slurry was then stirred for 16 hours under constant heating at 50 °C, and sonicated for approximately 60 minutes before casting in the normal manner described in Chapter 4. This method was utilised for SPEEK and TiO_2, SiO_2 and $Zr(HPO_4)_2$

Zirconium hydrogen phosphate ($Zr(HPO_4)_2$) (ZrP) was prepared by reacting a solution of $ZrOCl_2.{}_8H_2O$ (1 M), with a solution of H_3PO_4 (1 M). This reaction is known to form an insoluble white precipitate of $Zr(HPO_4)_2$ through ion-exchanging of the oxychloro group. The precipitate was filtered off and washed in DI water thoroughly before drying under vacuum at 80 °C for 12 hours. The solid was then combined with the polymer as mentioned above.

After all the casting solvent had been evaporated off, the polymer membranes that were remaining showed visible signs of separation and aggregation of the additive. The TiO_2, SiO_2 and ZrP added at the casting stage caused phase segregation, with the additive having sunk to the bottom of the casting dish. The membranes had two very different surfaces. The bottom of the membrane that was next to the substrate appeared somewhat grainy to the touch where the additive had accumulated. The top of the membrane was very smooth and the separation was very clear when the sample was

dipped in liquid nitrogen and snapped in half. Although when the quantity of additive was reduced this separation was less pronounced, the strength of the membranes (*ie*; their tear resistance and mechanical strength) was still retained and was superior to the standard membranes with no additive. The samples were briefly tested for their conductivity, but due to the non-ideal physical properties this route of investigation was not continued any further.

The focus was then turned to the ZrP additive which was known to ion-exchange relatively easily. Several groups have investigated the *in-situ* ion exchange of ZrP with positive results [2, 3]. The membranes were cast and dried in the normal manner. To ensure all sulfonic acid sites were protonated, the membranes were subjected to the standard pre-treatment and stored in DI water. The membranes were then immersed in $ZrOCl_2.{}_8H_2O$ (1 M) at 80 °C, whereby the samples were allowed to swell in the solution for 2 hours. Following this, the samples were immersed in H_3PO_4 (1 M) at 80 °C for 12 hours to ion-exchange the oxy-chloride for the phosphate. The samples were rinsed in boiling DI water for several hours to remove any traces of H_3PO_4 before drying and weighing to determine the mass of ZrP contained. The synthesis of ZrP occurs via the condensation of the zirconyl chloride and phosphoric acid as seen in Equation 7.1.1, while the ZrP is thought to join with the SPEEK structure as seen in Figure 7.1.1.

$$ZrOCl_2 + H_3PO_4 \rightarrow Zr(HPO_4)_2 \cdot H_2O$$

Equation 7.1.1

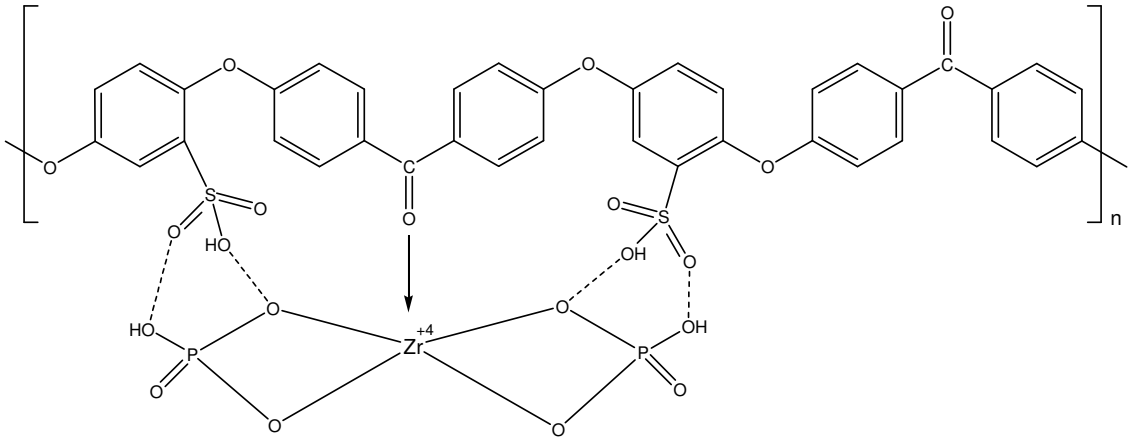

Figure 7.1.1 Possible molecular structure of SPEEK-ZrP.

7.1.3 SPEEK Blend Preparation

The blend polymer was prepared in a similar manner as detailed in Chapter 4. The raw polymer was dried after being stored in DI water and appropriate weights of each DS were weighed and mixed with the NMP casting solvent. The samples were mechanically stirred for 24 hours to ensure complete mixing had occurred before casting and drying in the usual manner. A range of different compositions were prepared which is detailed in Table 7.1.1.

Table 7.1.1 Specific weight % of SPEEK blends and corresponding DS.

Sample Ref.	wt % DS 0.47	wt % DS 0.75	Actual DS
1A	100	0	0.47
1B	92.73	7.27	0.49
1C	85.56	14.44	0.51
1D	78.47	21.53	0.53
1E	71.50	28.50	0.55
2A	64.41	35.59	0.57
2B	56.65	43.35	0.59
2C	49.87	50.13	0.61
3A	28.81	71.19	0.67
3D	7.15	92.85	0.73

The actual DS was calculated based upon the ratio of each component and their corresponding DS. The calculated IEC and EW values can be seen in Table 7.1.2.

Table 7.1.2 IEC and EW values for blended samples DS and was deemed accurate to 5 %.

Sample Ref.	IEC	EW
1A	1.40	715
1B	1.45	689
1C	1.50	666
1D	1.55	645
1E	1.60	626
2A	1.65	608
2B	1.70	589
2C	1.74	574
3A	1.88	532
3D	2.01	497

The samples were dried, cut to size and pre-treated as described previously. A separate sample was used for each experiment and each replica sample was labelled by the sample reference and 1,2, 3 and so forth. For each standard sample that was prepared, a second sample was prepared in parallel and treated to obtain the SPEEK-ZrP form as detailed previously. These were named as the sample reference plus the replica number and then Z to denote the ZrP form.

7.1.4 Physical Characterisation

7.1.4.1 Water Uptake

The water uptake was studied for the blended SPEEK and the blended SPEEK-ZrP samples. This was performed at the same temperatures and relative humidities as in Chapter 6 (*ie* 20 and 80 ° C immersed in water and 20 and 80 ° C in 95 % relative humidity).

7.1.5 Electrochemical Characterisation

The impedance of the samples was measured using the platinum wire multi-electrode cell in the *WKL* chamber as described in Chapter 6. The temperature and relative humidity was changed in order to further evaluate environmental effects on conductivity.

Table 7.1.3 Environmental conditions of the experiments and the samples that were used.

Experiment	T_{max}	RH	WKL Program	Samples Tested	Chapter
1	80	80	1	Nafion	6
2	80	80	1	SPEEK	6
3	80	95	2	Nafion	6
4	80	95	2	SPEEK	6
5	105	75	3	SPEEK	6
6	105	75	3	SPEEK-ZrP	7
7	80	75	4	SPEEK-ZrP blends	7
8	80	75	4	SPEEK blends	7
9	105	75	5	SPEEK-ZrP blends	7

7.2 Results

7.2.1 Physical Characterisation

7.2.1.1 Water Uptake

The water uptake of the blended SPEEK samples can be seen in Table 7.2.1 and Table 7.2.2.

Table 7.2.1 Lambda values of blended SPEEK samples immersed in water at varying temperatures.

Sample	20 ° C λ	80 ° C λ
1A	8.0	19.7
1AZ	19.3	22.5
1B	9.1	20.9
1BZ	19.6	23.2
1C	9.3	22.7
1CZ	21.6	24.2
1D	9.5	23.1
1DZ	20.7	25.6
1E	11.6	26.3
1EZ	21.9	28.9
2A	12.9	28.4
2AZ	24.5	35.1
2B	13.5	33.0
2BZ	25.1	42.6
2C	14.0	36.2
2CZ	27.6	49.5
3A	16.9	38.6
3AZ	36.1	53.1
3D	20.2	41.5
3DZ	38.6	63.2

Table 7.2.2 Lambda values of blended SPEEK samples in 95 % RH at varying temperatures.

Sample	20 ° C λ	80 ° C λ
1A	4.9	1.7
1AZ	5.5	3.3
1B	5.1	1.9
1BZ	5.8	3.6
1C	5.6	2.3
1CZ	6.3	4.0
1D	5.3	2.9
1DZ	6.9	4.4
1E	5.8	3.2
1EZ	7.2	5.3
2A	6.4	3.5
2AZ	7.8	7.5
2B	9.3	3.9
2BZ	11.3	10.3
2C	12.5	5.8
2CZ	15.7	12.2
3A	14.2	7.1
3AZ	19.5	13.6
3D	16.8	8.3
3DZ	24.2	14.7

The water uptake over the blend range for the standard samples shows a similar increase as seen in Chapter 6 in that as the weight fraction of the higher DS SPEEK is increased, the water content also increases. When the data from Table 7.2.1 and Table 7.2.2 is plotted graphically, a second trend is seen. There is a steep increase in the water content seen in Figure 7.2.1 after sample 2A (greater than 36 % SPEEK-75). At this blend level, the IEC is approximately 1.65 meq/g, and the unblended samples mentioned in Chapter 6 also showed a similar gradient change at this IEC value. This may be due to the sample reaching a critical composition whereby some elastic forces have been overcome purely by the number of sulfonate groups and their waters of solvation.

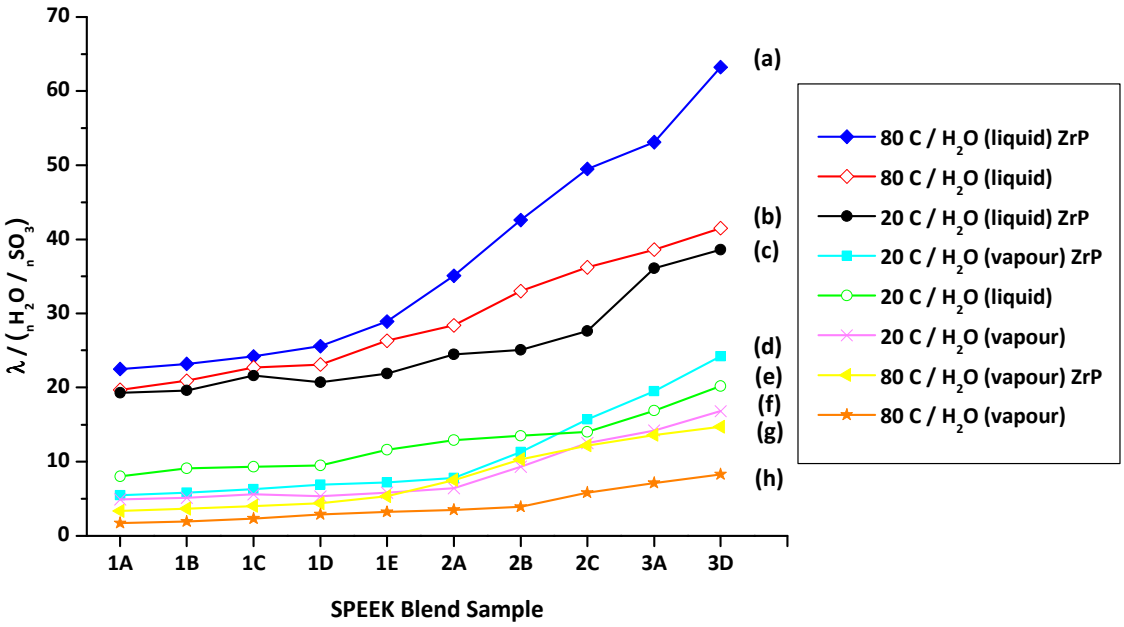

Figure 7.2.1 Water uptake of the blended SPEEK samples when subjected to various temperatures, water phases, with and without ZrP additive.

When the samples containing additives are evaluated, the water content is higher than that of the standard blend samples. The increase after sample 2A is seen to be greater in the blended samples containing the ZrP additive, especially when immersed in liquid water at high temperatures. The structure of SPEEK-ZrP detailed in Figure 7.1.1 would have most likely caused a volume expansion due to its structure alone. In addition, the ion-exchange reaction to ZrP requires two water molecules to hydrate the phosphate group, which could account for additional water content. This effect by the ZrP additive is likely to be enhanced when the content of SPEEK-75 is near its maximum, due to the weight fraction of the ZrP itself. When the membranes were dried to determine the ZrP content, it was found that typically 1-2 % ZrP was incorporated into samples 1A through to 1E. At the point when the sample was over 70 % SPEEK-75, the ZrP content has risen to over 10 % reaching 12.5 % for the sample 3D.

7.2.2 Electrochemical Characterisation

7.2.2.1 Experiment 6 – SPEEK-ZrP at Tmax = 105 ° C and 75 % Relative Humidity

This experiment was used to see any similarities or differences between the unmodified SPEEK samples and those that had been converted to the SPEEK-ZrP form. The unmodified SPEEK experiment was detailed in Experiment 5 in Chapter 6. The environmental conditions for Experiment 6 were kept at 105 ° C and 75 % relative humidity as in Experiment 5, but the samples had been converted to SPEEK-ZrP using the second experimental preparation method detailed in Section 7.1.2

The impedance data obtained followed that which has been seen previously, exhibiting parallel RC behaviour with a bulk resistance intercept of the real axis. The calculated conductivity trace can be seen in Figure 7.2.2.

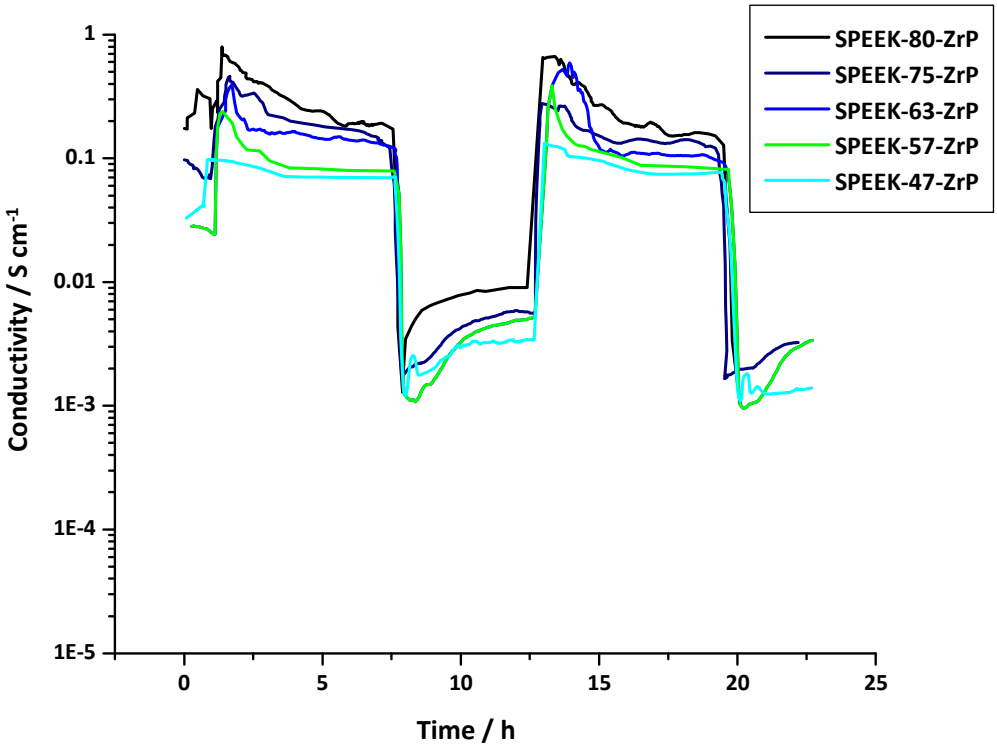

Figure 7.2.2 Experiment 6 (T_{max} = 105 °C, RH = 75 %) - Conductivity trace for all SPEEK-ZrP samples using WKL Program 3.

There is a marked difference in the shape of the conductivity trace compared with the samples that did not contain any ZrP. Instead of a rapid decrease in conductivity when the thermal cycle had reached its maximum, there appeared a more controlled gradual decrease. As discussed in Chapter 6, the decrease in the conductivity is due to less water being retained as the temperature is increased. The conductivity decrease being lessened indicates that the water content may be greater in samples containing the ZrP than in standard samples when equilibration is reached.

The ZrP structure, retains 2 water molecules per Zr ion as shown in Equation 7.1.1. It may be possible that the lesser degree of conductivity decay may be due to these water molecules staying within the structure at elevated temperatures. This may also be the reason behind the physical observations of the membrane after the experiment had been completed. In Experiment 5, Chapter 6, samples with a high DS were so severely dehydrated at T_{max} = 105 °C that the sample was somewhat deformed when removed from the multi-electrode cell. A similar effect was seen with the ZrP additive samples, however it was only significantly noticeable for the SPEEK-80.

7.2.2.2 *Experiment 7 – SPEEK-ZrP Blends at T_{max} = 80 ° C and 75 % Relative Humidity*

The samples in Experiments 5 and 6 still achieved relatively high conductivities at 75 % relative humidity so this value was deemed useful for this experiment but by employing a lower temperature. During the previous experiments on the second thermal cycle, no conductivity loss was seen at the second thermal plateau. Therefore, for this and future experiments a single thermal cycle with a plateau was used as seen in Figure 7.2.3.

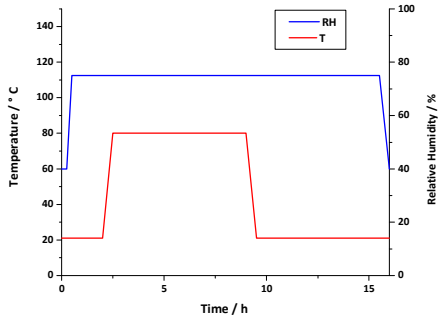

Figure 7.2.3 WKL Program 4 – Temperature and relative humidity profile – T_{max} 80 ° C and RH 75 %.

The conductivity trace for some of the samples in this experiment can be seen in Figure 7.2.4. As with previous experiments, the initial temperature ramp provides the rise in conductivity which then decays away as the sample equilibrates to a conductivity equilibrium plateau. The thermal program utilised in this experiment had an extended low temperature baseline after the temperature was ramped down. By contrast, with other experiments, the conductivity only just reached equilibrium before the second thermal cycle begun. This experiment shows that the conductivity is maintained after equilibration as long as the environmental conditions remain constant.

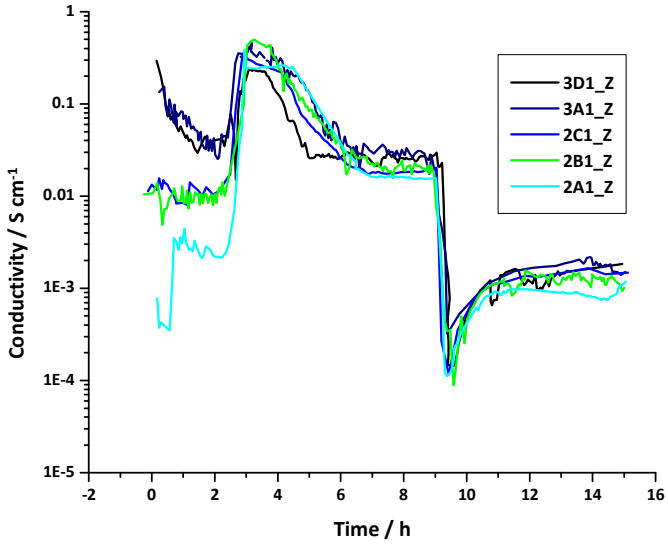

Figure 7.2.4 Experiment 7 (T_{max} = 80 °C, RH = 75 %) - Conductivity trace for some SPEEK-ZrP blended samples.

The conductivity results for all the blended SPEEK samples in Experiment 7 can be seen in Table 7.2.3.

Table 7.2.3 Conductivity data for the blended SPEEK-ZrP samples from Experiment 7 (T_{max} = 80 °C, RH = 75 %) .

Sample	Temperature / ° C	Relative Humidity / %	σ_{MAX} / S cm^{-1}	σ_P / S cm^{-1}
1A1_Z	80	75	0.117	0.015
1B1_Z	80	75	0.155	0.017
1C1_Z	80	75	0.154	0.018
1D1_Z	80	75	0.169	0.019
1E1_Z	80	75	0.186	0.020
2A1_Z	80	75	0.203	0.021
2B1_Z	80	75	0.295	0.026
2C1_Z	80	75	0.301	0.026
3A1_Z	80	75	0.350	0.030
3D1_Z	80	75	0.368	0.041

In this experiment, the water content effect is predominantly seen at the offset. The samples that have a greater weight content of SPEEK-75 have a much higher initial conductivity due to their ability to hold a greater amount of water. When the conductivity reaches σ_p, the effect is lessened, though generally speaking, the greater the content of SPEEK-75, the higher the conductivity. This agrees with the findings in Experiment 4 whereby the SPEEK-75 sample had a much higher σ_p than the SPEEK-47 sample.

7.2.2.3 *Experiment 8 – SPEEK Blends at T_{max} = 80 ° C and 75 % Relative Humidity*

It has been seen in Experiment 4, T_{max} = 80 ° C and RH = 95 % that the conductivity of SPEEK samples suffered only small degrees of decay after the temperature had been ramped to T_{max}. In Experiments 2 and 5, T_{max} = 80 ° C, RH = 80 % and T_{max} = 105 ° C, RH = 75 % respectively, the conductivity of SPEEK samples was shown to decay at T_{max}. The effect of the blended membrane under conditions that would normally cause conductivity decay was investigated, with the environmental profile WKL Program 4 being utilised for this experiment.

The data in Table 7.2.4 shows that a large difference between the σ_{MAX} and σ_P still remains. The decay in conductivity is not however as large as when the T_{max} = 105 ° C at the same relative humidity, which was over one order of magnitude. The samples in the Experiment 7 with the ZrP additive, had a larger σ_{MAX} but the σ_P was only slightly higher than the data in the table below.

Table 7.2.4 Conductivity data of the blended SPEEK samples from Experiment 8.

Sample	Temperature / ° C	Relative Humidity / %	σ_{MAX} / S cm^{-1}	σ_P / S cm^{-1}
1A2	80	75	0.011	0.006
1B2	80	75	0.016	0.007
1C2	80	75	0.018	0.008
1D2	80	75	0.019	0.008
1E2	80	75	0.019	0.009
2A2	80	75	0.028	0.009
2B2	80	75	0.030	0.001
2C2	80	75	0.036	0.011
3A2	80	75	0.040	0.013
3D2	80	75	0.046	0.014

7.2.2.4 *Experiment 9 – SPEEK-ZrP Blends at T_{max} = 105 ° C and 75 % Relative Humidity*

The environmental conditions used in Experiment 9 followed the recent single thermal cycle seen in WKL Program 4, except that the T_{max} was raised to 105 ° C again as seen in Figure 7.2.5.

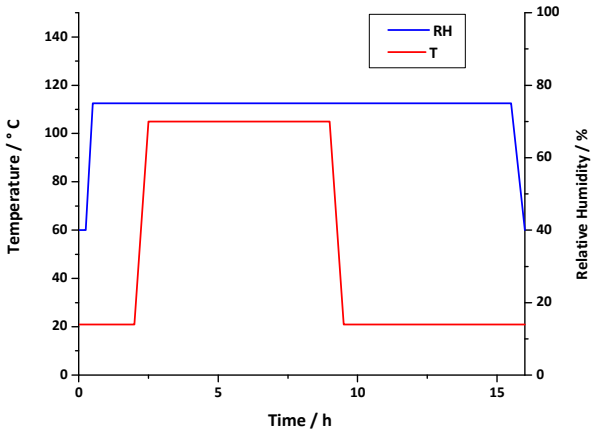

Figure 7.2.5 WKL Program 5 – Temperature and relative humidity profile – T_{max} 105 ° C and RH 75 %.

The visual observations from Experiment 9 showed that after the T_{max} was reached, the conductivity followed the same decay as previously seen, the data of which can be seen in Table 7.2.5

Table 7.2.5 Conductivity data for the blended SPEEK-ZrP samples from Experiment 9.

Sample	Temperature / ° C	Relative Humidity / %	σ_{MAX} / S cm^{-1}	σ_P / S cm^{-1}
1A3_Z	105	75	0.19080	0.02700
1B3_Z	105	75	0.27720	0.04729
1C3_Z	105	75	0.29050	0.06112
1D3_Z	105	75	0.29870	0.07573
1E3_Z	105	75	0.32640	0.08142
2A3_Z	105	75	0.35020	0.08870
2B3_Z	105	75	0.36820	0.09851
2C3_Z	105	75	0.41450	0.12278
3A3_Z	105	75	0.52080	0.16645
3D3_Z	105	75	0.71460	0.17860

The σ_{MAX} values across the range of samples is seen to have a shallow gradient which increases as the weight fraction of SPEEK-75 increases. This effect also appears to be visible in the σ_P values.

7.2.2.5 *SPEEK Comparisons With Respect to Temperature, Relative Humidity and Additive Effects*

A range of different environmental conditions coupled with the introduction of inorganic additives and blends has been investigated throughout the number of separate experiments detailed in this, and Chapter 6. While through each experiment, explanations of the processes involved have been discussed, the set of experiments as a whole was designed so that the different individual effects could be inter-related.

The σ_{MAX} and σ_P data from Experiments 4, 5 and 6 can be seen in Figure 7.2.6. These three experiments utilised the 5 different DS samples of SPEEK, and in the case of Experiment 6, the samples were ion-exchanged with ZrP.

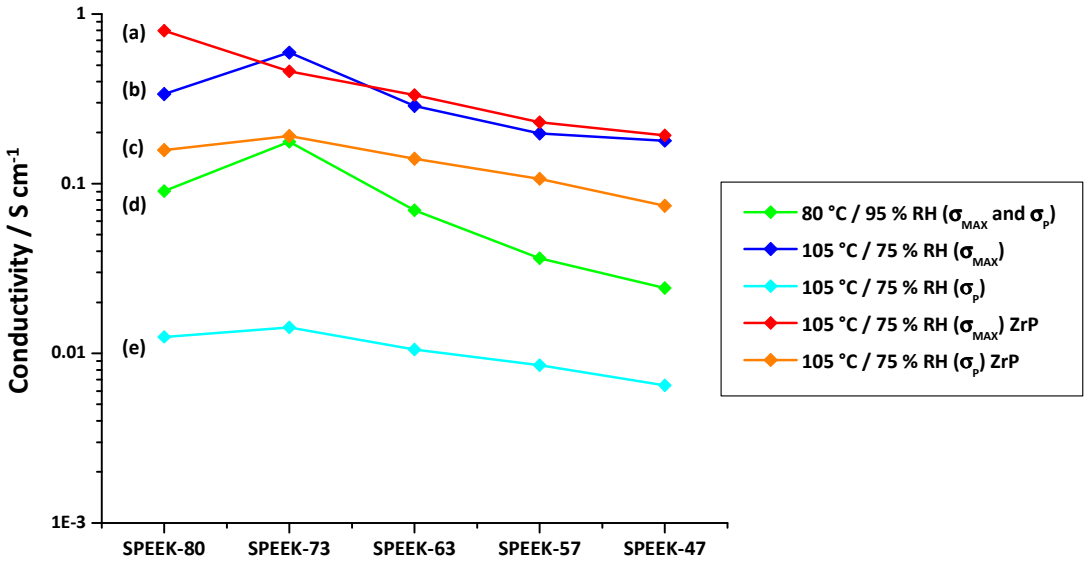

Figure 7.2.6 Graph illustrating the σ_{MAX} and σ_P of the range of varying DS samples under different environmental conditions with and without ZrP additive.

The data in Figure 7.2.6 shows that the greatest σ_{MAX} was achieved at 105 °C and 75 % relative humidity with the ZrP additive in the SPEEK-80 sample (a). The same sample that was without the ZrP additive (b) had the second highest σ_{MAX}, while for the SPEEK-47 sample (b), the σ_{MAX} was almost the same as the ZrP sample (a). However, the differences between the samples with additives and those without, was more pronounced in the σ_P values. The ZrP additive (c) at the same temperature and relative humidity (105 °C and 75 %) provided an increase in σ_P by on average one order of

magnitude across the DS range when compared to the standard samples (e). At lower temperature and higher relative humidity (d) an intermediate conductivity was achieved which was absent of any maximum or minimum due to faster equilibration. When the DS of the samples is considered, for both the σ_{MAX} and σ_P, an almost linear increase is seen. The failure of the highest DS sample to comply with this trend may be due to the excessive water uptake causing some mechanical abnormalities.

When the σ_{MAX} and σ_P values of the blended samples were compared as in Figure 7.2.7, a linear increase is seen as the weight fraction of SPEEK-75 within the blend is increased.

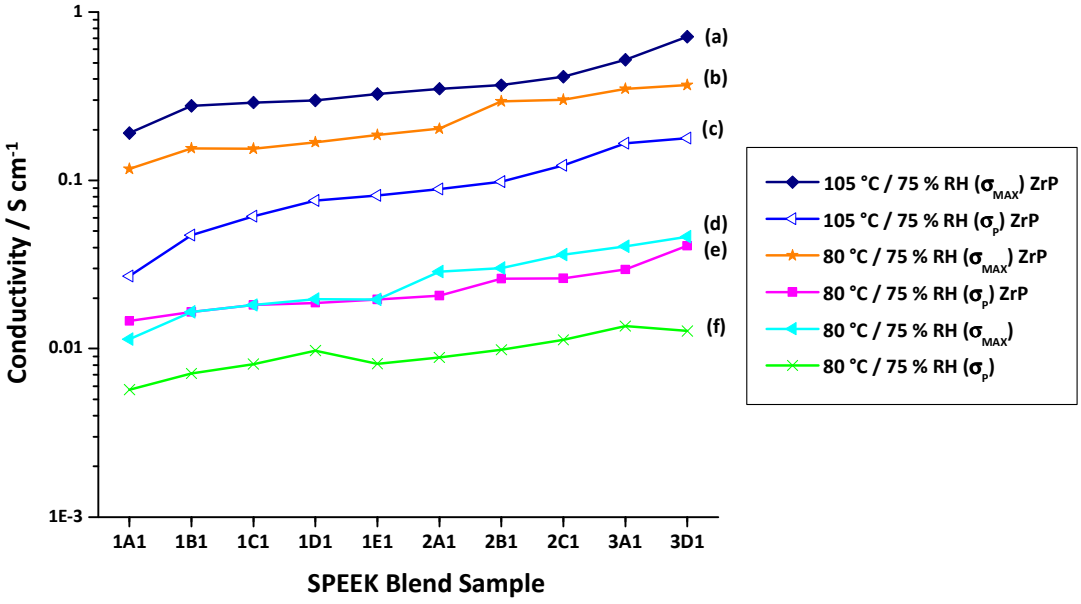

Figure 7.2.7 Graph illustrating the σ_{MAX} and σ_P of the range blended SPEEK samples under different environmental conditions with and without ZrP additive.

7.3 Chapter 7 Conclusions

By performing the additional experiments in Chapter 7, a much fuller picture is obtained on how SPEEK and blended SPEEK membranes with and without organic additives behave over a range of temperatures and relative humidities.

- The addition of ZrP into standard samples of varying DS provided some benefit with regards to the conductivity value retention at T_{max}. Whereas the standard samples suffered from very sharp conductivity decays, the ZrP samples possessed much shallower decays in all DS samples. The ZrP may be inhibiting water loss allowing for the higher σ_P, or it may simply be due to the higher water content of the ZrP samples.

- The blending of two different DS standard samples has shown that for both with and without the ZrP additive, the IEC and associated water content are significant factors in conductivity effects. For the experiments run at 80 °C and 75 %, the standard blended samples showed a gradual increase over the range for both σ_{MAX} and σ_P, with approximately half an order of magnitude difference. When this was compared to ZrP blends at the same temperature, the σ_{MAX} was half an order of magnitude higher than the standard blend σ_{MAX}. The difference between the σ_{MAX} and the σ_P, was approximately one order of magnitude, with the σ_P from ZrP samples being similar to the σ_{MAX} of standard samples.

- The effect of temperature on the samples could also be distinguished between Experiments 7 and 9. The σ_{MAX} of samples at 105 °C and at 80 °C was very similar with values in the region of 0.7 and 0.4 S cm^{-1} respectively. However, it was after the decay of conductivity to the σ_P that the greatest difference was seen. The samples at 105 °C had a σ_P half an order of magnitude lower than the σ_{MAX}. The samples at 80 °C had a drop of over one order of magnitude to their σ_P.

- The process of blending samples has shown that no detrimental effects on the conductivity and water content have been seen. This technique has seen beneficial effects in that the mechanical stability of lower DS SPEEK samples

has been preserved while allowing slight increases in conductivity as the content of higher DS SPEEK has been increased.

7.4 Chapter 7 References

1. H.-Y. Jung and J.-K. Park, *Electrochimica Acta*, 2007, **52**, 7464-7468.

2. S. D. Mikhailenko, S. M. J. Zaidi and S. Kaliaguine, *Catalysis Today*, 2001, **67**, 225-236.

3. B. P. Tripathi and V. K. Shahi, *Journal of Colloid and Interface Science*, 2007, **316**, 612-621.

Chapter 8

Conclusions

Chapter 8 Conclusions

8.1 Conclusions on the Developed Experimental Techniques

One of the main aims of this work was to develop new high-throughput methods for the discovery of materials that would be suitable for use as polymer electrolytes in battery and fuel cell applications.

In Chapter 3, a method based on previous works on positive electrode materials [1, 2] was found to be suitable for polymer electrolyte characterisation with simple modifications. Using a ternary system of a polymer, lithium salt and plasticiser, polymer electrolytes with different compositions of known material content were prepared by liquid mixing to cover the entire compositional spread. Through deposition and controlled evaporation of the co-solvent, thin film membranes were produced on each of the 64 electrodes of a combinatorial cell. The conductivity of the samples was analysed by means of AC Impedance over a range of frequencies using the through-plane method. The multi-electrode cell that was used was tested for individual cell divergence which was found to be minimal. A complete range of different compositions was measured and compositional plots, which were mapped for conductivity values were prepared, allowing any trends to be found.

In order to measure more highly conductive polymer electrolytes, a second technique was developed that utilised the in-plane measurement method. A single cell was constructed and tested with commercially available samples. This was then scaled up to a multi-electrode cell with 20 individual electrodes providing a maximum of 19, 2-electrode cells or 5, 4-electrode cells. The cell was designed specifically to allow gas access to the polymer samples from both sides and different electrode materials and substrates were evaluated. Platinum wire stretched over Macor was found to maintain the best contact for the duration of the experiments and remained durable over many experiments. The platinum-Macor multi-electrode cell was calibrated to ensure the true bulk conductance was being measured using commercial polymer samples. It was

found that the true bulk conductance was measured, and any secondary effects were minimal.

By connecting the multi-electrode cell to a connector box and a multi-channel potentiostat, the impedance of the samples was measured to calculate their conductivity. The cell was placed in an environmental chamber whereby the impedance was measured *in-situ* whilst a temperature and relative humidity profile was run. By creating a continuously looped impedance program, the conductivity was monitored on a real-time basis as temperature or relative humidity changed. By performing the measurements in this manner, certain characteristic behaviours that may normally be overlooked or not even measured using conventional methods, were recorded.

A HT preparation method was developed to some extent in that parallel synthesis of varying SPEEK samples was performed. By varying the reaction time, samples with varied DS's were produced. This proved to be of most use when characterising the polymer as only small samples were prepared. An overview of the spread of the properties was obtained through ^{1}H NMR analysis allowing certain samples to be isolated and used in a scaled up synthesis step.

8.2 Conclusions on Materials Studies

For the gel polymer electrolyte system involving PVdF-HFP, LiTFSI and PC, an optimum composition at 0.5/0.45/0.05 (PVdF-HFP / LiTFSI / PC) was found. The highest conductivity attainable in the ternary system was achieved at a composition around 0.75/0.25 (LiTFSI/PC) which corresponds to the maximum liquid electrolyte conductivity for these components. The samples that contained PVdF-HFP had an increasing trend in conductivity towards this point. However, it was only samples with higher weight fractions of polymer that could be considered as optimum for the system as they possessed both mechanical and electrochemical properties required for their intended use.

The proton conducting polymer work on SPEEK showed that conductivities in the order of 0.177 S cm^{-1} can be achieved under normal PEM fuel cell conditions with a SPEEK sample that has a DS of 75 %. Under these conditions (80 °C and 95 % relative

humidity) there is also little conductivity decay of any of the SPEEK samples. Effects of the % DS on the conductivity was found to be significant under these conditions, with the general trend showing that higher DS samples had higher conductivities. These samples compared well to commercial Nafion 117 samples that did show decay in the conductivity from very high values at T_{max} to equilibration values of 0.196 S cm^{-1}.

Using water uptake experiments, the decay in conductivity was found to correlate to water loss. At the same relative humidity, it was determined that both SPEEK and Nafion samples were able to hold more water at lower temperatures. This provided an explanation for the conductivity decay as the experiment began at low temperature. At the point of reaching T_{max}, the water content of the samples needed to reduce to reach equilibrium leading to a decrease in the conductivity. The fact that under PEM fuel cell conditions, the SPEEK had minimal decay may have indicated that equilibration was reached very fast on the temperature rise under those particular conditions.

When the environmental conditions were changed to higher temperatures and lower relative humidities, SPEEK samples began to exhibit the conductivity decay characteristic of the Nafion samples and the mechanical integrity of high DS samples was also compromised. Methods of reducing these undesirable properties were investigated by using an inorganic additive, ZrP, and by blending high and low DS samples. The addition of the additive allowed higher conductivities to be achieved due to the increase in water content, and the conductivity decay was also reduced, but it did not address the mechanical issues. This was however improved with the blended membranes when very similar values of conductivity were reached with structural stability remaining after the experiments were complete. At 105 °C and 75 % relative humidity, blended membranes showed maximum conductivities between 0.19-0.72 S cm^{-1} and equilibration values between 0.18-0.03 S cm^{-1}. The blended SPEEK-ZrP samples also showed beneficial properties at lower temperatures in that they had reduced conductivity decay at lower temperatures

8.3 Further Work

This work has shown two methods that could be optimised and honed for future high-throughput studies of polymer electrolytes. Very recently a commercial product has been developed by BekkTec LLC [3]. It is specifically for use with PEM's for fuel cell application and is based on a single cell 4 electrode measurement. The theoretical principles behind the design of this commercial cell and the multi-electrode cell fabricated for the work detailed in this thesis are fundamentally similar. The multi-electrode cell in this work has been proven to function as a single cell was expected to, so it is anticipated that with commercial manufacturing knowledge and finances, high-throughput methods should soon become available.

When considering further development of the high-throughput synthesis of polymer electrolytes there are two directions in which the work may proceed. The polymer electrolytes detailed in Chapter 3 were prepared by liquid mixing of constituents. This method may be appropriately used for any electrolytes that can have their components synthesised individually and then mixed by ratio to determine the optimum composition.

The proton conducting polymer electrolytes however pose more of a problem with respect to their future development. Synthesising fluorinated PEM's requires specialist equipment and is therefore expensive. However, the preparation of certain compositionally varied aromatic polymers can be done with relative ease when the nature of introducing a functional group follows simple organic reactions. The method of mixing constituents can also be applied to PEM's when using additives to make composite membranes and could be developed to an automated level. To truly achieve high-throughput PEM characterisation, a combinatorial approach to copolymer synthesis should be coupled with the measurement technique of the multi-electrode cell, though this would most probably require the collaboration of workers from the organic and electrochemical disciplines.

8.4 Chapter 8 References

1. A. D. Spong, G. Vitins, S. Guerin, B. E. Hayden, A. E. Russell and J. R. Owen, *J. Power Sources*, 2003, **119**, 778-783.

2. M. R. Roberts, A. D. Spong, G. Vitins and J. R. Owen, *Journal of The Electrochemical Society*, 2007, **154**, A921-A928.

3. Bekktech, *BT-112 Conductivity Cell (FCT)*, http://www.bekktech.com/BT112.html.